SEP. - DEC. 2023 • Volume XXIV Number

THE ASEAN
JOURNAL OF RADIOLOGY

Highlight

- Original Article
- Case Report
- Perspectives
- ASEAN Movement in Radiology
- Memorial

Official Journal of The

Royal College of Radiologists of Thailand

Radiological Society of Thailand

Foundation for Orphan and Rare Lung Disease

Thai Society of Vascular and Intervention Radiology

ASEAN Association of Radiology

ASEAN
JOURNAL OF RADIOLOGY

ISSN 2672-9393

The ASEAN
Journal of Radiology

CONTENTS

From The Editor

Original Article

Case Report

Perspectives

ASEAN Movement in Radiology

Memorial (Part 2)

THE ASEAN JOURNAL OF RADIOLOGY
ISSN 2672-9393

From The Editor

The passing 2023 remained the year of infection

Received 24 December 2023; revised 24 December 2023; accepted 24 December 2023
doi:10.46475/asean-jr.v24i3.893

Since the start of the year, the total number of Covid cases has reached 36,204, with 826 cumulative deaths [1]. The dominant sub-variants of COVID-19 in Thailand are XBB.1.9.2 (24.5%), followed by 23.3% of EG.5, 17.8% of XBB.1.16 and 11.9% of XBB.2.3 [2]. The XBB.1.16, or Arcturus is the descendent of Omicron. It was first detected in India in early January and has been steadily spreading in several countries. There is no proven evidence that the variant causes more symptoms, except for those suffering from underlying diseases. 2023 is the COVID-19 infections' fourth year of entering and the severity of the disease has declined substantially, even though the virus continues to mutate.

Starting from infected foreigners in May last year, the Monkeypox outbreak in Thailand has spread rapidly among Thai nationals in central and eastern Thailand to a total of 535 cases consisting of 481 Thais, 50 individuals of foreign origin, and 4 cases where the nationality was not disclosed [3]. More than 80% are homosexual males and almost half are HIV positive. Bangkok and central Thailand recorded the highest number, followed by eastern Thailand and Phuket. One casualty has been reported within the total cases.

The highest HIV infection rates in Thailand, previously among sex workers and men who had sex with men, has now shifted to the younger population. Nearly half of the annual 9,000-plus new HIV infections are individuals aged between 15 and 24 years old [4].

Melioidosis, also known as Whitmore's disease, is triggered by Burkholderia pseudomallei, and typically found in contaminated soil, water, rice paddies, and cropping farms. It is endemic in Southeast Asian countries. Thailand's Department of Disease Control (DDC) disclosed that 582 cases of the illness have been identified this year in lower northeastern and deep south of the country, claiming the lives of the approximately 10 farmers [5]. This is the first time in recent years that the disease has led to fatalities. Melioidosis can spread to both humans and animals through direct contact with a contaminated source. Humans can contract the disease by touching or ingesting contaminated soil and water, or even by inhaling the organism. Symptoms, which include high fevers, abscesses, and respiratory infections, can appear one to 21 days post-exposure, depending on the body's antibody levels [6]. A fatal case of typical melioidosis from India was reported in this issue.

Dengue fever is a clear and present danger for tropical countries, including Thailand. The number of dengue fever patients in Thailand recorded between January 1st and November 1st was more than 123,000, which is an increase up to three folds compared to last year. Among the 123,000 people infected, 139 died and most were in the 25-34 age group [7].

Between January 1 and November 25, there were 548 cases of meningitis caused by Streptococcus suis in Thailand, with 26 fatalities, mostly in the northeastern part of the country. It is likely attributable to consuming contaminated raw or undercooked pork. The public is advised not to consume undercooked pork and buy pork from reliable sources with standards, not from unknown sources [8,9].

When it comes to tuberculosis, the oldest and still number one enemy in the human history, Thailand is successful in remarkable reduction of the mortality rate in HIV-positive individuals. However, reductions in the incidence rate of and the number of deaths in tuberculosis in HIV-negative people are still far from milestones, even lower than the global current status [10] regardless of the fact that Thailand ranks number one in the Universal Health Coverage index. The National Plan of Action on tuberculosis phase 2 (2023-2027) determines new goals, indicators, measures and timeline. The chest radiograph remains the screening tool and will be used in all at-risk people. The shortage of radiologists in interpreting chest radiographs will be overcome by applying Artificial Intelligence (AI) in the triaging purpose. The Royal College of Radiologists of Thailand guides the proper use of AI and provides radiographic data set of pulmonary tuberculosis for external validation.

The editor, on behalf of the Royal College of Radiologists of Thailand (RCRT), gives a talk about the role of RCRT in guiding and promoting the proper use of AI on 14 December 2023 in the conference held by the Division of Tuberculosis, the Department of Disease Control, the Ministry of Health.

The Royal College of Radiologists of Thailand (RCRT) in collaboration with the Foundation for Orphan and Rare Lung Disease (FORLD) hosted the 2024 annual meeting among thoracic radiologists and participants during 20-22 October in Bangkok. The business meeting among thoracic radiologists, taking place on 20 October, focused on rising issues which were grouped into 5 agendas: a post implementation review of the National HRCT Protocol, the safety and effectiveness of the diagnostic imaging, HRCTinterpretation for suspected or at-risk or with known interstitial lung disease including the standard report of HRCT in patients with fibrotic lung disease, the recommended CT protocol for patients with thoracic malignancy in the public health universal coverage system, and a review of the guideline for determining the fibrotic extent on HRCT. The details and conclusions of all agendas were published in this issue.

THE ASEAN JOURNAL OF RADIOLOGY
ISSN 2672-9393

The editor together with the president of RCRT (middle), panellists and speakers in the 2024 annual meeting of thoracic radiology.

I sincerely wish all the readers, authors, our valued reviewers, and editors a more prosperous 2024.

Wiwatana Tanomkiat, M.D.
Editor,
The ASEAN Journal of Radiology
Email: aseanjournalradiology@gmail.com

References

1. Thaiger.com [Internet]. c2023 [cited 2023 Dec 27]. Westwood N. Thailand's weekly Covid-19 cases surge over 500 with three fatalities. Available from: https://thethaiger.com/news/national/thailands-weekly-covid-19-cases-surge-over-500-with-three-fatalities

2. Thaipbsworld.com [Internet]. Bangkok: Thailand's Public Broadcasting Service Act; c2023 [cited 2023 Dec 27]. No extraordinary preparations for Omicron XBB.1.16 sub-variant in Thailand. Available from: https://www.thaipbsworld.com/no-extraordinary-preparations-for-omicron-xbb-1-16-sub-variant-in-thailand/

3. Thaipbsworld.com [Internet]. Bangkok: Thailand's Public Broadcasting Service Act; c2023 [cited 2023 Dec 27]. Monkeypox morphs: Thailand reports 535 'mpox' cases in a year. Available from: https://thethaiger.com/news/national/monkeypox-cases-surge-to-535-in-thailand-bangkok-hardest-hit

4. aseannow.com [Internet]. c2023 [cited 2023 Dec 27]. Half of new HIV infections in Thailand among 15-24 year olds. Available from: https://aseannow.com/topic/1313134-half-of-new-hiv-infections-in-thailand-among-15-24-year-olds/

5. Thaiger.com [Internet]. c2023 [cited 2023 Dec 27]. Melioidosis outbreak in Thailand claims ten lives, farmers urged caution. Available from: https://thethaiger.com/news/national/melioidosis-outbreak-in-thailand-claims-ten-lives-farmers-urged-caution

6. www.ddc.moph.go.th [Internet]. นนทบุรี: กรมควบคุมโรค; c 2562 [cited 2023 Dec 27]. เมลิออยโดสิส (Melioidosis). Available from: https://www.ddc.moph.go.th/disease_detail.php?d=99

7. Thaipbsworld.com [Internet]. Bangkok: Thailand's Public Broadcasting Service Act; c2023 [cited 2023 Dec 27]. Dengue fever infections increase by about 300% this year. Available from: https://www.thaipbsworld.com/dengue-fever-infections-increase-by-about-300-this-year/

8. ddc.moph.go.th [Internet]. นนทบุรี: กรมควบคุมโรค; c 2562 [cited 2023 Dec 27]. กินหมูดิบ!! เสี่ยงโรคไข้หูดับ. Available from: https://ddc.moph.go.th/odpc9/news.php?news=38993&deptcode=odpc9

9. Thaiger.com [Internet]. c2023 [cited 2023 Dec 27]. Westwood N. Rise in meningitis cases sparks health concerns in Thailand ahead of new year. Available from: https://thethaiger.com/news/national/rise-in-meningitis-cases-sparks-health-concerns-in-thailand-ahead-of-new-year

10. www.who.int [Internet]. Geneva: WHO; c2023 [cited 2023 Dec 27]. Global tuberculosis report 2023. Available from: https://www.who.int/publications/i/item/9789240083851

Original Article

Comparison characteristic visibility of the lesions with automated whole breast ultrasound and handheld breast ultrasound in screening situation

Patteera Rohitopakarn, M.D.[(1)]
Varanatjaa Pradaranon, M.D.[(1)]
Anutida Limsuknirun, M.D.[(2)]
Wisarut Srisintorn, M.D., Ph.D.[(3)]
From [(1)] Department of Radiology, Faculty of Medicine, Prince of Songkla University, Hat-Yai, Songkla, Thailand.
[(2)] Makarak hospital, Kanjanaburi, Thailand.
[(3)] Occupational Medicine Unit, Division of Family and Preventive Medicine, Faculty of Medicine, Prince of Songkla University, Hat-Yai, Songkla, Thailand.
Address correspondence to P.R.(e-mail: RPatteera.edu@gmail.com)

Received 1 July 2023; revised 30 September 2023; accepted 30 September 2023
doi:10.46475/asean-jr.v24i3.867

Abstract

Background: Screening mammography and additional ultrasound are effective in detecting occult cancer. We know that handheld breast ultrasound (HHUS) depends on the operator. In comparison, automated whole breast ultrasound (ABUS) decreases these disadvantages of ultrasound procedures and can increase its sensitivity to cancer detection rates, but the results showed such studies, especially masses' characteristics, are different. Our study wants to evaluate the features of the lesions in all aspects of the masses by using ABUS compared to HHUS to increase overall interpretation confidence.

Objective: Comparison of visible breast lesions between ABUS and HHUS.

THE ASEAN JOURNAL OF RADIOLOGY
ISSN 2672-9393

Materials and Methods: Retrospective analysis was conducted with 168 screening mammography cases, the undergoing ABUS and HHUS interpreted as the detected lesion, mass characteristic and BI-RADS between October 2017 to May 2018. The investigator reviewed the pathologic or the 2-year follow-up from hand-held ultrasound results. The agreement measurements were assessed, using SD, ICC, percent agreement and Cohen kappa coefficient.

Results: Comparison of the mass's details between two radiologists by using ABUS, ICCs for the location and individual size of the lesion had good reliability. Localization ($\kappa = 0.81$) and BI-RADS ($\kappa = 0.82$) showed almost perfect agreement showing substantial agreement for mass margin ($\kappa = 0.78$), moderate agreement for mass shape ($\kappa = 0.48$) as well as 95% agreement for mass orientation. Intra-rater reliability between two modalities also revealed concordance in both radiologists in important ways for breast mass interpretation.

Conclusion: ABUS can detect lesions, give accurate locations, certain mass size and a few characteristics, is acceptable for screening and monitor detected lesions.

Keywords: Automatic whole breast ultrasound, Breast cancer, Handheld breast ultrasound, Screening.

Introduction

Breast cancer is the most common diagnostic malignancy in women worldwide, including Thailand [1-2]. Multiple studies show early detection of breast cancer by screening mammography can reduce mortality. However, the sensitivity of mammography is about 85% because it is not a particularly effective tool for screening cancer in women with dense breast tissue. Moreover, its sensitivity is reduced to 47.8-64.4% in this woman group because normal breast tissue could obscure the lesion [3-5].

The dense breast is categorized by expert consensus, as heterogeneously dense breasts (BI-RADS category C) and breasts with extremely dense fibroglandular tissue (BI-RADS category D) (more than 50% dense tissue, according to the BI-RADS fourth edition) are considered dense [6-7].

There are supplemental screening modalities that include whole-breast ultrasonography (US) and magnetic resonance (MR) imaging. Because the cost of MR imaging is too expensive, ultrasound is used more prevalently. Many studies supported the idea that ultrasound could detect mammographically occult and clinically significant small invasive breast cancers [8-11].

It is commonly known that more than 50% of women in Western countries have dense breast tissue [12]; meanwhile, more than 70% of women in Eastern countries also have dense breasts [13]. Therefore, in today's clinical practice, after the radiologist interprets screening mammography and the breast tissue of the patient has dense breast tissue or the radiologist suspects something in mammographic imaging, they will do an additional ultrasound to evaluate the findings.

Although many studies are showing that screening breast ultrasound in women is effective in detecting mammographically occult cancer, the practical workflow of nearly 20 minutes for the performance of bilateral handheld breast ultrasound (HHUS) makes it a challenge for screening [14]. Besides, the HHUS is operator-dependent which makes the number of false positives.

Currently, automated whole breast ultrasound (ABUS) is being developed. The ABUS is a technology in which ultrasound scanning is performed mechanically. The operation of the automated system to acquire the scanning data does not require an ultrasound technologist; anyone can be trained to operate the equipment for scanning. The unit acquired raw data via a larger transducer. The transducer paddle is placed over the breast with a small amount of compression. Three image acquisitions of each breast are usually sufficient to image virtually all of the breast tissue, excluding the axilla, including anterior-posterior, medial, and lateral positions. In women with large breasts, 4 or 5 acquisitions of each breast may be needed. The total time to complete the examination is about 15 minutes [15]. The images can be reviewed on a standard workstation. One study shows the interpretation time for each examination is about 3 minutes [16]. These advantages such as image consistency, reproducibility, independence from an operator, and a short time to interpret are feasible for screening situations as an adjunct to screening mammography.

A few studies supported that ABUS significantly increased the sensitivity cancer detection rate but increased recall and false-positive biopsy rates [17-19]. Some studies have made it suspicious that ABUS actually has a significant decrease in specificity [20].

However, a few studies showed that ABUS can help radiologists increase confidence in the visualization of suspicious and benign lesions in various aspects such as size, distance from the nipple, and other characteristics. The results of these studies show no significant difference in radiologists' detection performance, sensitivity, and specificity [21-26]. But different results are shown in separate ways in such studies, especially some mass characteristics. Regarding the results in previously mentioned studies, our study strives to evaluate and confirm characteristic visibilities of the lesions in all aspects of the detected lesions, which can help radiologists increase overall interpretation confidence and specificity and decrease a false-positive biopsy rate. It is useful for both new lesions and in a long-term follow-up of known benign-appearing lesions in a screening setting.

Materials and methods

A retrospective study of 168 cases of women who came to have mammography screening and needed an additional ultrasound between October 2017 to May 2018 was recruited to this study. Each case was combined with both HHUS and ABUS.

Automated ultrasound of the breast (Acuson S2000 automated breast volume scanner (ABVS), Siemens Healthcare) was performed by technologists who had trained to use the technique. A typical examination comprised three automated scans of each breast in the anteroposterior, lateral, and medial positions. Occasional additional views were required for larger breasts. Two breast radiologists with 7 and 9 years of experience independently evaluated the 3D volume data at the automated breast ultrasound workstation. They were blinded to the findings on the corresponding mammograms and handheld ultrasound images as well as to clinical information and tissue pathologic results.

Breast ultrasound with the handheld device (Siemens Acuson S2000) equipped with two linear-array transducers with a frequency bandwidth of 4-9 MHz and 5.5-18 MHz was performed by two breast radiologists with 7 and 9 years of experience according to a standardized scanning protocol. All images, previously interpreted by those two radiologists for a clinical service, were retrieved from the hospital database.

Data obtained from ABUS and HHUS ultrasound images were interpreted in the same detail including breast tissue echogenicity, mass characteristics such as shapes, orientation, margins, echo patterns, posterior features, calcification, associated features such as architectural distortion, duct changes, skin changes, edema, vascularity.

The sequence of images was independently randomized to reduce the risk of bias.

The investigator reviewed the pathologic result in which the suspicious masses (BI-RADS IV-V) were biopsied or the handheld ultrasonographic result in which the probably benign lesions (BI-RADS III) received a follow-up every 6 months for 2 years or until the last visit before December 2019 (The duration of the follow-ups was about 1-4 times, one time/person on average).

We used mean, (SD), and two-way interrater reliability (A,1) type of intra-class correlation coefficient (ICC) to calculate descriptive statistics such as the mass size.

Based on the 95% confident interval of the ICC, the estimated values were scored as poor (ICC< 0.5), moderate (ICC = 0.5-0.75), good (ICC = 0.75-0.9), and excellent reliability (ICC > 0.90) [27].

The agreement of detectable lesions, breast parenchymal echogenicity, and mass characteristics of each lesion between ABUS and HHUS, as well as agreement between radiologic interpretations of each modality, were compared by using percent agreement and Cohen's kappa (κ).

CI construction for the Cohen kappa coefficient was based on the asymptotic normality assumption, and Landis and Koch [28] reference intervals were used to assess the strength of agreement in terms of the Cohen kappa coefficient, where values of $\kappa \leq 0$ indicate no agreement; $0 < \kappa \leq 0.20$, slight agreement; $0.20 < \kappa \leq 0.40$, fair agreement; $0.40 < \kappa \leq 0.60$, moderate agreement; $0.60 < \kappa \leq 0.80$, substantial agreement; and $0.80 < \kappa < 1$, almost perfect agreement. A P-value of less than 0.05 is considered a statistically significant difference.

Results

The 168 women met the study criteria. Between 72 and 83 detected masses were depicted in ABUS examination, by 1st and 2nd radiologists, respectively. Also, 85 masses were results of HHUS, previously interpreted by those two radiologists from the hospital database.

All data from the 168 cases were compared between two breast radiologists using only imaging from ABUS to evaluate the inter-rate agreement. We also used the data to compare the consistency of the data obtained from each individual radiologist's interpretation of ultrasound images from hand-held ultrasound and ABUS which detect detectable lesions, localization, mass size, clock face position, mass characteristics and BI-RADS categories to evaluate inter-rater agreement of imaging interpretation by using ABUS.

A comparison between two radiologists with ABUS significantly showed good reliability for the mass size in width (ICC = 0.89), length (ICC = 0.81), and height (ICC = 0.87) as well as other important mass characteristics such as a substantial agreement for mass margin (κ = 0.78), fair agreement for posterior features (κ = 0.36) of mass and 95% agreement of mass orientation. The almost perfect agreement of the BI-RADS category assessment (κ = 0.82) by two radiologists using ABUS was also manifested.

The intra-rater reliability between the two modalities revealed concordance.

The 1st radiologist significantly showed excellent reliability for the mass size in width (ICC = 0.91) and length (ICC = 0.94), substantial agreement for mass orientation (κ = 0.65), 93% agreement for the shape of the mass*, moderate agreement for detected mass (κ = 0.52), a clock-face position (κ = 0.55), the mass size in height (ICC = 0.62), and the mass margin (κ = 0.45).

The 2nd radiologist significantly described substantial agreement for the clock-face position (κ = 0.68), the mass shape (κ = 0.78) and the margin (κ = 0.68) with

BI-RADS categories assessment ($\kappa = 0.76$), good agreement for the mass size in width (ICC = 0.87), moderate agreement for the mass size in length (ICC = 0.6), fair agreement for detected mass ($\kappa = 0.39$) and posterior features of the mass ($\kappa = 0.39$).

**Note: Some data cannot be calculated by using Cohen's kappa statistic because when one rater's ratings have no variation, the agreement corrected for chance (κ) is considered to be zero. Furthermore, our study shows a corresponding agreement between the percent agreement and the Cohen's kappa statistics. Consequently, we used percent agreement instead of Cohen's kappa statistics if the κ could not be assessed.*

We found that 40 masses matched between the two radiologists for ABUS imaging interpretation, with 25 masses matching those found in both HHUS and ABUS between the two radiologists.

BI-RADS categories assessment for ABUS, detectable lesions by 1st and 2nd radiologists were corresponding as 2.5%, 65%, 5% and 7.5% in BI-RADS II, III, IVa and IVc, respectively. However, 2.5% discordant BI-RADS categories assessment was shown in this study; interpreted as BI-RADS II and IVa that the pathologic result was invasive ductal carcinoma grade 1 (Table 1).

Table 1. *Comparison of BI-RADS categories assigned by 1st and 2nd radiologist for ABUS.*

			1st Radiologist						
			BI-RADS						
			I	II	III	IVa	IVb	IVc	V
2nd Radiologist	BI-RADS	I	0	0	0	0	0	0	0
		II	0	1 (2.5%)	0	1 (2.5%)	0	0	0
		III	0	0	26 (65%)	4 (10%)	0	0	0
		IVa	0	0	2 (5%)	2 (5%)	1 (2.5%)	0	0
		IVb	0	0	0	0	0	0	0
		IVc	0	0	0	0	0	3 (7.5%)	0
		V	0	0	0	0	0	0	0

A comparison of BI-RADS categories interpretation by two radiologists between ABUS and HHUS significantly reported reliability (Table 2). The pathologic results showed mostly benign such as fibroadenoma (Figure 1), intraductal papilloma, and stromal fibrosis; however, it had one malignancy as ductal carcinoma in situ (DCIS) high grade (Figure 2).

THE ASEAN JOURNAL OF RADIOLOGY
ISSN 2672-9393

Table 2. *Comparison of BI-RADS categories assigned by 1st and 2nd radiologist between ABUS and HHUS with the pathologic result.*

		1st Radiologist		2nd Radiologist		Mean	
		ABUS (n)	HHUS (n)	ABUS (n)	HHUS (n)	ABUS	HHUS
BI-RADS	I	0	0	0	0	0	0
	II	1	1	0	0	0.5	0.5
	III	21	20	20	20	20.5	20
	IVa	3	4	4	4	3.5	4
	IVb	0	0	0	0	0	0
	IVc	0	0	1	1	0.5	0.5
	V	0	0	0	0	0	0
Total		25	25	25	25	25	25
Pathologic result		- 4 masses with BI-RADS IVa are 2 fibroadenomas, 1 Intraductal papilloma and 1 stromal fibrosis		- 4 masses with BI-RADS IVa are fibroadenomas - 1 mass with BI-RADS IVc is DCIS high grade		-	

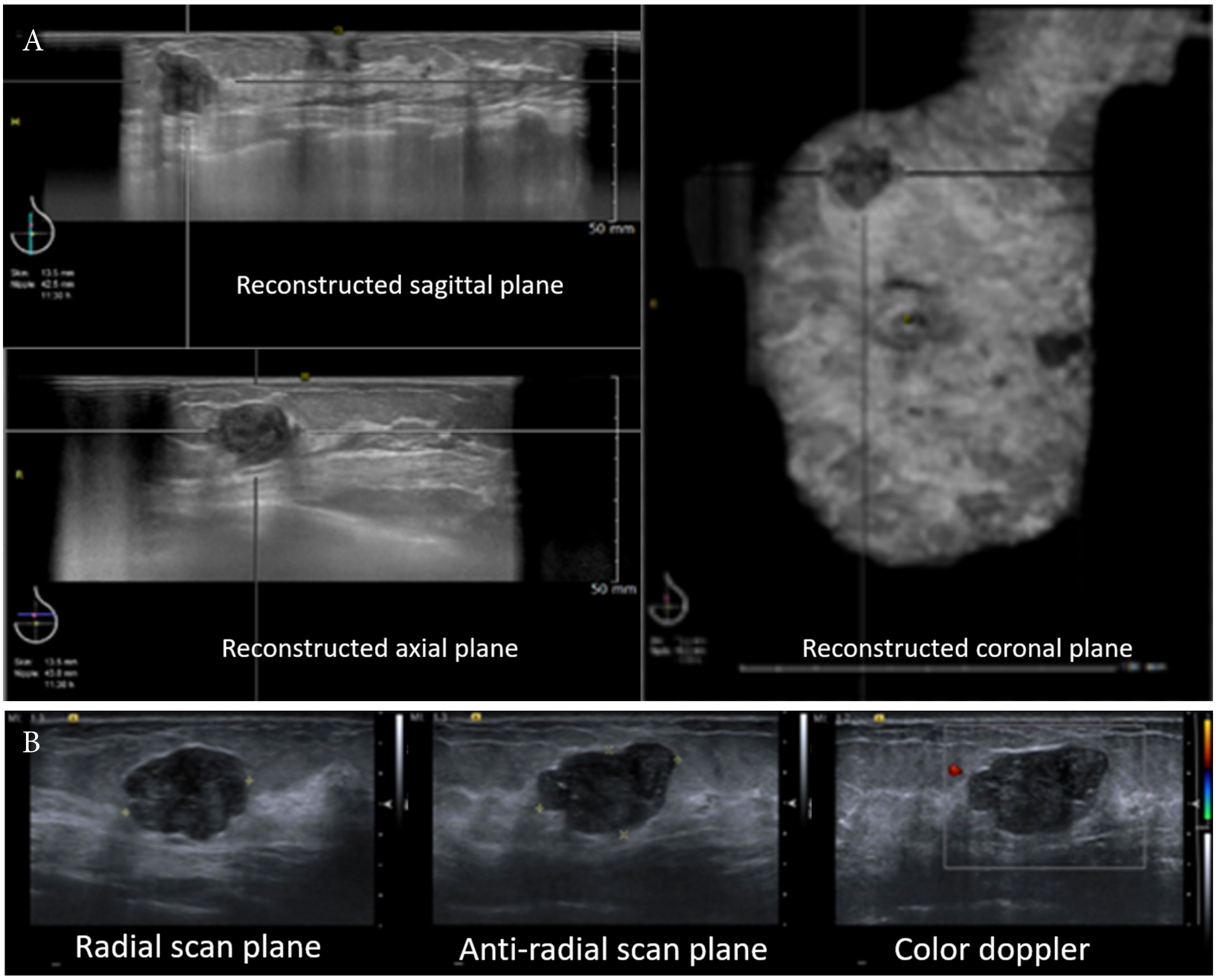

Figure 1. *Ultrasound findings in ABUS (A) and HHUS (B) showed an oval, microlobulated, heterogeneous hypoechoic mass with parallel orientation and enhancement of the posterior feature at 11-12 o'clock of the left breast. There was no vascularity. (BI-RADS IVa) The pathologic result was fibroadenoma at the left breast.*

THE ASEAN JOURNAL OF RADIOLOGY
ISSN 2672-9393

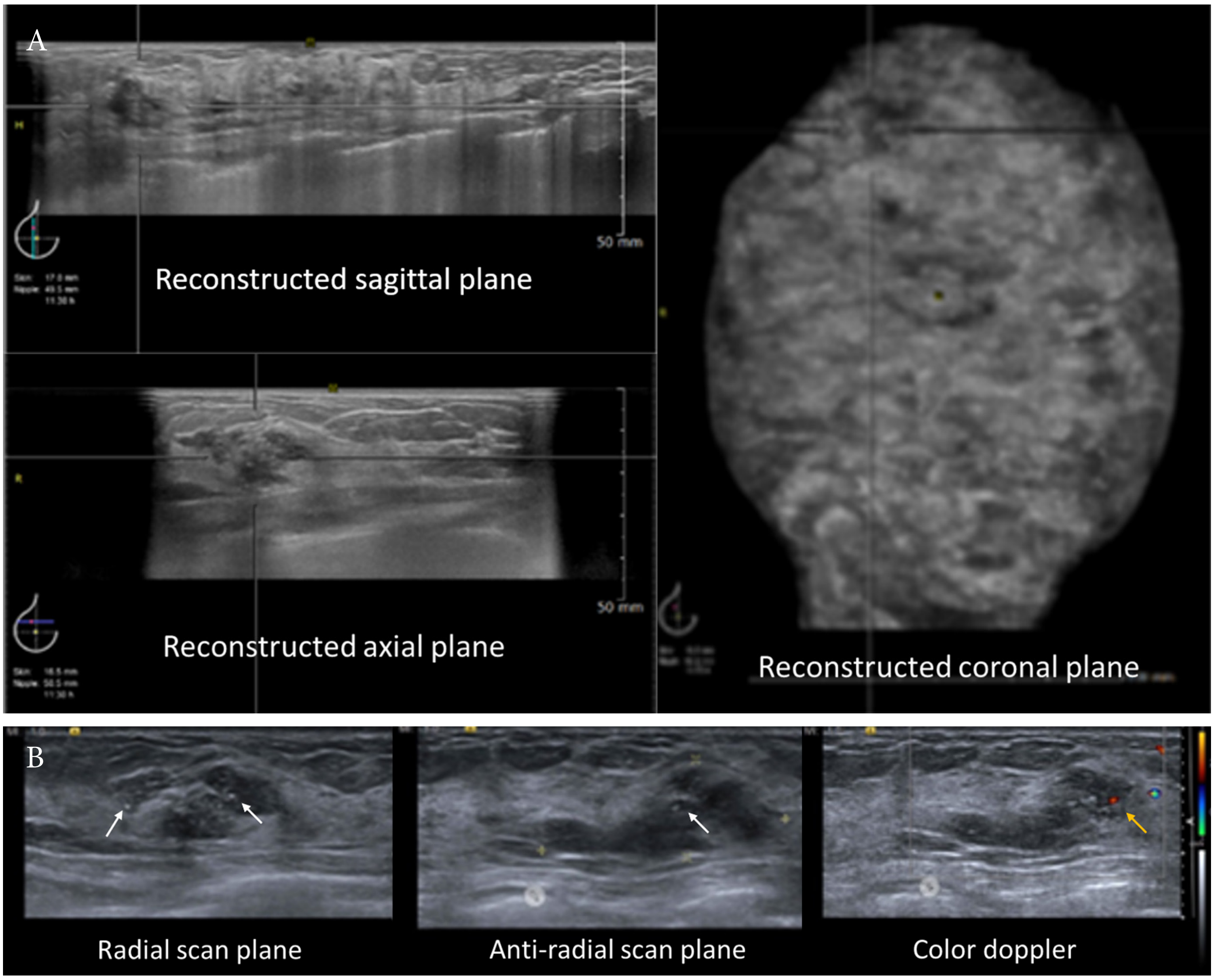

Figure 2. *Ultrasound findings in ABUS (A) and HHUS (B) showed an irregular, indistinct, hypoechoic mass with parallel orientation, the combined pattern of posterior features and internal calcification at 11-12 o'clock of the right breast (White arrow). Internal vascularity was seen at the medial portion of the mass (Yellow arrow). (BI-RADS IVc) The pathologic result was high-grade ductal carcinoma in situ (DCIS).*

Discussion

Unlike other breast imaging techniques, breast ultrasound is affected by a lack of reproducibility in lesion characterization. Also, the document data is not consistent and reproducible. ABUS has the potential for complete and standardized documentation which has several advantages over HHUS. As a matter of fact, there are a number of interesting studies showing equal efficacy between ABUS and HHUS [22-25, 29-31], but those studies were done in people with the diagnostic groups, differently from this study which was in a screening situation to assess the reliability of ABUS compared with HHUS for lesion detection, description, and interpretation, that may be useful to allow delayed interpretation both inside and outside the workplace.

Consistent reporting with reproducible localization of detected breast lesions is critical for the clinical application of ABUS. We found ICCs for the lesion localization (clock face location, distance from nipple, deep from skin) were 0.9, 0.82, and 0.8, indicating excellent and good reliability, respectively. The individual size of detected lesions (wide, long and height) was 0.89, 0.81, and 0.87, indicating good reliability. This information is consistent with previous reports in Chang et al and Shin et al, except for skin depth locations, in which our study was more reliable [21,23].

Practicable reasons for the higher rate of reliability when using ABUS could be due to readers being able to reproduce whole breast scans in multiple orientations, selecting the longest dimension plane, and measure the size, by using the 3D volume data. The reader can link the image to the coronal scan plane performed using ABUS and provide a center of the lesion to access the distance from the nipple and the depth from the skin and the workstation also has the software to help us measure automatically. Therefore, in the follow-up of multiple benign lesions or probably benign lesions in people with dense breasts and still requiring a mammogram every year, changes in size can be monitored, precisely. ABUS is also important for education hospitals where different inexperienced radiologists may perform each examination. On the other hand, like any imaging technique, ABUS has disadvantages and some limitations. Disadvantages regarding image acquisition are the inability to assess the axilla, the vascularization, and the elasticity of a lesion while concerning the interpretation, the disadvantages are the artifacts due to poor positioning, a lack of contact, a motion, or lesion related factors. Therefore, the technician should be aware of these aspects and scan the entire breast by obtaining supplemental acquisitions on the superior and inferior parts of the breasts. Furthermore, suspicious lesions detected with ABUS and requiring further assessment need to be reevaluated with HHUS.

The result of this study about the characteristic visibility of the breast lesions using ABUS almost resembles other studies such as Zhang et al, Shin et al, and Kim et al, in some aspects [23,25,31] (Table 3).

Table 3. *Compared results of localization, size, and characteristics of lesions between our study and other studies.*

Variable	This study	Chang et al.	Zhang et al.	Shin et al.	Kim et al.
Location (ICC)	Excellent (0.90)	Excellent (0.99)	-	Good (0.75)	Substantial (κ= 0.74)
Distance from nipple (ICC)	Good (0.82)	Excellent (0.93)	-	Good (0.89)	-
Deep from skin (ICC)	Good (0.80)	Fair (0.34)	-	Good (0.89)	-
Size(W-L-H) (ICC)	Good (0.89-0.81-0.87)	Excellent (0.98)	-	Excellent (0.94)	Moderate (κ =0.43)
Shape (κ)	Moderate (0.48)	-	Substantial (0.79)	Substantial (0.71)	Moderate (0.45)
Orientation(κ)	95% agreement	-	Substantial (0.74)	Substantial (0.72)	Moderate (0.50)
Margin(κ)	Substantial (0.78)	-	Substantial (0.76)	Substantial (0.61)	Fair (0.25)
Echo pattern(κ)	Fair (0.31)	-	Substantial (0.69)	Moderate (0.45)	Substantial (0.65)
Posterior feature(κ)	Fair (0.36)	-	Substantial (0.68)	Moderate (0.42)	Moderate (0.45)
BI-RADS (κ)	Almost perfect (0.82)	-	Substantial (0.70)	Substantial (0.63)	Substantial (0.57)

We found substantial agreement on the description of the margin (κ=0.78), moderate agreement on the description of the shape (κ=0.48), and fair agreement on the description on mass echogenicity, and posterior acoustic features (κ= 0.31 and κ= 0.36, respectively). Anywise, this study shows 95% agreement instead of Cohen's kappa value to assess the concordance of orientation due to statistic κ cannot be assessed because of no variation from most of the lesions in screening situation which were horizontal appearing masses and our study already proved concordance agreement between the percent agreement and the Cohen's kappa statistics (Table 1). Prominently, almost perfect agreement was found in BI-RADS assessment in this study (κ= 0.82), distinguished from previous studies.

Based on the data obtained from this research together with the facts supported by other studies, this makes us certain that ABUS can be used to detect new lesions, monitor identified known lesions, localization, description, and interpretation.

However, in our study, one radiologist missed one lesion from ABUS image (Figure 3) that was malignancy from the pathologic result (invasive ductal carcinoma grade 1). Also, this lesion was a subareolar region which is a limit position for the lesion detection of ABUS.

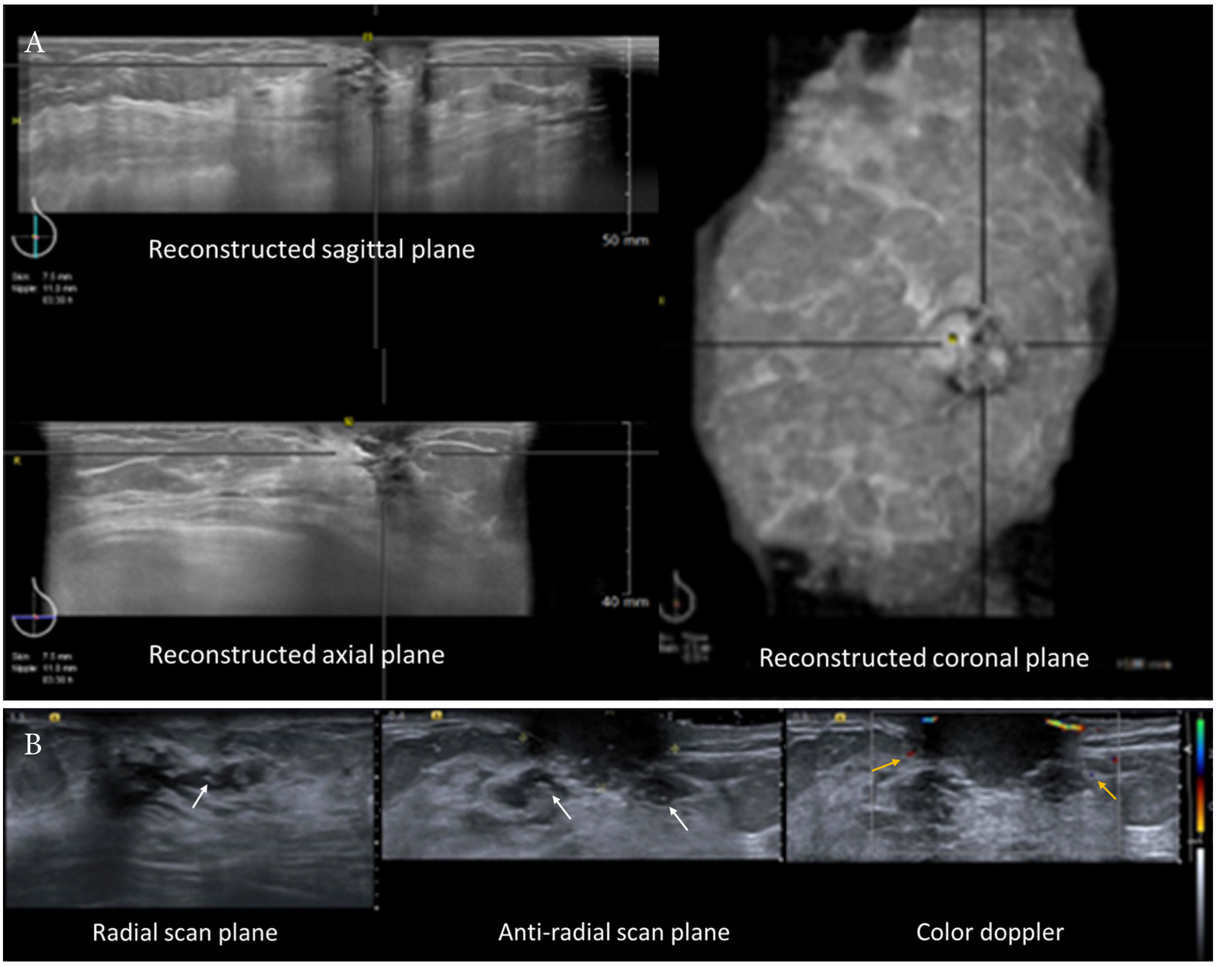

Figure 3. *Ultrasound findings in ABUS (A) and HHUS (B) showed an irregular, indistinct, hypoechoic mass with parallel orientation, the enhancement pattern of posterior features and internal calcification at 3-4 o'clock at the subareolar region (White arrow). Adjacent subareolar duct dilatation with internal echogenic content and calcification was noted. Vascularity was seen as a vessel in the rim (Yellow arrow). (BI-RADS IVc) The pathologic result was invasive ductal carcinoma grade 1 (IDC).*

In daily practice, ABUS may have more benefits than HHUS in several respects. First, patients with multiple lesions might benefit from the faster examination time. Second, for patients with dense breast tissue, additional screening ABUS may be beneficial because of improved workflow efficiency and a lack of operator dependence. Third, to monitor the previously detected lesion might be standard and reproducible. Last, for surgical planning, surgeons who are familiar with the coronal plane may appreciate the multiplanar images obtained with ABUS.

Our study had some limitations. First, the readers were blinded to the mammographic and clinical findings, and BI-RADS categorization established only with the ultrasound features does not always reflect actual practice. Second, our study included a relatively small number of patients with malignancy, so the mass characteristics were more similar, for example, the oval mass-shaped and parallel orientation of mass which represent mostly benign lesions. Moreover, the number of associated features, such as calcification, architectural distortion, skin, or duct change as well as special finding, for example, lymph node, cluster microcyst, vascularity abnormalities or fat necrosis, were too small sample size for available interpretation. Third, our study was a retrospective study; thus, some data were incomplete. Fourth, our study including only two radiologists was small to assess the reliability agreement. A further evaluation of the interobserver agreement among multiple radiologists is needed.

Conclusion

ABUS is a useful tool for detecting lesions and providing accurate information on their locations, sizes, and key characteristics, making it ideal for screening breast lesions and monitoring any detected lesions although ABUS may have limitations related to the technique, for example, air interposition or insufficient compression which can be effectively managed with extensive training and attention to image acquisition and interpretation.

References

1. Cancer Prevention and Control. Centers for Disease Control and Prevention Division. Breast cancer statistic [Internet]. 2023 Jun 8 [cited 2023 Oct 7]. Available from: https://www.cdc.gov/cancer/breast/statistics/

2. Virani S, Bilheem S, Chansaard W, Chitapanarux I, Daoprasert K, Khuanchana S, et al. National and subnational population-based incidence of cancer in Thailand: assessing cancers with the highest burdens. Cancers (Basel) 2017;9:108. doi: 10.3390/cancers9080108.

3. Tabár L, Fagerberg CJ, Gad A, Baldetorp L, Holmberg LH, Gröntoft O, et al. Reduction in mortality from breast cancer after mass screening with mammography. Randomised trial from the Breast Cancer Screening Working Group of the Swedish National Board of Health and Welfare. Lancet 1985;1: 829-32. doi: 10.1016/s0140-6736(85)92204-4.

4. Shapiro S, Venet W, Strax P, Venet L, Roeser R. Ten- to fourteen-year effect of screening on breast cancer mortality. J Natl Cancer Inst 1982;69:349-55.

5. Kolb TM, Lichy J, Newhouse JH. Comparison of the performance of screening mammography, physical examination, and breast US and evaluation of factors that influence them: an analysis of 27,825 patient evaluations. Radiology 2002;225:165-75. doi: 10.1148/radiol.2251011667.

6. D'orsi CJ, Sickles EA, Mendelson EB, Morris EA, editors. ACR BI-RADS atlas: breast imaging reporting and data system; mammography, ultrasound, magnetic resonance imaging, follow-up and outcome monitoring, data dictionary. 5 th ed. Reston (FL) : ACR American College of Radiology; 2013.

7. Winkler NS, Raza S, Mackesy M, Birdwell RL. Breast density: clinical implications and assessment methods. Radiographics 2015;35:316-24. doi: 10.1148/rg.352140134.

8. Kolb TM, Lichy J, Newhouse JH. Occult cancer in women with dense breasts: detection with screening US--diagnostic yield and tumor characteristics. Radiology 1998;207:191-9. doi: 10.1148/radiology.207.1.9530316.

9. Berg WA, Gilbreath PL. Multicentric and multifocal cancer: whole-breast US in preoperative evaluation. Radiology 2000;214:59-66. doi: 10.1148/radiology.214.1. r00ja2559.

10. Buchberger W, DeKoekkoek-Doll P, Springer P, Obrist P, Dünser M. Incidental findings on sonography of the breast: clinical significance and diagnostic workup. AJR Am J Roentgenol 1999;173:921-7. doi: 10.2214/ajr.173.4.10511149.

11. Gordon PB, Goldenberg SL. Malignant breast masses detected only by ultrasound. A retrospective review. Cancer 1995;76:626-30. doi: 10.1002/1097-0142(19950815)76:4<626: aid-cncr2820760413>3.0.co;2-z.

12. Nazari SS, Mukherjee P. An overview of mammographic density and its association with breast cancer. Breast Cancer 2018;25:259-67. doi: 10.1007/s12282-018-0857-5.

13. Park B, Cho HM, Lee EH, Song S, Suh M, Choi KS, et al. Does breast density measured through population-based screening independently increase breast cancer risk in Asian females? Clin Epidemiol 2017; 10:61-70. doi: 10.2147/CLEP.S144918.

14. Berg WA, Blume JD, Cormack JB, Mendelson EB, Lehrer D, Böhm-Vélez M, et al. Combined screening with ultrasound and mammography vs mammography alone in women at elevated risk of breast cancer. JAMA 2008;299:2151-63. doi: 10.1001/jama.299.18.2151.

15. Kaplan SS. Automated whole breast ultrasound. Radiol Clin North Am 2014; 52:539-46. doi: 10.1016/j.rcl.2014.01.002.

16. Brem RF, Rapelyea JA, Torrente J, Kann M, Coffey C, Lieberman J, et al. Interpretation time of 3D automated breast ultrasound (AWUS). AJR Am J Roentgenol [Internet]. 2012 May [cited 2023 Oct 7]. Available from: https://www.researchgate.net/publication/296032869_Interpretation_Time_of_3D_Automated_Breast_Ultrasound.

17. Kelly KM, Dean J, Comulada WS, Lee SJ. Breast cancer detection using automated whole breast ultrasound and mammography in radiographically dense breasts. Eur Radiol 2010;20:734-42. doi: 10.1007/s00330-009-1588-y.

18. Kelly KM, Dean J, Lee SJ, Comulada WS. Breast cancer detection: radiologists' performance using mammography with and without automated whole-breast ultrasound. Eur Radiol 2010;20:2557-64. doi: 10.1007/s00330-010-1844-1.

19. Brem RF, Tabár L, Duffy SW, Inciardi MF, Guingrich JA, Hashimoto BE, et al. Assessing improvement in detection of breast cancer with three-dimensional automated breast US in women with dense breast tissue: the SomoInsight Study. Radiology 2015;274:663-73. doi: 10.1148/radiol.14132832.

20. Giger ML, Miller DP, Brown JB, Inciardi MF, Metz CE, Jiang Y, et al. Clinical reader study examining the performance of mammography and automatic breast ultrasound in breast cancer screening. Radiological Society of North America 2012 Scientific Assembly and Annual Meeting, November 25 - November 30, 2012, Chicago IL. [Internet] 2012 [cited 2023 Oct 7] Available from: http://archive.rsna.org/2012/12029472.html

21. Chang JM, Cha JH, Park JS, Kim SJ, Moon WK. Automated breast ultrasound system (ABUS): reproducibility of mass localization, size measurement, and characterization on serial examinations. Acta Radiol 2015;56:1163-70. doi: 10.1177/0284185114551565.

22. Kuzmiak CM, Ko EY, Tuttle LA, Steed D, Zeng D, Yoon SC. Whole breast ultrasound: comparison of the visibility of suspicious lesions with automated breast volumetric scanning versus hand-held breast ultrasound. Acad Radiol 2015;22:870-9. doi: 10.1016/j.acra.2015.03.006.

23. Shin HJ, Kim HH, Cha JH, Park JH, Lee KE, Kim JH. Automated ultrasound of the breast for diagnosis: interobserver agreement on lesion detection and characterization. AJR Am J Roentgenol 2011;197(:747-54. doi: 10.2214/AJR.10.5841.

24. An YY, Kim SH, Kang BJ. The image quality and lesion characterization of breast using automated whole-breast ultrasound: A comparison with handheld ultrasound. Eur J Radiol 2015;84:1232-5. doi: 10.1016/j.ejrad.2015.04.007.

25. Kim SH, Kang BJ, Choi BG, Choi JJ, Lee JH, Song BJ, et al. Radiologists' performance for detecting lesions and the interobserver variability of automated whole breast ultrasound. Korean J Radiol 2013;14:154-63. doi: 10.3348/kjr.2013.14.2.154.

26. Hellgren R, Dickman P, Leifland K, Saracco A, Hall P, Celebioglu F. Comparison of handheld ultrasound and automated breast ultrasound in women recalled after mammography screening. Acta Radiol 2017;58:515-20. doi: 10.1177/0284185116665421.

27. Koo TK, Li MY. A Guideline of selecting and reporting intraclass correlation coefficients for reliability research. J Chiropr Med 2016;15:155-63. doi: 10.1016/j.jcm.2016.02.012.

28. Landis JR, Koch GG. The measurement of observer agreement for categorical data. Biometrics 1977;33:159-74.

29. Bassett LW. Imaging of breast masses. Radiol Clin North Am 2000;38:669-91, vii-viii. doi: 10.1016/s0033-8389(05)70193-7.

30. Wenkel E, Heckmann M, Heinrich M, Schwab SA, Uder M, Schulz-Wendtland R, et al. Automated breast ultrasound: lesion detection and BI-RADS classification --a pilot study. Rofo 2008;180:804-8. doi: 10.1055/s-2008-1027563.

31. Zhang J, Lai XJ, Zhu QL, Wang HY, Jiang YX, Liu H, et al. Interobserver agreement for sonograms of breast lesions obtained by an automated breast volume scanner. Eur J Radiol 2012;81:2179-83. doi: 10.1016/j.ejrad.2011.06.043.

Original Article

Ultrasound-guided percutaneous nephrostomy: Analysis of early complications in a prospective descriptive cross-sectional study at a tertiary care center

Bishnu Pandey, M.D.[1]
Shailendra Katwal, M.D.[2]
Sushmita Bhandari, M.B.B.S.[3]
Mukhtar Alam Ansari, Ph.D.[4]
From [1] Department of Radiology, TUTH, Institute of Medicine, Kathmandu, Nepal.
[2] Department of Radiology, Dadeldhura Subregional Hospital, Dadeldhura, Nepal.
[3] Shankar nagar health post, Butwol, Nepal.
[4] Department of Radiology, National Medical college, Birgunj, Nepal.
Address correspondence to S.K.(e-mail: shailendrakatwal@gmail.com)

Received 12 June 2023; revised 20 August 2023; accepted 25 September 2023
doi:10.46475/asean-jr.v24i3.866

Abstract

Background: Percutaneous nephrostomy (PCN) is a crucial intervention for urinary obstruction. Understanding indications, complications, and materials used enhances its clinical application.

Objective: This study aims to identify PCN indications, assess tube types/materials, evaluate early complications, and determine PCN success rates, fostering improved outcomes and procedural refinement.

Materials and Methods: This study was carried out in the interventional radiology suite of the Department of Radiodiagnosis and Imaging, Tribhuvan University Teaching Hospital (TUTH) on 74 patients for one year. Patients of all age groups who underwent PCN were included in the study. Indications for PCN were identified before the procedure using various imaging modalities like Ultrasonography (USG), Computed Tomography (CT) scan, and more. The type of approach, calyx punctured, the size of the tube chosen, and the type of the drain material were all recorded during the procedure or in the post-procedure note. The patients were evaluated daily, and USG was done in every patient after 48 hours of the procedure to evaluate in terms of any complications.

Results: Ninety-eight PCNs were done on 74 patients, of whom 58 were males and 40 were females. The main reasons for PCN were calculus disease with hydronephrosis (44.9%), calculus disease with pyonephrosis (22.4%), and obstructive uropathy due to bladder or cervix carcinoma. The success rate for PCN on the first attempt was 89.8%, while 6.1% required two attempts and 4.1% needed more than two attempts. Complications included tube dislodgement (8.2%), urinoma (5.1%), major bleeding (3%), and retroperitoneal hematoma (1%). No new cases of sepsis occurred post-procedure.

Conclusion: Percutaneous nephrostomy is a safe and simple procedure with low morbidity and no life-threatening complications.

Keywords: Early complications, Obstructive uropathy, Percutaneous nephrostomy, Ultrasonography.

Introduction

Percutaneous nephrostomy (PCN) is an interventional procedure used to relieve obstruction in the urinary collecting system when natural drainage or surgical nephrostomy is not feasible. PCN was first performed in 1955 for draining hydronephrotic kidneys [1]. The advantages of percutaneous insertion under local anesthesia include quick recovery and early discharge without general anesthesia-related complications. The imaging modalities commonly used for the localization of the pelvicalyceal system are ultrasound and fluoroscopy. Sometimes CT scan may be required in case of emphysematous pyelonephritis where the visualization of the pelvicalyceal system is difficult because the air obscures its visualization. Magnetic resonance imaging (MRI) presents an appealing option for guiding percutaneous procedures, such as percutaneous nephrostomy (PCN), due to its radiation-free nature and the ability to provide high-resolution and multiplanar visualization [2,3]. PCN is crucial in patients with pyonephrosis, allowing urinary tract decompression and direct sampling of urine for culture and sensitivity to initiate appropriate antibiotic treatment. In cases of ureteral obstruction caused by stones, PCN provides immediate decompression, protects renal function, and allows elective management of the underlying cause [4,5]. Prolonged obstruction with infection can lead to progressive damage to the nephrons [6].

PCN may have a higher success rate than retrograde double J ureteral stenting in patients with malignancy, especially when there is an extrinsic compression [7]. Decompressing the renal pelvicalyceal system improves the renal function in pelvic malignancies [8].

This procedure is also valuable for evaluating the functional reserve of hydronephrotic kidneys in benign conditions and is the preferred procedure for temporary urinary tract drainage in both adults and children. It is often sufficient for healing post-surgical leaks.

Under local anesthesia, PCN is a feasible life-saving procedure for critically ill patients who cannot undergo general anesthesia due to various conditions. It also serves as an entry point for other interventional uro-radiological and endo-urological procedures [1].

Major contraindications to PCN include uncorrected coagulopathy and uncooperative patients. Severe hyperkalemia(>7mEq/L) can be managed with dialysis before the procedure [1].

However, complications can still occur following this seemingly simple intervention. Early complications of PCN, occurring immediately or within 48 hours, include bleeding, infection, retroperitoneal hematoma, extravasation, urinoma, and perforation of adjacent viscera. Tube dislodgement and blockage, typically considered late complications, can also occur within 24 hours.

A comprehensive assessment is required to determine the incidence of various early complications linked with diverse PCN approaches and drainage materials within the Nepalese population. There's also a lack of holistic evaluation regarding the success rate of PCN, insights into optimal procedural techniques and material selection, as well as a complete understanding of image-guided PCN.

Our study aims to investigate image-guided percutaneous nephrostomy (PCN), encompassing common indications, procedural techniques, and the incidence of early complications. Additionally, the research seeks to evaluate the overall success rate of PCN procedures. Through these objectives, a more comprehensive understanding of image-guided PCN is aimed to be achieved.

Materials and methods

Study design and target population

This descriptive prospective cross-sectional study was carried out in the interventional radiology suite of the Department of Radiodiagnosis and Imaging, Tribhuvan University Teaching Hospital (TUTH) for one year. Ethical approval was obtained from the Institutional Review Committee. Consent was taken from each participant.

The study included all patients who underwent PCN in the department, totaling 98 procedures in 74 patients. Inclusion criteria were patients of all ages and genders who underwent PCN and gave consent for the study, while those who did not give consent or attend follow-up sessions were excluded.

Methodology and data collection

Patients were informed about the purpose of the procedure, anesthesia options, potential complications, and benefits compared to other surgeries. Platelets and coagulation were checked and corrected if abnormal. Urine analysis was checked for infection. Intravenous antibiotics were initiated based on a positive urine analysis. Imaging via ultrasound or fluoroscopy localized the pelvicalyceal system. Patients were positioned and secured, and the puncture site was marked using ultrasound. Local anesthetics were used, with sedation if needed. Infants received general anesthesia.

The marked site was incised, and an 18-gauge Chiba needle punctured the selected calyx under ultrasound. Contrast and a guidewire were introduced. Serial dilators expanded the tract, using 8-10 F catheters for non-infected drainage. A contrast check ensured proper catheter placement. Sutures secured the catheter, connected to a collection bag for gravity drainage.

Data on indications, drain tube size, material drained, and intra-procedural complications were recorded from the procedure note. Common complications

THE ASEAN JOURNAL OF RADIOLOGY
ISSN 2672-9393

included bleeding, subcapsular hematoma, sepsis, vessel and bowel injury, urinoma formation, tube dislodgement, and unsuccessful drainage. Major bleeding requiring intervention was documented, while minor bleeding and hematuria were not.

Sepsis was defined based on specific Severe Inflammatory Response Syndrome (SIRS) criteria with documented infection [9].

Vessel and bowel punctures occurred when contrast entered these structures. The procedure was considered unsuccessful if no urine was drained despite pelvicalyceal system dilatation. The success rate was determined based on the number of attempts in the study.

Definition

Technical success of percutaneous nephrostomy refers to ensuring effective urinary drainage, extracting stone or ureteral stent placement with a catheter of a suitable diameter and route. The success rate should involve the consideration of the number of kidneys treated and the number of patients undergoing treatment [10].

Minor and Major complications: Complications were classified by the guidelines set forth by the Society of Interventional Radiology (SIR) [11].

Minor complications include:

(A) cases without the need for therapy or resulting consequences,
(B) cases requiring only nominal therapy with no subsequent consequences.

Major complications include:

(C) complications necessitating therapy and resulting in brief hospitalization (<48 hours),
(D) requiring significant therapy and associated with an unplanned escalation in the level of care, extended hospitalization (>48 hours),
(E) leading to permanent adverse effects,
(F) ultimately resulting in death.

Results

The study included 74 patients who underwent a total of 98 PCNs for various indications. The age of the patients ranged from 1 month to 80 years, categorized into age groups: 0-10 years, 10-40 years, and >40 years. The highest number of patients was in the ≥40 years age group (69.4%). All the PCN cases were carried out with a pigtail catheter.

Calculus disease accounted for over 50% of the PCNs performed (44 PCN for hydronephrosis and 22 for pyonephrosis), followed by malignant etiology, ureteric stricture, PUJ stenosis, and posterior urethral valves. Most PCNs (58) were performed in the right kidney, with one case involving a grafted kidney located in the right iliac fossa.

In our study, the posterolateral approach was the most commonly used for PCN insertion (93.9%), followed by the posterior approach (5.1%). An anterior approach was used in a single case involving a grafted kidney. The interpolar region was punctured in nearly two-thirds of PCNs, while the upper pole calyx was chosen only for the grafted kidney. The majority of drained kidneys had an 8F tube, and turbid material was obtained in 60% of PCNs, with clear fluid obtained in the remaining 40%.

Complications associated with PCN are listed below:

- Tube dislodgement,
- Sepsis,
- Urinoma,
- Major bleeding,
- Retroperitoneal hematoma,
- Injury to vessels,
- Injury to viscera,
- Cardiac arrest,
- Pneumothorax.

THE ASEAN JOURNAL OF RADIOLOGY
ISSN 2672-9393

Tube dislodgement was the most common complication. Major bleeding as a complication was seen but none required embolization or blood transfusion. Perinephric urinoma was also noted; however, none of the patients developed cardiac arrest, pneumothorax, or hydrothorax (Figure 1).

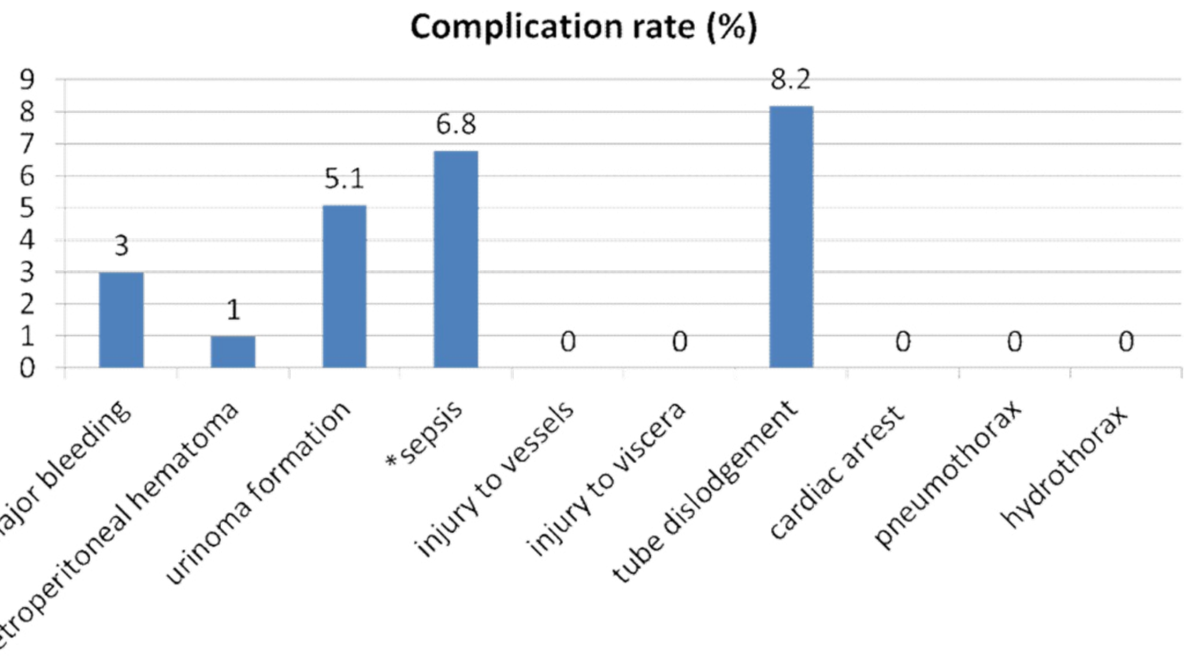

Figure 1. *Complication rate as per the number of PCN performed.*

*The number and percentage calculated in sepsis as a complication was based on the number of patients, unlike other complication rates which were calculated based on the number of PCNs done.

The success rate of PCN in our department was 100% despite the number of attempts. Nearly 90% of PCNs were successful in the first attempt, while approximately 6% of PCNs required two attempts for successful insertion of the PCN tube.

Discussion

PCN as a urinary diversion procedure is relatively safe and effective and can be performed under local anesthesia. PCN is a commonly performed procedure to preserve the renal function in any case with post-renal obstruction.

In a study (n=300) conducted by Ali et al, the commonest cause for PCN was obstructive uropathy due to stone diseases either in the kidney or in the ureter which accounted for 77.3% of patients. Malignancy was the second largest group with 13.3% of patients having carcinoma of the urinary bladder and 4.0% having carcinoma of the cervix, rectum, prostate, abdominal lymphoma, and retroperitoneal fibrosis. In 4.33% of patients, upper urinary tract obstruction was seen, of which 3.33% patients were due to ureteric stricture and 1% was due to accidental ligation of the ureter during an obstetric surgery [12]. Similar to this study, our study also showed the commonest (67.3%) indication for PCN to be obstruction due to the calculus disease. Although malignancy was also the second most common (23.5%) reason for PCN in our study, only carcinoma bladder (13.3%) and carcinoma cervix (10.2%) were seen. Other indications were PUJ stenosis (3.1%), ureteric stricture (4.1%), and posterior urethral valve (2%).

The success rate of PCN in many previous studies was found to be between 84 to 100% [13-15]. In our study, the success rate was calculated as per the number of attempts made because all the patients who had PCN attempts ultimately became successful despite the number of attempts. Therefore, the ultimate success rate came out to be 100%. However, only 89.8% of PCNs were successful in the first attempt.

In a study conducted by E. Radecka and A. Magnusson (n=401), in 569 PCN performed, the early major complications (within 2 days) were cardiac arrest (0.24%), major bleeding requiring transfusion (0.24%), hydrothorax (0.24%), and urosepsis (0.5%) [14]. In the study conducted by Ali et al (n=300), early complications comprised sepsis (2%), retroperitoneal hematoma (1.6%), hematuria (0.6%), and urinoma (0.3%). Total early complications were noted in 4.66% of patients, while late complications were noted in 7.33% of patients. The low incidence of complications observed in this study shows that PCN is a safe technique with low morbidity and no major life-threatening complications [12]. In a study performed by Farrel et al (n=303), major bleeding requiring transfusion was seen in 2.8% [4]. In a study conducted by Lee et al (n=160), the complications seen were sepsis (6%), hematuria requiring blood transfusion (2.4%), catheter displacement or mal-position (4.8%), pelvic perforation (4.3%), paralytic ileus (2.4%), pneumonia/atelectasis (1.8%) and pleural effusion (1.2%). The overall complication rate was 34%, of which 6% were major and 28% were minor [13]. In our study, none of the patients developed cardiac arrest. Pneumothorax or hydrothorax was not seen in our study probably because none of the native kidneys were punctured via the upper pole calyx as puncturing the upper pole calyx increases the chances of traversing the pleura compared to puncturing the interpolar region or lower pole calyx [16]. In our study, major bleeding was seen in 3% of the PCNs performed which were managed by providing a tamponade effect in the form of clamping of the catheter for 24 hours and none of them required blood transfusion or embolization of the bleeding vessel.

Tube dislodgement in our study came out to be the most common complication probably because of mishandling of the tube while flushing the tube or during tube site dressing. Besides, the higher rate of tube dislodgement could be due to the insertion of a PCN tube even in kidneys with thinned-out renal parenchyma which cannot provide an adequate anchoring effect to the tube. Moreover, PCNs were performed in kidneys with large sialolithiasis in which the PCN tube was placed in the calyx rather than in the renal pelvis preventing adequate coiling of the tube and resulting in the easy displacement of the tube. These may be the reasons for tube dislodgement to be the commonest complication. A retrospective study conducted by Bayne et al in 475 PCNL cases showed the BMI of the patient is a major determinant of tube dislodgement instead of the tube properties [17].

Perinephric urinoma formation was seen in 5.1% of PCNs performed which were all seen in difficult cases necessitating multiple punctures for successful insertion of the tube creating the tract between the pelvicalyceal system and the perinephric space resulting in urinary leakage into the perinephric space.

This study includes single-center nature, a relatively small sample size, and a short duration, which might restrict the extrapolation of findings to larger and more diverse populations. Additionally, the study's reliance on participant consent and follow-up attendance could introduce selection bias, and the exclusion of certain complications like minor bleeding, and hematuria might lead to an incomplete understanding of the overall procedure-related outcomes. Future research should encompass multi-center collaboration, larger sample sizes, longer study durations, and comprehensive complication assessment to enhance validity.

Conclusion

This study on percutaneous nephrostomy (PCN) assessed its effectiveness, complications, and success rates. Conducted over a year at a teaching hospital, the study reported a 100% success rate, with 90% achieving success on the first attempt. Major complications were infrequent, including manageable cases of tube dislodgement and perinephric urinoma formation. These findings underscore PCN's feasibility and safety for urinary obstruction management, aiding future patient care enhancements.

References

1. Young M, Leslie SW. Percutaneous Nephrostomy. [Updated 2023 June 26]. In: StatPearls [Internet]. Treasure Island (FL): StatPearls Publishing; 2023 Jan- [cited 2023 Aug 13]. Available from: http://www.ncbi.nlm.nih.gov/books/NBK493205/

2. Egilmez H, Oztoprak I, Atalar M, Cetin A, Gumus C, Gultekin Y, et al. The place of computed tomography as a guidance modality in percutaneous nephrostomy: analysis of a 10-year single-center experience. Acta Radiol 2007;48:806–13. doi: 10.1080/02841850701416528.

3. Kariniemi J, Sequeiros RB, Ojala R, Tervonen O. MRI-guided percutaneous nephrostomy: a feasibility study. Eur Radiol 2009;19:1296–301. doi: 10.1007/s00330-008-1235-z.

4. Farrell TA, Hicks ME. A review of radiologically guided percutaneous nephrostomies in 303 patients. J Vasc Interv Radiol 1997;8:769–74. doi: 10.1016/s1051-0443(97)70658-4.

5. Joshi HB, Adams S, Obadeyi OO, Rao PN. Nephrostomy tube or "JJ" ureteric stent in ureteric obstruction: assessment of patient perspectives using quality-of-life survey and utility analysis. Eur Urol 2001;39:695–701. doi: 10.1159/000052529.

6. Chung SY, Stein RJ, Landsittel D, Davies BJ, Cuellar DC, Hrebinko RL, et al. 15-year experience with the management of extrinsic ureteral obstruction with indwelling ureteral stents. J Urol 2004;172:592–5. doi: 10.1097/01.ju.0000130510.28768.f5.

7. Kraemer PC, Borre M. [Relief of upper urinary tract obstruction in patients with cancer of the prostate]. Ugeskr Laeger 2009;171:873–6. Danish.

8. Aravantinos E, Anagnostou T, Karatzas AD, Papakonstantinou W, Samarinas M, Melekos MD. Percutaneous nephrostomy in patients with tumors of advanced stage: treatment dilemmas and impact on clinical course and quality of life. J Endourol 2007;21:1297–302. doi: 10.1089/end.2006.0104.

9. Comstedt P, Storgaard M, Lassen AT. The Systemic Inflammatory Response Syndrome (SIRS) in acutely hospitalised medical patients: a cohort study. Scand J Trauma Resusc Emerg Med 2009;17:67. doi: 10.1186/1757-7241-17-67.

10. Pabon-Ramos WM, Dariushnia SR, Walker TG, d'Othée BJ, Ganguli S, Midia M, et al. Quality improvement guidelines for percutaneous nephrostomy. J Vasc Interv Radiol 2016;27:410–4. doi: 10.1016/j.jvir.2015.11.045.

11. Turo R, Horsu S, Broome J, Das S, Gulur DM, Pettersson B, et al. Complications of percutaneous nephrostomy in a district general hospital. Turk J Urol 2018;44:478–83. doi: 10.5152/tud.2018.37336.

12. Ali SM, Mehmood K, Faiq SM, Ali B, Naqvi SA, Rizvi AU. Frequency of complications in image guided percutaneous nephrostomy. J Pak Med Assoc 2013;63:816–20.

13. Lee WJ, Patel U, Patel S, Pillari GP. Emergency percutaneous nephrostomy: results and complications. J Vasc Interv Radiol 1994;5:135–9. doi: 10.1016/s1051-0443(94)71470-6.

14. Radecka E, Magnusson A. Complications associated with percutaneous nephrostomies. A retrospective study. Acta Radiol 2004;45:184–8. doi: 10.1080/02841850410003671.

15. Sood G, Sood A, Jindal A, Verma DK, Dhiman DS. Ultrasound guided percutaneous nephrostomy for obstructive uropathy in benign and malignant diseases. Int Braz J Urol 2006;32:281–6. doi: 10.1590/s1677-55382006000300004.

16. Dyer RB, Regan JD, Kavanagh PV, Khatod EG, Chen MY, Zagoria RJ. Percutaneous nephrostomy with extensions of the technique: step by step. Radiographics 2002;22:503–25. doi: 10.1148/radiographics.22.3.g02ma19503.

17. Bayne D, Taylor ER, Hampson L, Chi T, Stoller ML. Determinants of nephrostomy tube dislodgment after percutaneous nephrolithotomy. J Endourol 2015;29:289–92. doi: 10.1089/end.2014.0387.

Original Article

Noninvasive postmortem investigation of cases refusing autopsy using computed tomography

Pakorn Wasinrat, M.D.[1]
Jitladda Wasinrat, M.D.[2]
From [1] Institute of Forensic Medicine, Police General Hospital, Thailand.
[2] Department of Radiology, Faculty of Medicine Siriraj Hospital, Mahidol University, Thailand.
Address correspondence to P.K.(e-mail: pakorn_wsr@yahoo.com)

Received 13 November 2022; revised 11 October 2023; accepted 13 October 2023
doi:10.46475/asean-jr.v24i3.194

Abstract

Background: CT is a well-known tool to assess several conditions in living patients. The post-mortem CT (PMCT) has been introduced to determine the cause of death in dead subjects. CT is also the imaging modality of choice for the analysis of autopsy findings including fracture, hematoma, gas collection and gross tumor injury. The rate of standard autopsy is continuing to decline and there are several reasons for refusing autopsy.

Objective: The current research endeavor is investigate the usefulness of computed tomography (CT) in cases refusing autopsy.

Materials and Methods: In this study, the PMCT were evaluated in 150 subjects in different contexts of death. The causes of death were classified into four categories which include a definite cause of death, a possible cause of death, a minor pathological finding and no fatal findings. For the definite cause of death and the possible cause of death, the specific lesions are described in detail.

Results: The definite cause of death was detected in 48 (32%) of the subjects. The possible cause of death was detected in 18 (12%) of the subjects. The remaining 84 subjects were classified into minor pathological findings and no fatal findings in 46 (30.7%) and 38 (25.3%) of the patients, respectively. The fatal lesions of PMCT were found in 93 lesions (48 subjects) that were demonstrated by anatomical locations into the traumatic bone, intracranial, spine, thoracic, heart leak and abdominal lesions. We found definite causes of death in 6 subjects, which had no history of trauma and malignancy and were mentioned about a cardiopulmonary failure as a cause of death at first.

Conclusion: The PMCT is a useful tool for identifying the cause of death in many cases that have limitations for conventional autopsy. The morphological change such as intracranial hemorrhage is easily diagnosed with PMCT. The PMCT appears to be an alternative tool to assess the cause of death in any reason of objections.

Keywords: Cause of death, Postmortem CT, Refusing autopsy case, Virtual autopsy.

Introduction

To investigate the cause of death, an autopsy is the reference standard for postmortem evaluation in a modern clinical practice. In recent years, the autopsy rate has declined in most developed countries [1]. Computed tomography (CT) and magnetic resonance imaging (MRI) is a well-known imaging tool to investigate the internal organs of living patients. Several studies have reported the use of these imaging tools to identify postmortem causes of death. Robert et al.[2] reported that whole body CT is more accurate than MRI to investigate the cause of death in adults. Takahashi et al.[3] demonstrates that postmortem CT (PMCT) is a feasible tool to detect the morphological cause of death in non-traumatic cases in the emergency department. Le Blanc-Louvry et al.[4] compares the PMCT with standard autopsy in different contexts of death. They found that PMCT is an effective tool as a standard autopsy in determining the cause of death. Wichmann et al.[5] reported that advanced radiographic techniques provide an alternative approach for postmortem evaluation. Yukihiro et al. reported PMCT in the investigation of non-traumatic death in infants and children.

Although the conventional autopsy is a standard tool to determine the cause of death in all contexts of death, several reasons to object conventional autopsy are found. CT is an advanced radiographic imaging tool to evaluate the morphological change of internal organs. CT provides a better spatial resolution than MRI and less scan time. CT is also a useful tool for showing fractures and internal hemorrhage. CT is more widely available in most of hospitals particularly in rural areas.

In this study, we evaluate the usefulness of the PMCT to diagnose possible causes of death in cases refusing conventional autopsy.

Materials and methods

This study is a retrospective review and approved by the institutional review board (No.147/2564). The study subjects were unnatural death bodies of any age who were sent to the Institute of Forensic Medicine, Police General Hospital, Thailand between 31 October 2017 and 30 September 2018 with the conventional autopsy not performed due to the refusal of conventional autopsy. The informed consent was waived due to retrospective review. The exclusion criteria were failure to perform PMCT imaging.

All PMCT images were performed on a 16-slice multidetector row CT scanner (Alexion, Canon Medical Systems; Toshiba Medical Systems). The acquisitions were obtained with contiguous axial slices with spiral mode from the vertex to the pelvis with 5 mm slice thickness.

The PMCT was interpreted by the consensus of one radiologist and one forensic doctor. The clinical history was given to the radiologist and forensic doctor during the imaging interpretation. The CT images were visualized in axial images on computer workstation with DICOM viewing software. For better image visualization, the coronal and sagittal images were reconstructed during the imaging interpretation. All abnormalities were noted in the case record form. To define the cause of death, the CT findings are classified in four categories: definite causes of death, possible causes of death, minor pathological findings and no fatal findings. For the definite causes of death and possible causes of death, the specific lesions are described in detail.

The demographic data including ages, genders and clinical data were collected. The PMCT findings were presented in non-contiguous variables.

Results

Out of the total of 153 decedents enrolled in the study, three were excluded because the PMCT was not available (data loss). The remaining 150 decedents were employed in the study. The demographic data of the subjects were males and females in 123 and 27, respectively. The average age of the subject is 42.6 years old (Table 1). The definite causes of death were detected in 48 (32%) of the subjects. The possible causes of death were detected in 18 (12%) of the subjects. The remaining 84 subjects were classified into minor pathological findings and no fatal findings in 46 (30.7%) and 38 (25.3%) of the patients, respectively (Table 2).

Table 1. *Patient characteristic.*

No of cases	150
Male	123
Female	27
Age (years)	42.6 years (range 1-96)

Table 2. *Classification of causes of death by post mortem CT.*

	No of cases
Definite cause of death	48 (32%)
Possible cause of death	18 (12%)
Minor pathological finding	46 (30.7%)
No fatal finding	38 (25.3%)
Total	150

The fatal lesions of PMCT in definite causes of death were found in 93 lesions (48 subjects) that were demonstrated by anatomical locations into traumatic bones (Figure 1), intracranium, and spine (Figure 2), thoracic, heart leak and abdominal lesions. In the definite causes of death, two most common lesions are subarachnoid hemorrhage and skull fractures (Table 3). The traumatic bone and intracranial lesions are also the most common anatomical locations for the fatal lesions.

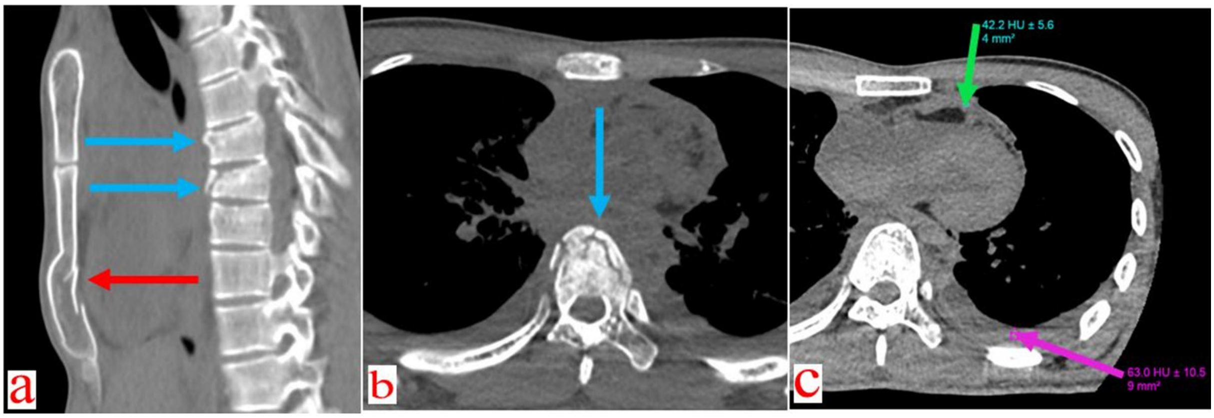

Figure 1. *A 24-year-old male who fell from height. PMCT in the bone windowed in (a and b) sagittal and axial views found a fracture at sternum (red arrow) and a fracture in vertebral bodies at T6-7 levels (arrow head). (c) axial image soft tissue windowed showed hemopericardium (green arrow) and hemothorax (pink arrow).*

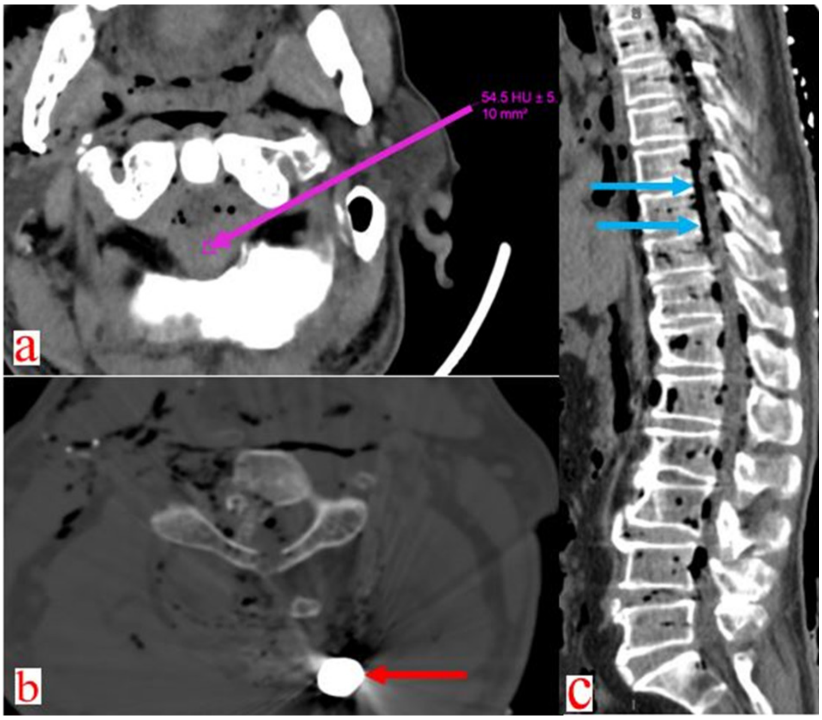

Figure 2. *A 70-year-old male with multiple gunshot wounds at the right shoulder. PMCT showed (a) hemorrhage in the spinal canal (pink arrow) in the bone windowed (b) found multiple fractures along bony vertebrae with retained bullet (arrow-head). (c) Sagittal image showed pneumorrhachis along the spinal canal (blue arrow).*

Table 3. *Post-mortem CT findings in definite causes of death and possible causes of death by the specific lesion.*

Category	Lesion	No. of lesion
	Traumatic bone lesions	
Definite causes of death	- skull fractures	12
	-Facial fractures	1
	-Vertebral fractures	9
	-Pelvic fractures	5
	Intracranial lesions	
	-Pneumocephalus	1
	-Intracranial hemorrhage	5
	-Subarachnoid hemorrhage	14
	-Epidural hematoma	1
	-Subdural hematoma	2
	-Intraventricular hemorrhage	8
	-Cerebral contusion	2
	-Cerebral edema	1
	Spines lesions	
	-Intraspinal hemorrhage	1
	Neck lesions	
	-Neck injury	1
	Thoracic lesions	
	-Pulmonary congestion	1
	-Pleural fluids	1
	-Pneumothorax	9
	-Hemothorax	9
	-Thoracic cancer	2
	Heart leakage lesions	
	-Hemopericardium	5
	Abdominal lesions	
	-Hemoperitoneum	3
	-Abdominal cancer	1
	Thoracic lesions	
Possible causes of death	-Pulmonary infiltration	4
	-Pulmonary mass	4
	-Pulmonary edema(drowning)	1
	-Pleural effusion	4
	-Pulmonary congestion	1
	-Hemopneumothorax	3
	Cardiac lesions	
	-Markedly cardiomegaly	2
	Abdominal lesions	
	-Kidney atrophy(ESRD)	1
	-Ascites fluid	2

We found definite causes of death in 6 subjects, which had no history of trauma and malignancy and were mentioned about the cardiopulmonary failure for the cause of death at first (Table 4, Figure 3-5).

Table 4. *Post-mortem CT findings with definite causes of death in six subjects, which were mentioned about the cardiopulmonary failure for the cause of death at first.*

Case	History	Cause of death from CT
1	Male 57 years, unconsciousness	Massive left hemothorax
2	Male 61 years, unconsciousness	Hemopericardium
3	Male 62 years, unconsciousness	Subarachnoid hemorrhage
4	Female 65 years, unconsciousness	Subarachnoid hemorrhage
5	Male 50 years, unconsciousness	Subarachnoid hemorrhage, intraventricular hemorrhage
6	Male 40 years, unconsciousness	Intraventricular hemorrhage, intracerebral hemorrhage

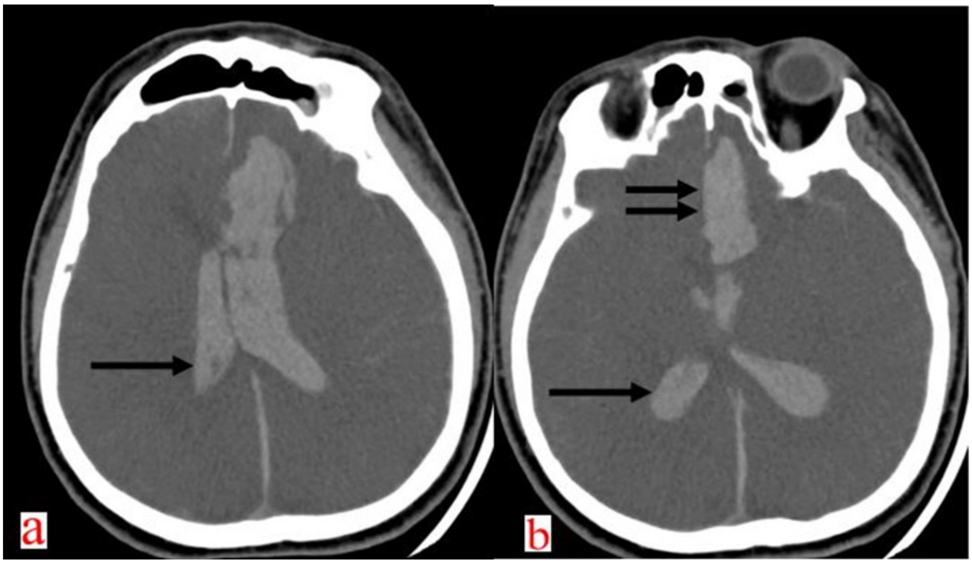

Figure 3. *A 61-year-old male with unconsciousness and PMCT showed (a and b) intraventricular hemorrhage (arrow) and intracerebral hemorrhage (double arrow).*

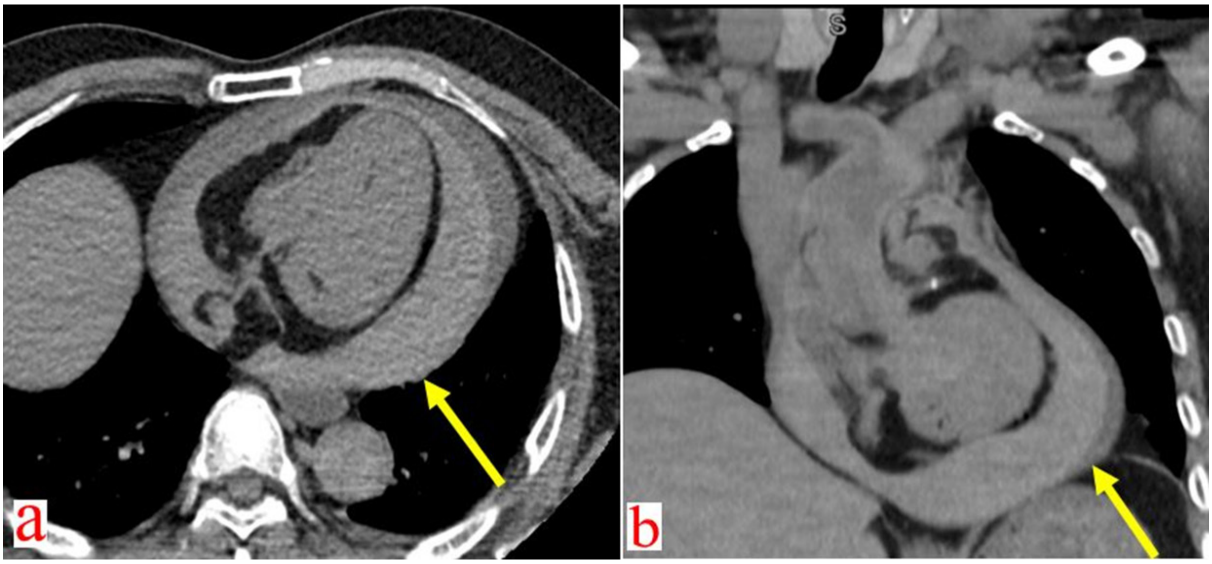

Figure 4. *A 62-year-old male with unconsciousness and PMCT axial and coronal views (a and b) showed hemopericardium (arrow).*

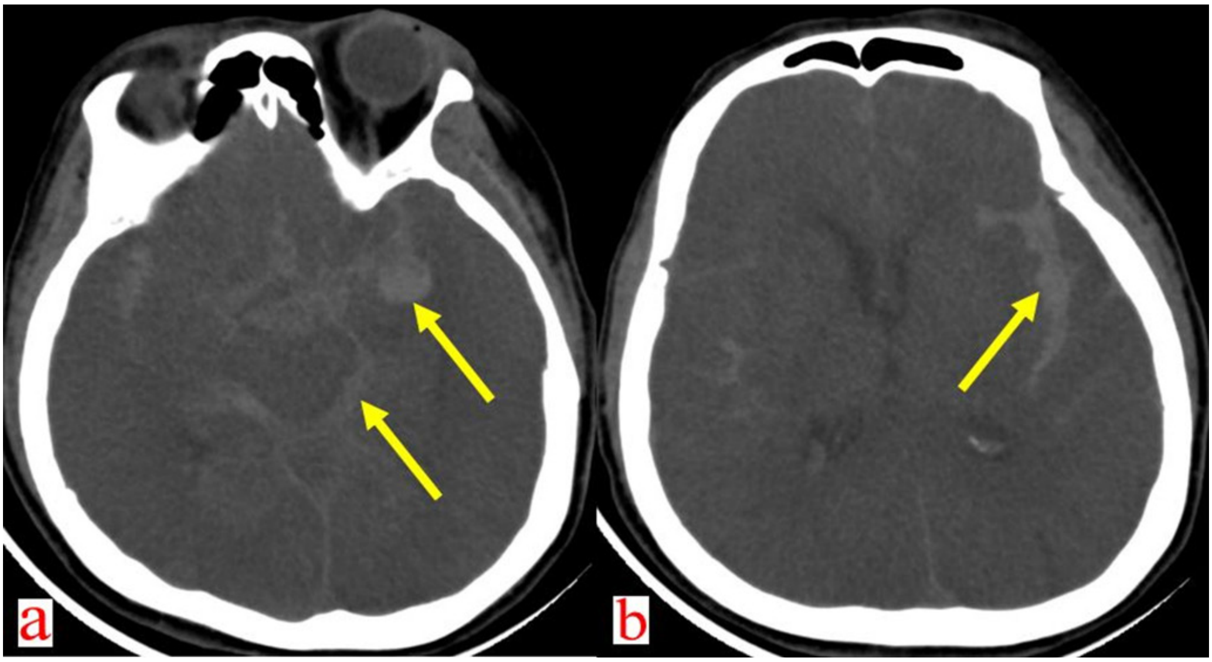

Figure 5. *A 65-year-old female with unconsciousness and PMCT brain axial view (a and b) showed subarachnoid hemorrhage (arrow).*

Discussion

The PMCT is a non-invasive method to visualize the internal organ after death. Recently, several studies have proposed the use of PMCT to determine the cause of death [1-10]. The PMCT is considered the most feasible imaging modality because it is widely available. In our study, we demonstrate the usefulness of PMCT to determine the cause of death in cases refusing autopsy. We can determine the definite and possible causes of deaths in 66 (44%) subjects. The remaining are minor pathological and no fatal findings. The anatomical change of the internal organ can be detected in PMCT. Conventional CT is a well-known diagnostic tool to access the internal organ. The most common fatal anatomical locations in PMCT are traumatic bones and intracranial lesions. The traumatic bone lesions are skull, facial, vertebral and pelvic fractures. The intracranial lesions are pneumocephalus, intracranial hemorrhage, subarachnoid hemorrhage, epidural hematoma, subdural hematoma, intraventricular hemorrhage, cerebral contusion and cerebral edema. The most common lesion of traumatic bone lesions is skull fractures, which is in concordance with the previous study [4]. The PMCT is more frequently detected for facial and vertebral fractures than conventional autopsy because these areas are not in routine dissection [4]. The intracranial lesions are well-demonstrated in PMCT. The hyperattenuation of blood clot or hematoma can be easily visualized in conventional methods and PMCT. Elkhateeb et al. [7] reported that PMCT was as valuable as autopsy for detecting the direction of firing and internal bleeding of gunshot injuries.

In 86 subjected who were diagnosed with the cardiopulmonary failure from only an external body exam, we found definite causes of death from PMCT in six subjects. Four of them had intracranial hemorrhage and two of them had intrathoracic hemorrhage. This is about 7% in cases of a diagnosed cardiopulmonary failure.

PMCT is less sensitive than autopsy in vascular injury because of no contrast enhancement in vessels. The direct evidence of blood leakage is demonstrated as an isoattenuation on CT images. If leakage is small, it is difficult to be detected in

PMCT. However, the indirect evidence of blood leakage is perivascular hematoma, which is slightly hyperattenuation of lesion adjacent to the vessel. In this study, no direct evidence of perivascular hematoma is detected in all subjects. The hemopericardium is indirect evidence of ascending aortic or heart rupture that is frequently found in autopsy observation [6]. In this study, we can detect hemopercardium in five subjects. The acute coronary syndrome is one of the commonest causes of death worldwide. The absence of post mortem coronary angiography may lead to underdiagnosis of an acute coronary syndrome [6]. The Agatston score measured in non-contrast CT more than 400 may indicate the likely presence of the significant coronary artery disease but it is not a definite diagnosis. Nevertheless, the PMCT is not sufficient in the diagnosis of this sudden death. Pulmonary embolism is also a diagnostic pitfall of PMCT. The pulmonary embolism is one the most common sudden deaths that is presented with cardiovascular collapse. However, the pulmonary embolism is limited for diagnosis in non-contrast PMCT [3, 6].

The PMCT is an effective tool similar to the conventional autopsy in diagnosis of airway, lung and thoracic diseases [6]. The airway obstruction by foreign body or food aspiration may be secondary to a cardiac arrest. The opaque foreign body can be detected in non-contrast PMCT. However, post mortem redistribution of gastric contents into the airways and lungs are commonly misdiagnosed as aspiration in PMCT [6].

The abdominal region is one of the causes of sudden death. The solid organ injuries may be visualized as hyperattenuation hematoma. The gastrointestinal perforation may reveal gas and free air in the abdomen but the perforation site cannot be visualized [6]. The hemoperitoneum or blood leakage in the abdomen may be a possible result of solid organ injury or aortic rupture. In this study, we found hemoperitoneum in three subjects. Takahashi et al. [3] reported the usefulness of PMCT in detecting bowel lesions such as bowel strangulation and ischemic colitis.

The limitation of this study is no confirmation by conventional autopsy. Non-contrast of CT imaging is also a major limitation of vascular lesions. Prospective studies with a larger sample size are required to investigate the additional value of PMCT.

Conclusion

The PMCT is a useful tool for identifying the causes of death in many cases that have limitations in a conventional autopsy. The morphological change such as intracranial hemorrhage is easily diagnosed with PMCT. The PMCT appears to be an alternative tool to assess the causes of death in any reason of objections.

References

1. Burton JL, Underwood J. Clinical, educational, and epidemiological value of autopsy. Lancet 2007;369:1471-80. doi: 10.1016/S0140-6736(07)60376-6.

2. Roberts IS, Benamore RE, Benbow EW, Lee SH, Harris JN, Jackson A, et al. Post-mortem imaging as an alternative to autopsy in the diagnosis of adult deaths: a validation study. Lancet 2012;379:136-42. doi: 10.1016/S0140-6736(11)61483-9.

3. Takahashi N, Higuchi T, Shiotani M, Hirose Y, Shibuya H, Yamanouchi H, et al. The effectiveness of postmortem multidetector computed tomography in the detection of fatal findings related to cause of non-traumatic death in the emergency department. Eur Radiol 2012;22:152-60. doi: 10.1007/s00330-011-2248-6.

4. Le Blanc-Louvry I, Thureau S, Duval C, Papin-Lefebvre F, Thiebot J, Dacher JN, et al. Post-mortem computed tomography compared to forensic autopsy findings: a French experience. Eur Radiol 2013;23:1829-35. doi: 10.1007/s00330-013-2779-0.

5. Wichmann D, Obbelode F, Vogel H, Hoepker WW, Nierhaus A, Braune S, et al. Virtual autopsy as an alternative to traditional medical autopsy in the intensive care unit: a prospective cohort study. Ann Intern Med 2012;156:123-30. doi: 10.7326/0003-4819-156-2-201201170-00008.

6. Burton JL, Kitsanta P. Daily application of post-mortem computed tomography digital autopsy in a public mortuary. Diagn Histopathol 2020;26:358-67.

7. Elkhateeb SA, Mohammed EB, Meleka HA, Ismail AAE. Postmortem computed tomography and autopsy for detection of lesions and causes of death in gunshot injury cases: a comparative study. Egypt J Forensic Sci 2018;8:50. doi:10.1186/s41935-018-0078-2.

8. Mentink MG, Latten BGH, Bakers FCH, Mihl C, Rennenberg RJMW, Kubat B, et al. Clinical relevance of unexpected findings of post-mortem computed tomography in hospitalized patients: an observational study. Int J Environ Res Public Health 2020;17:7572. doi: 10.3390/ijerph17207572.

9. Dirnhofer R, Jackowski C, Vock P, Potter K, Thali MJ. VIRTOPSY: minimally invasive, imaging-guided virtual autopsy. Radiographics 2006;26:1305-33. doi: 10.1148/rg.265065001.

10. Badam RK, Sownetha T, Babu DBG, Waghray S, Reddy L, Garlapati K, et al. Virtopsy: touch-free autopsy. J Forensic Dent Sci 2017;9:42-. doi: 10.4103/jfo.jfds_7_16.

Original Article

Relationship of pericardial effusion thickness and volume measurement by non-ECG gated computed tomography

Karnkawin Patharateeranart, M.D.
Jidapa Stapornchaisit, M.D.
Jitladda Wasinrat, M.D.
From Division of Diagnostic Radiology, Department of Radiology,
Faculty of Medicine Siriraj Hospital, Mahidol University, Bangkok, Thailand.
Address correspondence to J.W.(e-mail: Jitladda.siriraj@gmail.com)

Received 8 April 2023; revised 31 October 2023; accepted 3 December 2023
doi:10.46475/asean-jr.v24i3.349

Abstract

Background: An accurate estimation of pericardial fluid volume could improve communication between radiologists and the multidisciplinary team.

Objective: To find the correlation between the volume and thickness of pericardial effusion measured by CT scan.

Materials and Methods: The chest CT scans of 38 patients with pericardial effusion were measured for volume using manual segmentation and for thickness on axial and 3-chamber planes from the anterior and posterior aspects. The correlation between volume and thickness was evaluated using Pearson's correlation coefficient (r). The reliability of the measurements was tested using intraclass correlation coefficient (ICC) and Bland-Altman analysis.

Results: There was a fair to moderately strong correlation between the volume and thickness of pericardial effusion (r= 0.435-0.625, p= <0.01). An ICC of 0.452-0.703 indicated moderate inter-observer agreement. The best measurement is the sum of the anterior and posterior thicknesses on the axial plane (ICC of 0.703) that correlates well with the volume (r= 0.624). A linear regression equation demonstrating the relationship between pericardial effusion thickness and the effusion volume was computed as; Volume (mL) = 73 + 71*(the sum of anterior and posterior thicknesses on axial view in cm). The equation was applied: a value of approximately 3 cm = small, 6 cm = moderate, and 9 cm = large pericardial effusion.

Conclusion: There is a moderate correlation between the sum of the anterior and posterior pericardial thicknesses and the pericardial volume. Our preliminary formula enables a rapid estimation of the effusion volume. Further validation and refinement of the formula in a larger, prospective study is needed.

Keywords: Computed tomography, Estimation of pericardial effusion volume, Pericardial effusion.

Introduction

The diagnosis of pericardial effusion is usually made by echocardiography. (1) An estimation of the size of the effusion and its important hemodynamic is the first step in clinical management. Large pericardial effusions have the potential risk for cardiac tamponade [1]. An estimation of the pericardial effusion size is done by measuring the distance of the anechoic space between the epicardium and the parietal pericardium during end-diastole [2]. An echocardiographic quantitative assessment of pericardial effusion with a 3-dimensional disk method has a strong correlation with drained pericardial fluid [3]. However, echocardiography has limitations such as a poor acoustic window and loculated fluid [4].

Pericardial effusion is detected incidentally by computed tomography (CT) in up to 5% of patients [5]. Various methods to quantify the amount of pericardial effusion with CT have been reported. In 2012, Ebert et al. proposed that measuring the fluid volume in the phantom by using the segmentation technique was highly accurate [6]. Other studies have reported that the pericardial effusion volume estimated from CT was moderately correlated with the actual volume drained from aspiration [7,8]. However, due to leakage during incision or retained unmeasured hematoma, the drained fluid volume is usually less than that estimated by CT [6], suggesting that even surgically drained fluid does not accurately measure the pericardial effusion volume.

Therefore, we aimed to determine if the pericardial effusion thickness in the axial plane and the 3-chamber plane can be used to precisely estimate the pericardial effusion volume. We also aimed to identify the specified position or plane that could best represent the pericardial effusion volume and to calculate an equation demonstrating the relationship between the pericardial effusion thickness and the pericardial effusion volume. An accurate estimation of the fluid volume using pericardial wall thickness could reduce interpretation time and improve communication between radiologists and the multidisciplinary team.

Materials and methods

Study Population

We searched the picture archive and communication system (PACS) of a tertiary hospital in Bangkok, Thailand using the terms “moderate amount of pericardial effusion”, “moderate pericardial effusion”, and “large amount of pericardial effusion” from January to December 2019. The query returned 59 cases. Non-ECG gated CTs of the chest with contrast media administration were included. Patients with other pericardial pathology such as pericardial mass, pericardial calcification, or loculated pericardial effusion were excluded. Images with artifacts that caused evaluation limits, such as motion or metallic artifacts, were excluded. Finally, 38 cases (14 males) were included with a median age of 60 years. This retrospective study was approved by the Siriraj Hospital’s institutional review board. (SIRB Protocol No. 828/2563 IRB3).

Imaging Technique

All CT studies were performed by one of three multidetector CT scanners (MDCT) at our institution, including Lightspeed VCT 64-slice (GE Healthcare, Milwaukee, USA), Discovery 750HD 64-slice (GE Healthcare, Milwaukee, USA), and Revolution CT 256-slice (GE Healthcare, Milwaukee, USA). Scanning parameters included three protocols; A) CT chest with contrast, B) CT pulmonary artery (CTPA), and C) CTA thoracoabdominal aorta. All protocols used 120 kVp tube voltage. However, the tube current and rotation time depended on each machine. The scanning volume for all studies included the entire chest from lung apex to base, in the supine position with a one-breath-hold at the end-inspiration phase.

For Protocol A, iodinated contrast was administered at 2 ml/kg of body weight, followed by 20 ml of saline at 3 ml/sec. For Protocol B, < 50 ml of iodinated contrast was administered at 4 ml/sec, then a mixture of contrast and saline (50:50 ratio) 5-10ml at a rate of 5 ml/sec, followed by 40 ml of saline at 5 ml/sec. For Protocol C, < 100 ml of iodinated contrast was administered followed by 40 ml of saline at a rate of 4 ml/sec.

Image Analysis

The images were reviewed using PACS for thickness evaluation and GE AW VolumeShare 5 for volume evaluation. Post contrast or delayed chest phase (approximately 45 sec after contrast injection) images were used. The window width and level were changed according to the reviewer preferences. The CT data were reconstructed with 1.25-mm slice thicknesses and reformatted into the 3-chamber plane. Each CT image was reviewed separately by three radiologists (K.P., J.W., and J.S., with 5, 15, and 4 years of experience in diagnostic radiology, respectively).

The pericardial effusion thicknesses were measured by K.P and J.W. with a one-week interval between readings. Pericardial effusion thicknesses were measured at two locations on two planes; maximal thickness at anterior to the right ventricle and maximal thickness at posterior to the free wall of the left ventricle on the axial and the 3-chamber planes (Figure1). Measurements of the pericardial fluid volume were measured twice by J.S. with a 1-week interval between readings and once by K.P, by drawing the region of interest (ROI) of the pericardial effusion area of every slice of CT with 2.5 mm thickness (Figure 2) using GE AW VolumeShare 5 software.

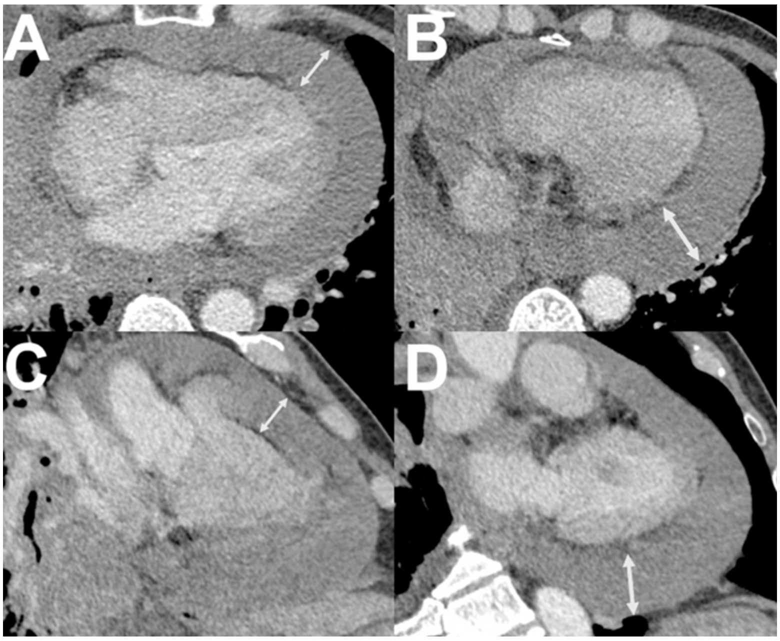

Figure 1. *Imaging planes used for measurement of pericardial effusion thickness*
A and B: axial plane images for measurement of anterior and posterior thickness,
C and D: 3-chamber plane for measurement of anterior and posterior thickness.

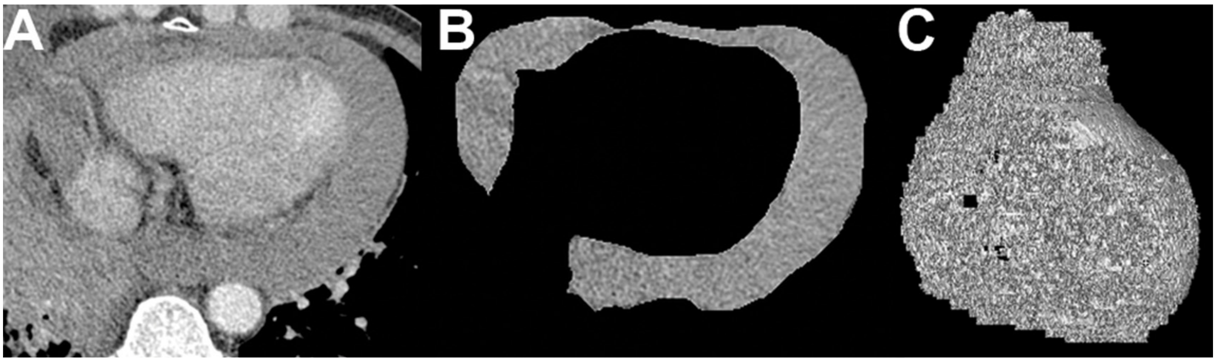

Figure 2. *Pericardial effusion volume measurement*
A: Axial CT shows pericardial effusion,
B: Image after manually drawn region of interest for pericardial effusion,
C: Volume-rendered image after drawing ROI of every slice demonstrates pericardial effusion volume.

Statistical Analysis

The statistical analysis was performed using SPSS version 23 and Medcalc. Intra- and inter-observer reliability were calculated to express the reproducibility, using the intraclass correlation coefficient (ICC) to assess the agreement of measurements and Bland-Altman analysis to present the bias and limits of agreement. An ICC <0.50 is considered poor, 0.50-0.75 moderate, 0.75-0.90 good and >0.90 excellent [9].

Validity was assessed by comparing the volume and thickness measured by both observers using Pearson's correlation coefficient. A linear equation was derived for the best thickness (best ICC). A correlation coefficient at least 0.80 is considered very strong, 0.60 up to 0.80 moderately strong, 0.30 to 0.50 fair, and less than 0.3 poor [10]. A P value of < 0.05 was considered statistically significant. For validity testing, a sample size of 38 provided 90% power to detect a correlation of 0.8 with an α value of 0.05.

Results

Pericardial effusion

The median pericardial effusion volume (n=38) measured by drawing the ROI technique was 203.50 ml (range 50 – 635 ml). There were 28 patients (73.6%) who had a pericardial effusion volume < 300 ml and 10 patients who had a pericardial effusion volume between 300 – 700 ml. No amount exceeding a volume of 700 ml was manifest in any patient.

Reliability of the measurements

There were excellent interobserver and intra-observer agreements of pericardial effusion volume measurement. The ICC of interobserver and intra-observer agreements were 0.902 and 0.968, respectively. The Bland-Altman analysis revealed a mean bias of -20.6 mL (95% limits of agreement between -128.8 mL to 87.5 mL) for interobserver agreement and -3.3 mL (95% limits of agreement between -67.6 mL to 61.0 mL) for intra-observer agreement (Table 1). Inter-observer agreements

(ICC 0.535-0.703) were moderate for thickness measurement in all locations, except for poor agreement in the posterior thickness on the 3-chamber plane (ICC 0.452). The strongest ICC was the sum of the anterior and posterior thicknesses on the axial plane (ICC = 0.703). Intra-observer agreement was moderate for the 1st reviewer and excellent for the 2nd reviewer. The sum of anterior and posterior thicknesses on the axial plane showed the strongest ICC (ICC = 0.997) (Table 2).

Table 1. *Intra- and inter-observer agreement of pericardial volume measurement.*

	Intraclass correlation coefficient (ICC)	Bland-Altman (mL)
Inter-observer agreement	0.902	-20.6 (-128.8, 87.5)
Intra-observer agreement	0.968	-3.3 (-67.6, 61.0)

Table 2. *Intra- and inter-observer agreement of pericardial thickness measurement.*

	Axial plane			3-chamber plane		
	Anterior	Posterior	Sum	Anterior	Posterior	Sum
Correlation for R1	0.435	0.599	0.613	0.505	0.523	0.625
P-value	0.006	0	0	0.001	0.001	0
Correlation for R2	0.404	0.578	0.624	0.381	0.596	0.63
P-value	0.012	0	0	0.018	0	0

Correlation between volume and thickness measurements

The correlation between thickness measurements and the pericardial volume for the sum of anterior and posterior thicknesses was moderately strong on both the axial and 3-chamber planes. The most robust Pearson's correlation coefficient was the sum of anterior and posterior thicknesses on the 3-chamber plane (r = 0.625 and 0.630) (Table 3).

Table 3. *Pericardial thicknesses and pericardial volume correlation.*

	Axial plane			3-chamber plane		
	Anterior	**Posterior**	**Sum**	**Anterior**	**Posterior**	**Sum**
Inter-observer agreement						
ICC	0.631	0.535	0.703	0.581	0.452	0.571
Bland-Altman (cm)	0.03 (-0.81, 0.88)	-0.2 (-1.7, 1.3)	-0.2 (-1.8, 1.5)	0.13 (-0.68, 0.93)	-0.35 (-1.58, 0.88)	-0.2 (-1.8, 1.4)
Intra-observer agreement (R1)						
ICC	0.806	0.702	0.774	0.732	0.678	0.716
Bland-Altman (cm)	-0.14 (-0.63, 0.36)	-0.28 (-1.22, 0.66)	-0.42 (-1.49, 0.66)	-0.18 (-0.74, 0.38)	-0.30 (-1.09, 0.50)	-0.48 (-1.48, 0.52)
Intra-observer agreement (R2)						
ICC	0.995	0.995	0.997	0.991	0.993	0.991
Bland-Altman (cm)	0 (-0.10, 0.10)	0.03 (-0.14, 0.20)	0.03 (-0.15, 0.21)	0.02 (-0.10, 0.13)	0.03 (-0.11, 0.17)	0.05 (-0.16, 0.26)

The summation of anterior and posterior thicknesses on the axial plane was selected to calculate a formula for the pericardial volume estimation with the best inter-observer agreement (ICC = 0.703 and correlation = 0.624). (Table 2 and 3) Using this correlation, we created a linear regression equation, from which we obtained the formula. The linear regression equation for summation of anterior and posterior thicknesses on axial view against the pericardial volume was simplified into the formula (Figure 3):

Volume (mL) = 73 + 71(the sum of anterior and posterior thicknesses on axial view in cm).*

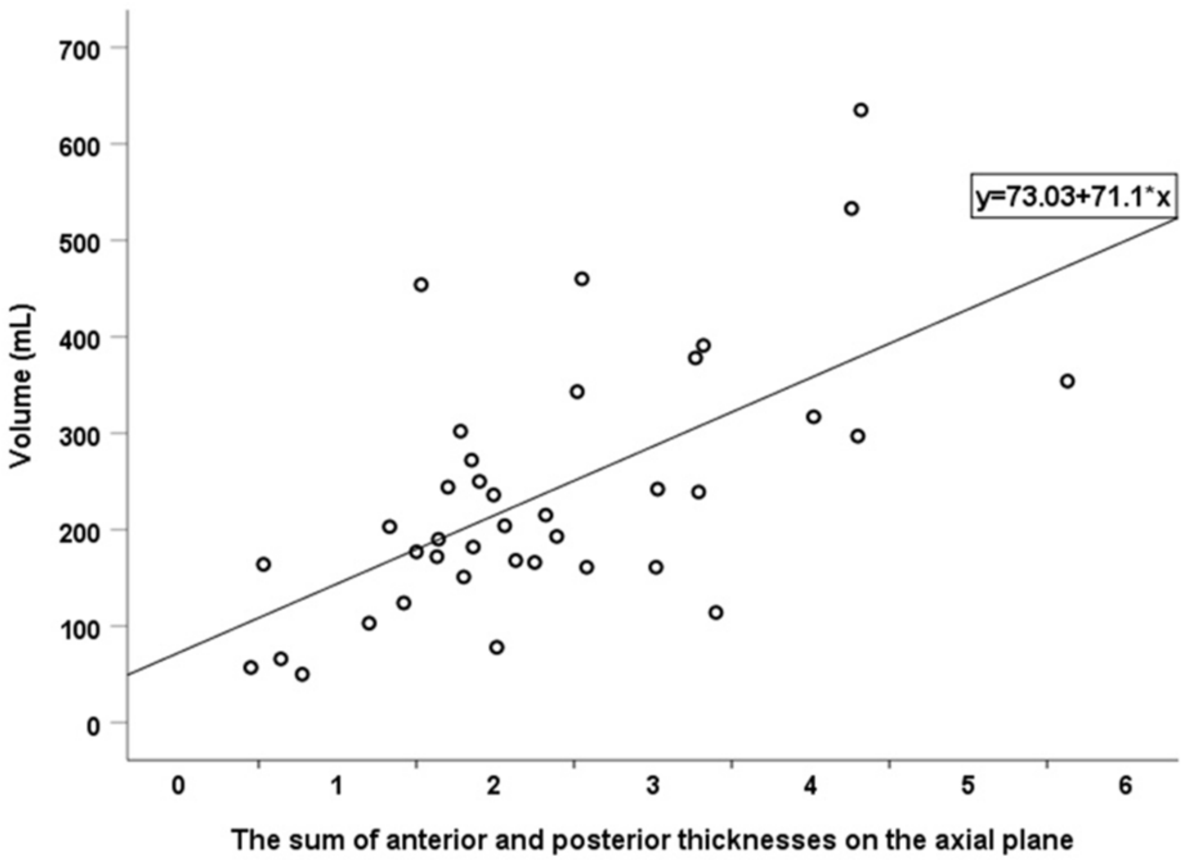

Figure 3. *The correlation between pericardial volume and thickness.*

Discussion

We found that the posterior thickness and the sum of the anterior and posterior thicknesses of both the axial and the 3-chamber planes had a moderately strong correlation, with Pearson's correlation coefficients of 0.613 and 0.624 for the axial plane and 0.625 and 0.630 for the 3-chamber plane. Therefore, the sum of the anterior and posterior thicknesses reveals a moderately strong correlation with the pericardial effusion volume.

Frank and colleagues suggested a thickness of the pericardial effusion anterior to the right ventricle of more than 5 mm represented a moderate amount of pericardial effusion [11]. We cannot find an explanation from the previous reports for why 5 mm would represent a moderate amount. However, we found anterior thickness to be poorly correlated with the volume which may be explained by the fact that gravity causes fluid to accumulate at the posterior aspect of the heart, making the anterior measurement alone a poor proxy for the volume.

Ohta et al. proposed that if a combination of anterior and posterior maximal thicknesses on the axial view exceeded 25.5 mm, this would indicate cardiac tamponade with an odds ratio of 12.7 [12]. Using our proposed equation would result in 254 mL of fluid, a small amount by echocardiography standards. However, the increment rate has more effect than the volume with respect to cardiac tamponade [13], and Ohta et al. did not evaluate the volume on CT or echocardiogram to compare with the mentioned thicknesses [12].

The intra-observer agreements for both thicknesses and volume measurements were excellent. However, the inter-observer agreements were moderate to weak, with the highest ICC for the sum of anterior and posterior thicknesses on the axial plane. This is different from a study by Groth et al. that reported excellent intra- and inter-observer agreement in a study of 20 patients with a different position for measurement than the one we used [14]. In our study, each reviewer scrolled through the entire scan/ set and selected the maximal anterior and posterior thicknesses.

The semiquantitative measurement from echocardiography is small (< 10 mm, representing 300 ml), moderate (> 10 mm, representing 500 ml), and large (> 20 mm, representing 700 ml [15]. When our formula is applied to calculate the thickness of pericardial effusion from CT scan for volumes of 300, 500 and 700 ml, the corresponding summation of anterior and posterior thicknesses is 3.19, 6.01 and 8.83 cm, respectively. To simplify the calculation, we round to the nearest whole number. Therefore, the sum of the anterior and posterior thicknesses on the axial plane of approximately 3 cm, 6 cm, and 9 cm represents small, moderate, and large pericardial effusion, respectively.

This equation can reduce the typical interpretation time using the drawing the ROI technique, which is normally between 40 and 50 minutes, to fewer than five minutes using thickness measured on the axial plane, which is almost always available in a routine practice. Our method may also help create a standard reference for what constitutes small, moderate, and large pericardial effusions on CT scan. Nonetheless, further validation is needed.

Limitations

There is currently no gold standard for the estimation of the volume of a pericardial effusion. Most patients with pericardial effusions are treated medically, and none of our patients were surgically drained. Moreover, post-mortem studies have showed that surgically drained fluid is often less than the volume estimated by CT, which can be explained by the inability to drain all of the pericardial effusion or errors during autopsy measurement [6,16]. Ebert et al. also validated volume measurement using CT compared with the phantom, which accurately measured the amount of pericardial effusion [6]. Thus, we used CT volume measured from every slice to be the standard to compare with thicknesses. Second, due to the variable size of pericardial effusion and although we used the key search terms “moderate amount”, “moderate” and “large amount” of pericardial effusion, 73.6% of our cases had a small pericardial effusion volume per echocardiography estimation [2,15]. As the present study is a retrospective, single-center experience with potential selection bias and the sample size of relatively small; hence, further prospective studies with larger recruited patients should be considered.

Conclusion

The sum of the anterior and posterior pericardial thicknesses and pericardial volume for both the axial and 3-chamber planes are moderately correlated. Our formula enables a rapid estimation of pericardial effusion volume and could help create a standard reference for what constitutes small, moderate, and large pericardial effusions on CT scan. Further validation and refinement of the formula in a larger, prospective study is needed.

Acknowledgements

The authors acknowledge Siriraj Institute of Clinical Research (SICRES) for supporting the manuscript development.

References

1. Adler Y, Charron P, Imazio M, Badano L, Barón-Esquivias G, Bogaert J, et al. 2015 ESC guidelines for the diagnosis and management of pericardial diseases: The task force for the diagnosis and management of pericardial diseases of the European Society of Cardiology (ESC) endorsed by: The European Association for Cardio-Thoracic Surgery (EACTS). Eur Heart J 2015;36:2921-64. doi: 10.1093/eurheartj/ehv318.

2. Ceriani E, Cogliati C. Update on bedside ultrasound diagnosis of pericardial effusion. Intern Emerg Med 2016;11:477-80. doi: 10.1007/s11739-015-1372-8.

3. DeMaria DM, Waring AA, Gregg DE, Litwin SE. Echocardiographic assessment of pericardial effusion size: time for a quantitative approach. J Am Soc Echocardiogr 2019;32:1615-7.e1. doi: 10.1016/j.echo.2019.08.019.

4. Unal E, Karcaaltincaba M, Akpinar E, Ariyurek OM. The imaging appearances of various pericardial disorders. Insights Imaging 2019;10:42. doi: 10.1186/s13244-019-0728-4.

5. Moustafa A, Liu X, Ye F, Khuder S, Alhazmi L, Youssef E, et al. Computed tomography scan overestimates the size of pericardial effusion compared to echocardiography. Cureus 2019;11:e5182. doi: 10.7759/cureus.5182. doi: 10.7759/cureus.5182.

6. Ebert LC, Ampanozi G, Ruder TD, Hatch G, Thali MJ, Germerott T. CT based volume measurement and estimation in cases of pericardial effusion. J Forensic Leg Med 2012;19:126-31. doi: 10.1016/j.jflm.2011.12.007.

7. Tomoda H, Hoshiai M, Furuya H, Oeda Y, Matsumoto S, Tanabe T, et al. Evaluation of pericardial effusion with computed tomography. Am Heart J 1980;99:701-6. doi: 10.1016/0002-8703(80)90618-3.

8. Leibowitz D, Perlman G, Planer D, Gilon D, Berman P, Bogot N. Quantification of pericardial effusions by echocardiography and computed tomography. Am J Cardiol 2011;107:331-5. doi: 10.1016/j.amjcard.2010.08.072.

9. Koo TK, Li MY. A guideline of selecting and reporting intraclass correlation coefficients for reliability research. J Chiropr Med 2016;15:155-63. doi: 10.1016/j.jcm.2016.02.012.

10. Chan YH. Biostatistics 104: correlational analysis. Singapore Med J 2003;44:614-9.

11. Frank H, Globits S. Magnetic resonance imaging evaluation of myocardial and pericardial disease. J Magn Reson Imaging 1999;10:617-26. doi: 10.1002/(sici)1522-2586(199911)10:5<617::aid-jmri5>3.0.co;2-z.

12. Ohta Y, Miyoshi F, Kaminou T, Kaetsu Y, Ogawa T. The evaluation of cardiac tamponade risk in patients with pericardial effusion detected by non-gated chest CT. Acta Radiol 2016;57:538-46. doi: 10.1177/0284185115592272.

13. Spodick DH. Acute cardiac tamponade. N Engl J Med 2003;349:684-90. doi: 10.1056/NEJMra022643.

14. Groth M, Regier M, Muellerleile K, Bannas P, Adam G, Henes FO. A new formula for rapid assessment of pericardial effusion volume by computed tomography. Acad Radiol 2012;19:718-22. doi: 10.1016/j.acra.2012.01.008.

15. Cosyns B, Plein S, Nihoyanopoulos P, Smiseth O, Achenbach S, Andrade MJ, et al. European Association of Cardiovascular Imaging (EACVI) position paper: Multimodality imaging in pericardial disease. Eur Heart J Cardiovasc Imaging 2015;16:12-31. doi: 10.1093/ehjci/jeu128.

16. Watanabe S, Hyodoh H, Shimizu J, Okazaki S, Mizuo K, Rokukawa M. Classification of hemopericardium on postmortem CT. Leg Med (Tokyo) 2015;17:376-80. doi: 10.1016/j.legalmed.2015.05.004.

Original Article

The study on the predictive accuracy of artificial intelligence (AI) Lunit INSIGHT CXR Version 3.0 for pneumonia diagnosis in COVID-19 patients

Wayupa Wongwikrom, M.D.
Arkrom Chaiwerawattana, M.D.
From Department of Radiology, National Cancer Institute, Bangkok, Thailand.
Address correspondence to W.W. (e-mail: wongwayupa@gmail.com)

Received 14 September 2023; revised 25 December 2023; accepted 25 December 2023
doi:10.46475/asean-jr.v24i3.881

Abstract

Background: Millions of people in Thailand have been infected and died from the infection of the COVID-19. As a result, the country's public health system is greatly affected due to the limitation of the number of physicians. Artificial intelligence (AI) is, therefore, used to reduce the working load of physicians in the diagnosis of COVID-19 patients.

Objective: To study on the predictive accuracy of AI Lunit INSIGHT CXR Version 3.0 for pneumonia diagnosis in COVID-19 patients.

Materials and Methods: This study was a retrospective study. The data was collected from 256 confirmed cases of COVID-19 infection admitted as new patients in the Nimibutr Pre-Admission Centre of the Institute of Neurology, the Ministry of Public Health. They were randomly selected from the database.

Seven radiologists and Lunit INSIGHT CXR Version 3.0 software interpret the CXR film to diagnose pneumonia in COVID-19 patients from chest radiographs (CXR).

Results: The research results of the diagnosis of pneumonia in patients infected with COVID-19 between from radiologists and using AI Lunit INSIGHT CXR Version 3.0 software revealed 97.87% (95%CI 88.71-99.95%) of sensitivity, 99.04% (95%CI 96.59-99.88%) of specificity, accuracy = 98.83%, positive predictive value (PPV) = 95.83%, and negative predictive value (NPV) = 99.52%, positive likelihood ratio (+LR) = 102.28, negative likelihood ratio (-LR) = 0.02.

Conclusion: The artificial intelligence software Lunit INSIGHT CXR Version 3.0 can be used to interpret the diagnosis of pneumonia in patients infected with COVID-19 in order to reduce radiologists' workloads during the COVID pandemic when medical staff were limited.

Keywords: Artificial intelligence, Chest radiograph, COVID-19, Diagnosis, Pneumonia.

Introduction

The 2019 coronavirus was officially detected in Wuhan, China in December 2019. It later spread worldwide and was called a pandemic by the World Health Organization (WHO) [1]. During this outbreak, the demand for medical care increased at a rapid rate. Meanwhile, the capacity of medical facilities and health personnel did not increase accordingly [2].

Furthermore, numerous medical officials became afflicted with this disease. As a result, a bigger supply of medical workers was required. Also, because doctors were required to work long hours, they could not provide comprehensive patient care. Many hospitals were opened temporarily to treat the enormous number of patients, and regular hospitals could not accept them. The Nimibutr Pre-Admission Center in the National Stadium was one of many temporary hospitals serving COVID-19 patients [3].

Most COVID-19 patients have respiratory problems, and some have pneumonia, which causes severe symptoms and deaths. Patients with severe symptoms must be rapidly diagnosed to detect pneumonia as soon as possible to provide effective treatment to prevent life-threatening conditions. On the other hand, some cases with positive CXR findings may present with negative RT-PCR testing revealing ground-glass opacity and mixed ground-glass opacity and mixed consolidation [4].

Numerous techniques can be used to examine lung inflammation, including chest computed tomography (Chest CT scan) and chest radiography (CXR). Cleaning the chest computed tomography after use was challenging and time-consuming, which made using it on COVID-19 patients an uphill task. Therefore, the World Health Organization (WHO) does not recommend using chest computed tomography for screening patients [5-9]. The early diagnosis of COVID-19 could control and prevent the spread of the disease and enable physicians to manage patients' disease control [10]. However, a chest radiograph is complicated for general physicians in reading and interpretation [8], and radiologists have difficulty reading CXR due to the indistinct manifestation of radiological features such as consolidation and hazy increased opacities [12-14]. In contrast, radiologists' performance in diagnosing COVID-19 is moderate [10].

Artificial intelligence (AI) is a type of computer science that aims to simulate tasks related to human intelligence and the learning process. In recent years, medical diagnosis employing AI-driven systems has made significant progress in supporting radiologists and clinicians with disease detection, characterization, and monitoring [15]. The application of AI in medical care has been intensively debated to assist medical personnel with the increasing workload in their daily routines—particularly in highly specialized domains such as radiological departments that deal with image-based duties [16,17]. It is a tool that can quickly learn and analyze data in various forms to assure diagnosis accuracy and speed [18]. By easing the burden on medical staff, AI can be used to make interpretations before radiologists confirm them. AI can speed up the performance of chest radiographs [19] and aid in the diagnosis of pneumonia brought on by COVID-19 [20].

During the COVID-19 pandemic, the Nimibutr Pre-Admission Center, the Ministry of Public Health, Thailand, was the temporary center responsible for curing COVID-19 patients because of the limited capacities to receive patients in regular hospitals. Lunit INSIGHT CXR is the AI Software for computer-assisted detection that assists physicians in interpreting chest radiography images which are used in the Nimibutr Pre-Admission center. Despite the fact that there are many studies pertinent to AI use, each AI may result in varied diagnosis results, but only a few researchers explore Lunit INSIGHT CXR.

The effectiveness of using AI to help diagnose pneumonia from COVID-19 is still limited and unclear. The researcher is, therefore, interested in studying the utility of AI in helping clinical diagnosing pneumonia caused by COVID-19 by helping detect lung abnormalities from chest radiographs in patients diagnosed by RT-PCR testing confirmed to be infected. Patients infected with COVID-19 who received care, treatment, and referral at the Nimibutr Pre-Admission Center of the Institute of Neurology, the Ministry of Public Health, between 1 – 30 September 2021 and had their CXR results confirmed by a radiologist by comparing the results of AI for diagnosing pneumonia in patients infected with COVID-19 and the team of radiologists.

Materials and methods

This study was a retrospective study collected from a database of medical records and chest radiographs of a positive RT-PCR confirmed COVID-19 patient admitted as a new patient at Nimibutr Pre-Admission Center of the Institute of Neurology, the Ministry of Public Health. The sample group was the confirmed case of COVID-19, receiving treatment at Nimibutr Pre-Admission Center Between 1 -30 September 2021. The sample size was calculated using G*Power [21] with the result of the suggested collection of 256 patients. Therefore, 256 out of 831 patients who received treatment at Nimibutr Pre-Admission Center Between 1 -30 September 2021 were selected as the sample for this study. Sample random sampling from a medical records database and chest radiographs was employed. Descriptive statistics to analyze general patient information by calculating sensitivity, specificity, and accuracy, including the positive and negative predictive values, were all used to confirm AI's benefits in diagnosing pneumonia caused by COVID-19.

AI, Lunit INSIGHT CXR Version 3.0 software

Lunit INSIGHT CXR is the AI Software for computer-assisted detection that assists physicians in interpreting chest radiography images. The device was designed to analyze chest radiographs via deep learning technology automatically and creates secondary capture DICOM objects reporting the analysis results. Each finding will report the detection-specific radiographic finding: Atelectasis, calcification, cardiomegaly, consolidation, fibrosis, mediastinal widening, nodule, pleural effusion, pneumoperitoneum, and pneumothorax according to the radiographs.

Data collection

The research requested a database of medical records and chest radiographs of a confirmed COVID-19 patient admitted as a new patient at Nimibutr Pre-Admission Center, receiving treatment between 1 -30 September 2021. Those reports included the COVID-19 screening record form, a Lab report of COVID-19 detection, radiography images, and the finalized report. The CXR film's x-rays were obtained into the LUNIT AI system and then were interpreted by radiologists. All the reported cases had the CXR films x-ray from radiologists and AI. Seven radiologists worked under the Department of Medical Services and had expertise in reading films responsible for that.

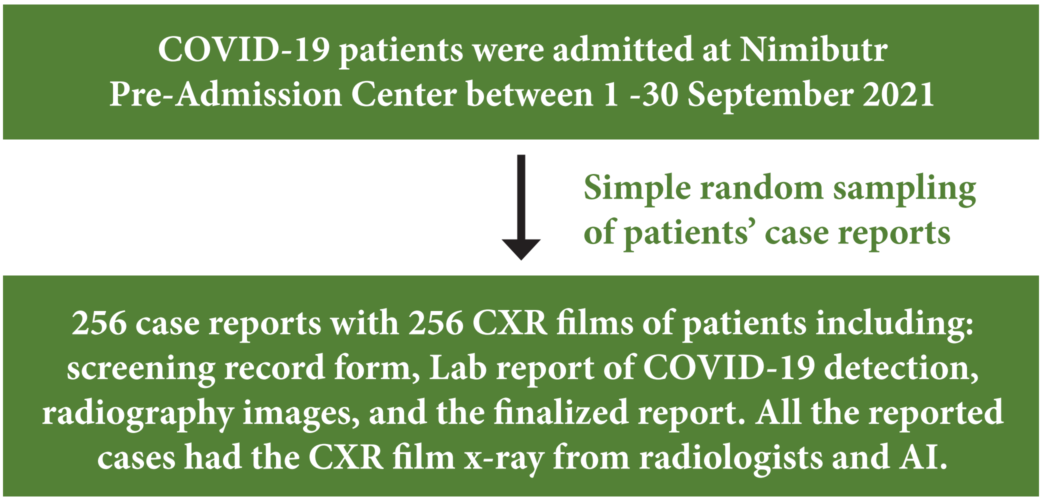

Figur 1. *Flowchart of patient selection.*

Criteria for separating abnormalities from chest radiographs for diagnosing pneumonia in patients with confirmed COVID-19.

Rama Co-RADS was developed by Suwatanaponched et al. [5] as the categorical assessment scheme of chest radiographic findings in diagnosing pneumonia in confirmed COVID-19 patients. There are six categories of chest radiographic diagnosis. Pneumonia will be confirmed if the CXR film was detected under the category 3 to category 5 of Rama Co-RADS. In this research study, the researcher used the result from radiologists and AI which was interpreted according to the Rama Co-RADS to confirm pneumonia in the patients.

This research received an ethical approval from the Human Research Ethics Committee, the Institute of Neurology, the Department of Medical Services, the Ministry of Public Health, No. 66034.

THE ASEAN JOURNAL OF RADIOLOGY
ISSN 2672-9393

Results

The study consisted of 256 patients, 140 males (54.69%) and 116 females (45.31%). There were 164 Burmese (64.10%), 41 Cambodians (16.00%), 20 Thais (7.80%), 14 Guineas (5.50%), 15 Laos (5.90%), and two not specified (0.80%) patients' cases in this study (Table 1). Most patients did not have any symptoms during the confirmation of COVID-19. An analysis of the different diagnoses between the demographic data of the patients showed no statistically significant difference (p = .46) between males and females, however, it showed a statistically significant difference between age (p =.00) and nationality (p = .01).

Table 1. *Demographic information of the patients.*

Characteristics	Total (n = 256)	Pneumonia	Non-Pneumonia	P-value
Gender				
Male	140 (54.69)	28	112	.46
Female	116 (45.31)	19	97	
Age (year) **categories**				
< 16	25 (9.77)	4	21	.00**
16 – 30	108 (42.19)	14	94	
31 – 45	99 (38.67)	16	83	
46 – 60	23 (8.98)	12	11	
> 60	1 (0.39)	1	0	
Nationality				
Thai	20 (7.80)	10	10	.01**
Burmese	164 (64.10)	24	140	
Cambodia	41 (16.00)	8	33	
Lao	15 (5.90)	3	12	
Guineas	14 (5.50)	2	12	
Not specifies	2 (0.80)	0	2	
Symptoms				
No	140 (54.69)			
Yes	116 (45.31)			
Pneumonia				
Pneumonia	48(18.75)			
Non-pneumonia	208(81.25)			

Note: * $p < .05$
** $p < .01$

There are three symptom categories of COVID-19 patients classified into three traffic light groups-green, red, and yellow- according to the seriousness of their symptoms. Red refers to the most severe symptoms typically with breathing difficulty; yellow represents mild symptoms; and green means with no signs or such fever, dry cough, or skin rashes. Figure 2 demonstrates the AI chest radiographs of three patients with different symptom categories. Each patient has two radiographs of contour and heatmap films.

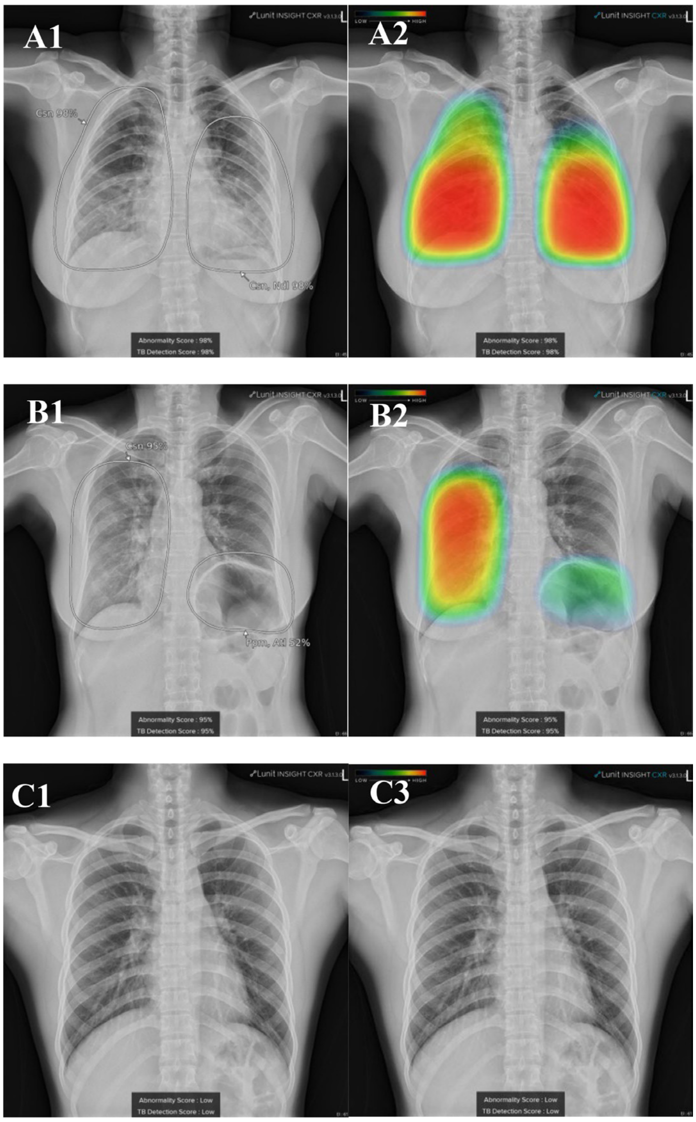

Figure 2. *Chest radiographs with AI interpretation of three different patients. (A1 and A2) The patient diagnosis in red categories with an abnormality score of 98.56% from AI chest radiographs showed that she had pneumonia. (B1 and B2) The patient diagnosis in yellow categories with an abnormality score of 95.11% from the AI chest radiograph showed that she had pneumonia. (C1 and C2) The patient diagnosis in green categories with an abnormality score of 3.54% from AI chest radiograph showed he had pneumonia.*

Test results for diagnosis of pneumonia in patients infected with COVID-19 between radiologists and AI, Lunit INSIGHT CXR Version 3.0 software, following the criteria for separating abnormalities from CXR of Rama Co-RADS [5], had a sensitivity of 97.87% (95%CI 88.71-99.95%), specificity of 99.04% (95%CI 96.59-99.88%) and accuracy of 98.83%. PPV=95.83. % and NPV=99.52%, positive likelihood ratio (+LR) = 102.28, negative likelihood ratio (-LR) = 0.02.

Table 2. *The sensitivity, specificity, and accuracy of AI.*

AI	Detected	Not Detected	Total
Positive	46 (Ture Positive)	2 (False Positive)	48
Negative	1 (False Negative)	207 (True Negative)	208
Total	47	209	256
Sensitivity	97.87% (95%CI 88.71-99.95%)		
Specificity	99.04% (95%CI 96.59-99.88%)		
Accuracy	98.83%		
Positive predictive value (PPV)	95.83%		
Negative predictive value (NPV)	99.52%		
Positive likelihood ratio (+LR)	102.28		
Negative likelihood ratio (-LR)	0.02		

Discussion

The use of imaging in speedy and accurate diagnosis has become extremely critical in the context of the COVID-19 epidemic. This study demonstrated that the commercial AI Lunit INSIGHT CXR Version 3.0 software used was able to identify consolidations associated with pneumonia with a high sensitivity (97.87%) and specificity (99.04%).

Diagnosis of pneumonia in patients infected with COVID-19 requires examination and interpretation of chest radiographs by a team of radiologists, which may take a long time. Due to the limited number of radiologists, it may not be possible to make a timely diagnosis if there are many patients, such as the recent COVID-19 infection. CXRs are the most popularly performed imaging tests; yet, a rapid interpretation of CXRs by radiologists is problematic in hospitals, especially for those with severe lesions [22] and rapid identification of lung infections may result in speedier isolation of patients, potentially reducing the risk of infection spread [23]. Recently, many studies have demonstrated the potential for AI application in radiology as the clinical decision support system (CDSS) or even as a second reading [24] and has great potential for the analysis of large amounts of data. It has played an essential role in preventing the COVID-19 outbreak [25].

For COVID-19 patients, as soon as they receive the treatment, the seriousness of the disease can be reduced. During an ongoing pandemic, chest X-rays were utilized more often, considering their availability and a lower cost [26]. AI in assisting radiologists in diagnosing patients is believed to provide an accurate rate, not a difference from experienced radiologists [19, 27, 25, 28, 29]. With radiologists' workloads increasing, whether AI could be a feasible solution for lowering fatigue and improving the predictive accuracy in an interpreting the diagnosis [30] and it is the other advantage of using AI as non-existence of fatigue, which leads to the risk of errors in interpreting CXRs [31].

The interpretation of CXR, especially regarding pneumonia, is subject to high variability even among radiologists; accordingly, the additional evaluation and highlighting of findings in CXRs by AI is advisable [23]. This AI performed slightly the same level as radiologists, with no statistically significant differences [24], and the AI system can accurately discern between normal and abnormal patients' radiographs and can be used as a triage tool [32]. A study in the same region (Samut Sakhon, central Thailand) in the same year showed that 91.7% of chest radiographs of 629 patients infected with COVID-19 were normal [33]. Our study confirmed that even though there were some false positive and false negative of the AI diagnosis, the amount was still little and likely insignificant for a triage purpose.

Moreover, according to the study of AI Lunit INSIGHT CXR on diagnosis of pneumonia showed no statistically significant differences between AI and radiologists with sensitivity, and specificity of AI of 0.94 (CI95%: 0.94-1.00), 0.90 (CI95%: 0.79-1.00), and 0.95 (CI95%: 0.89-1.00) [24]. Becker et al. [23] study AI can detect pneumonia in chest radiographs with a sensitivity of 95.4%, a specificity of 66.0%, PPV of 80.2% and NPV of 90.8%. Thus, the result from this research can help to confirm the result of the previous studies even though with differences in nationalities.

This study has some limitations. First, it was a retrospective study collected from a database of medical records and chest radiographs of a confirmed COVID-19 patient, with 256 samples from only Nimibutr Pre-Admission Center Between 1 -30 September 2021. This number was very little compared to other studies; however, the researcher employed simple random sampling to select the cases to prevent biases in this study. Second, this study did not measure the accuracy of the radiologists because the study cases were collected from the database. However, all seven radiologists were experts responsible for interpreting the films in the Nimibutr Pre-Admission Center Between 1 -30 September 2021.

Conclusion

The AI of Lunit INSIGHT CXR Version 3.0 software can help read and interpret pneumonia in patients infected with Coronavirus 2019 by sensitivity, specificity, and accuracy equivalent to the interpretation of radiologist results. Therefore, the use of this AI at Nimibutr Pre-Admission Center can assist radiologists in the understanding of CXR. This AI software is recognized and approved for use in helping physicians. In addition, the research results confirm the specificity and accuracy. Moreover, the fact that AI can help read CXR results can be counted as satisfying to confirm the reading results of the first radiologists. Therefore, as the study mainly compared AI with radiologists, it is worth pointing out that it is comparable to the radiologists' reading and thus may potentially be implemented as a decision support or screening tools.

Conflict of interest

The authors declare no conflict of interest.

Acknowledgement

The authors would like to sincerely thank the Neurological Institute of Thailand for providing the database of medical records and chest radiographs and Ms. Chanmeardey Chiv for her assistance in statistical analysis.

References

1. who.int [Internet]. Geneva: WHO; c2023 [cited 2023 Dec 27]. Coronavirus disease (COVID-19) pandemic. Available from: https://www.who.int/emergencies/diseases/novel-coronavirus-2019

2. Thanachotiphan K, Kalyanamitra K, Niyomyaht S, Kakkhanpichonchat T. [Management of Thai Health Service Systems During the Covid-19 Crisis]. J L G ISRRU 2022; 6(2):111-29. Thai.

3. Department of Physical Education, Ministry of Tourism and Sports [Internet]. 2021 [cited 2023 Dec 27]. Opening the Nimibutr Pre-Admission Center ready to support those infected with COVID-19. Available from: https://dpe.go.th/news-preview-431191791858. Thai.

4. Xie X, Zhong Z, Zhao W, Zheng C, Wang F, Liu J. Chest CT for typical coronavirus disease 2019 (COVID-19) pneumonia: relationship to negative RT-PCR testing. Radiology 2020;296:E41-5. doi: 10.1148/radiol.2020200343.

5. Suwatanapongched T, Nitiwarangkul C, Sukkaseam W, Phongkitkarun S. Rama Co-RADS: Categorical Assessment Scheme of Chest Radiographic Findings for Diagnosing Pneumonia in Patients with Confirmed COVID-19. Rama Med J 2022; 44(2):50-62.

6. Benza RL, Gomberg-Maitland M, Elliott CG, Farber HW, Foreman AJ, Frost AE, et al. Predicting survival in patients with pulmonary arterial hypertension: the REVEAL risk score calculator 2.0 and comparison with ESC/ERS-based risk assessment strategies. Chest 2019;156:323-37. doi: 10.1016/j.chest.2019.02.004.

7. Kwee TC, Kwee RM. Chest CT in COVID-19: what the radiologist needs to know. Radiographics 2020;40:1848-65. doi: 10.1148/rg.2020200159.

8. Larici AR, Cicchetti G, Marano R, Merlino B, Elia L, Calandriello L, et al. Multimodality imaging of COVID-19 pneumonia: from diagnosis to follow-up. A comprehensive review. Eur J Radiol 2020;131:109217. doi: 10.1016/j.ejrad.2020.109217.

9. Litmanovich DE, Chung M, Kirkbride RR, Kicska G, Kanne JP. Review of chest radiograph findings of COVID-19 pneumonia and suggested reporting language. J Thorac Imaging 2020;35:354-60. doi: 10.1097/RTI.0000000000000541.

10. Ardakani AA, Kanafi AR, Acharya UR, Khadem N, Mohammadi A. Application of deep learning technique to manage COVID-19 in routine clinical practice using CT images: Results of 10 convolutional neural networks. Comput Biol Med 2020;121:103795. doi: 10.1016/j.compbiomed.2020.103795.

11. Gatt ME, Spectre G, Paltiel O, Hiller N, Stalnikowicz R. Chest radiographs in the emergency department: is the radiologist really necessary?. Postgrad Med J 2003;79(930):214-7. doi: 10.1136/pmj.79.930.214.

12. Jacobi A, Chung M, Bernheim A, Eber C. Portable chest X-ray in coronavirus disease-19 (COVID-19): A pictorial review. Clin Imaging 2020;64:35–42. doi: 10.1016/j.clinimag.2020.04.001.

13. Guo W, Wang J, Sheng M, Zhou M, Fang L. Radiological findings in 210 paediatric patients with viral pneumonia: a retrospective case study. Br J Radiol 2012;85:1385–9. doi: 10.1259/bjr/20276974.

14. Lomoro P, Verde F, Zerboni F, Simonetti I, Borghi C, Fachinetti C, et al. COVID-19 pneumonia manifestations at the admission on chest ultrasound, radiographs, and CT: single-center study and comprehensive radiologic literature review. Eur J Radiol Open 2020;7:100231. doi: 10.1016/j.ejro.2020.100231.

15. Baltazar LR, Manzanillo MG, Gaudillo J, Viray ED, Domingo M, Tiangco B, et al. Artificial intelligence on COVID-19 pneumonia detection using chest xray images. PloS One 2021;16:e0257884. doi: 10.1371/journal.pone.0257884.

16. Hosny A, Parmar C, Quackenbush J, Schwartz LH, Aerts HJWL. Artificial intelligence in radiology. Nat Rev Cancer 2018;18:500-10. doi: 10.1038/s41568-018-0016-5.

17. Syed AB, Zoga AC. Artificial intelligence in radiology: current technology and future directions. Semin Musculoskelet Radiol 2018;22: 540-5. doi: 10.1055/s-0038-1673383.

18. Ávila-Tomás JF, Mayer-Pujadas MA, Quesada-Varela VJ. [Artificial intelligence and its applications in medicine II: current importance and practical applications]. Aten Primaria 2020;53:81-8. Spanish. doi: 10.1016/j.aprim.2020.04.014.

19. Mahatchariyapong P. Evaluation of the diagnostic accuracy of Artigivisl Intelligence detection of pulmonary tuberculosis on Chest Radiograph among outpatients in Maeramard district, Thailand. J Prim Care Fam Med 2022; 4:35-45.

20. Borkowski AA, Viswanadhan NA, Thomas LB, Guzman RD, Deland LA, Mastorides SM. Using artificial intelligence for COVID-19 chest X-ray diagnosis. Fed Pract 2020;37:398-404. doi: 10.12788/fp.0045.

21. Faul F, Erdfelder E, Lang AG, Buchner A. G* Power 3: A flexible statistical power analysis program for the social, behavioral, and biomedical sciences. Behav Res Methods. 2007;39:175-91. doi: 10.3758/bf03193146.

22. Shin HJ, Han K, Ryu L, Kim EK. The impact of artificial intelligence on the reading times of radiologists for chest radiographs. NPJ Digit Med 2023;6:82. doi: 10.1038/s41746-023-00829-4.

23. Becker J, Decker JA, Römmele C, Kahn M, Messmann H, Wehler M, Schwarz F, Kroencke T, Scheurig-Muenkler C. Artificial intelligence-based detection of pneumonia in chest radiographs. Diagnostics (Basel) 2022;12:1465. doi: 10.3390/diagnostics12061465.

24. Vasilev Y, Vladzymyrskyy A, Omelyanskaya O, Blokhin I, Kirpichev Y, Arzamasov K. AI-Based CXR First Reading: Current Limitations to Ensure Practical Value. Diagnostics (Basel) 2023;13:1430. doi: 10.3390/diagnostics13081430.

25. Mei X, Lee HC, Diao KY, Huang M, Lin B, Liu C, et al. Artificial intelligence-enabled rapid diagnosis of patients with COVID-19. Nat Med 2020;26:1224–8. doi: 10.1038/s41591-020-0931-3.

26. Khanna VV, Chadaga K, Sampathila N, Prabhu S, Chadaga R, Umakanth S. Diagnosing COVID-19 using artificial intelligence: A comprehensive review. Network Modeling Analysis in Health Informatics and Bioinformatics 2022;11(1):25.

27. Harmon SA, Sanford TH, Xu S, Turkbey EB, Roth H, Xu Z, et al.Artificial intelligence for the detection of COVID-19 pneumonia on chest CT using multinational datasets. Nature communications. 2020 Aug 14;11(1):4080. doi: 10.1038/s41467-020-17971-2.

28. Noisiri W, Vijitrsaguan C, Lertrojpanya S, Jiamjit K, Chayjaroon J, Tantibundhit C. Sensitivity and Specificity of Artificial Intelligence for Chest Diagnostic Radiology in Lung Cancer. J Depart Med Ser 2021;45(4):55-61.

29. Dorr F, Chaves H, Serra MM, Ramirez A, Costa ME, Seia J, et al. COVID-19 pneumonia accurately detected on chest radiographs with artificial intelligence. Intell Based Med 2020;3:100014. doi: 10.1016/j.ibmed.2020.100014.

30. Alexander R, Waite S, Bruno MA, Krupinski EA, Berlin L, Macknik S, et al. Mandating limits on workload, duty, and speed in radiology. Radiology 2022 ; 304:274-82. doi: 10.1148/radiol.212631.

31. Taylor-Phillips S, Stinton C. Fatigue in radiology: a fertile area for future research. Br J Radiol 2019;92:20190043. doi: 10.1259/bjr.20190043.

32. Van Beek EJR, Ahn JS, Kim MJ, Murchison JT. Validation study of machine-learning chest radiograph software in primary and emergency medicine. Clin Radiol 2023 ;78:1-7. doi: 10.1016/j.crad.2022.08.129.

33. Trimankha P, Lakkana Jirapong L, Rungsin R, Autravisittikul O, Deesuwan PDM, Mekavuthikul Y, et al. Utility of screening chest radiographs in patients with asymptomatic and mildly symptomatic COVID-19 at a field hospital in Samut Sakhon, Thailand. ASEAN J Radiol [Internet]. 2021[cited 2023 Dec 28];22(2):05-20. Available from: https://www.asean-journal-radiology.org/index.php/ajr/article/view/119.

THE ASEAN JOURNAL OF RADIOLOGY
ISSN 2672-9393

Case Report

Faecaloid like material in the urinary bladder: A radiological finding in a patient with urinary tract fungal bezoar infection

Abdul Hadi Shamsul Bahrin, M.D.[(1)]
Ahmad Aizuddin Mohamad Jamali, M.D.[(2)]
Khairil Amir Sayuti, M.D.[(2)]
Juhara Haron, M.D.[(2)]
Zul Khairul Azwadi Ismail, M.D.[(2)]
Othman Puteh, M.D.[(2)]
Mohamed Ashraf Mohamed Daud, M.D.[(3)]
From [(1)] Medical Officer, Department of Radiology, School of Medical Sciences, Universiti Sains Malaysia, Kubang Kerian, Kelantan, Malaysia.
[(2)] Radiologist, Department of Radiology, School of Medical Sciences, Universiti Sains Malaysia, Kubang Kerian, Kelantan, Malaysia.
[(3)] Urologist, Department of Surgery, School of Medical Sciences, Universiti Sains Malaysia, Kubang Kerian, Kelantan, Malaysia.
Address correspondence to A.A.M.J.(e-mail: aizuddinjamali@usm.my)

Received 30 June 2023; revised 10 October 2023; accepted 10 October 2023
doi:10.46475/asean-jr.v24i3.870

Abstract

Fungal colonization or infection of the urinary tract system is caused by *Candida* species. Fungal intravesical bezoars, however, are extremely rare. Radiological features may mimic the appearance of emphysematous cystitis, which makes the radiological diagnosis challenging. We present an unusual case of urinary bladder fungal bezoar caused by *Candida tropicalis.*

Keywords: Computed tomography, Cystoscopy, Radiography, Urinary tract fungal bezoar.

Introduction

Infection of the urinary tract due to candida is rare and occurs in about 2% of the urinary tract infection [1,2]. It usually happened in a host with a compromised immune function. Predisposing factors include diabetes mellitus, immunocompromise, a steroid therapy, a neurogenic bladder, antibiotic usage, and an indwelling Foley catheter. A rare complication that might happen is the formation of a fungus ball leading to urinary tract obstruction. The radiological appearance of urinary tract bezoar infection is the purpose of the discussion of this rare entity.

Case summary

A 47-year-old male patient with underlying type 2 diabetes mellitus and a history of bladder calculus was referred to the emergency department for intermittent macroscopic hematuria with lower urinary tract symptoms. The patient had no fever and dysuria. Blood investigations showed no leukocytosis, creatinine of 176 umol/L and hemoglobin of 10.7 g/dl. A urinalysis showed mixed pus and red blood cells. The patient was started empirically on cefuroxime with a provisional diagnosis of urinary tract infection secondary to possible urinary tract calculi.

The initial radiograph showed a large amount of faecal-like material seen in the pelvic region (Figure 1). Subsequently, the patient underwent plain computed tomography of kidneys, ureters, and the urinary bladder. The study showed a dilated left pelvicalyceal system with multiple faecaloid materials within the left renal pelvis until the proximal ureter (Figure 2). The Axial and coronal section showed distended urinary bladder with numerous faecaloid materials which caused obstruction of the bilateral vesicoureteral junction (Figure 3 and 4). The faecaloid material appeared like faeces within the colon. No perinephric, periureteric or peri-vesical fat stranding was seen. Adjusting to wide windowing contrast of the CT image could depict a spherical shape of fungal bezoar much better[3](Figure 5).

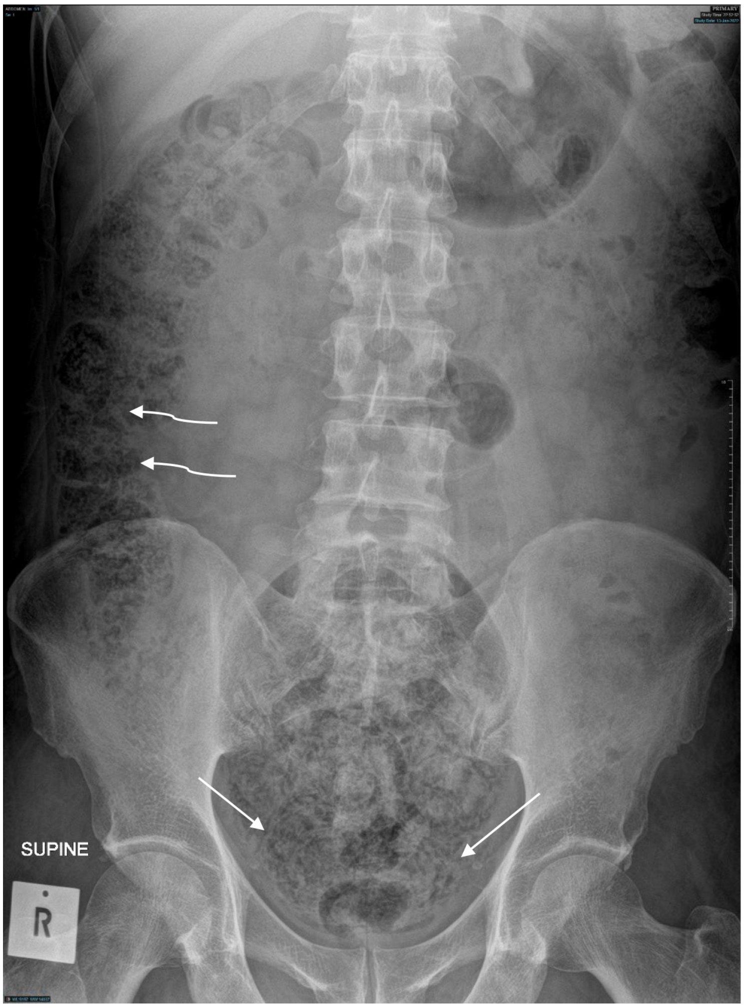

Figure 1. *Supine abdominal radiograph. It showed faecal loaded appearance at the pelvic region (arrow) similar to faecal loaded seen along the ascending colon (curve arrow).*

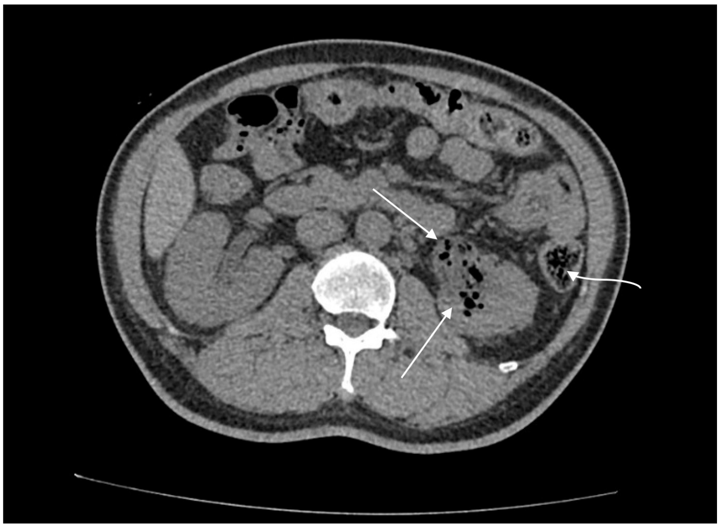

Figure 2. *Axial image of plain computed tomography at the renal level. The dilated left pelvicalyceal system with multiple fecaloid materials within the left renal pelvis(arrow) until the proximal ureter was observed. Note that it appears similar to faecal materials within the descending colon (curve arrow).*

Figure 3. *Axial image of plain computed tomography at the urinary bladder level. The distended urinary bladder with numerous fecaloid materials (arrow) which caused obstruction of the bilateral vesicoureteral junction was observed.*

Figure 4. *Coronal image of plain computed tomography. It showed faecaloid materials filling the urinary bladder and the left pelvicalyceal system(arrow). Note how it appears similar to the faecal materials in the sigmoid and the descending colon (curve arrow).*

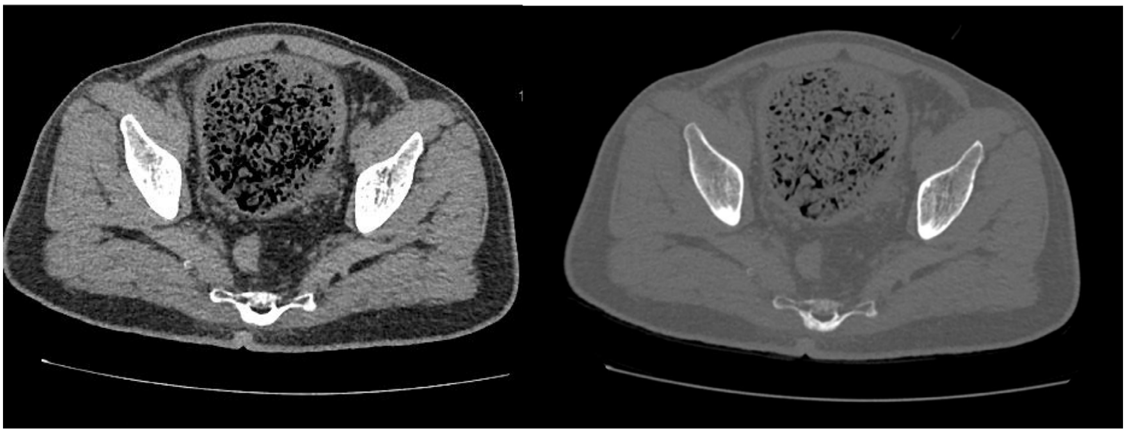

Figure 5. *Same axial images of plain computed tomography were shown in different windowing settings. The left image showed narrow windowing (WW400, WL40), while the right image showed more wider windowing (WW1000, WL100). The right image showed a better delineate spherical shape of fungal bezoars.*

Urine cultured yielded *Candida tropicalis* and intravenous micafungin were initiated. Subsequent cystoscopy was performed which shows numerous matrix stones consisting of fungal bezoar with minimal blood clots (Figure 6). The matrix stones and blood clots were evacuated endoscopically using an ellick evacuator. Approximately 400g of matrix stones were evacuated (Figure 7). Chronic cystitis features were noted in the bladder wall. A biopsy from the bladder wall was taken. Microscopic examination of the biopsy showed features of fungal cystitis.

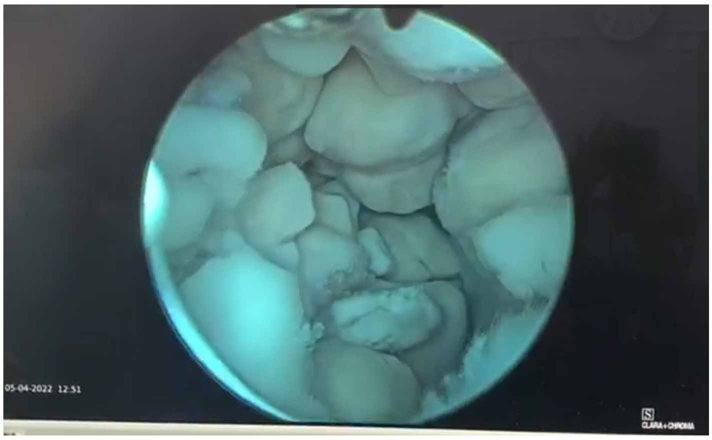

Figure 6. *Cystoscopy showed matrix stones consisting of fungal bezoars.*

Figure 7. *The picture showed content evacuated from the urinary bladder. Approximately 400g of matrix stones were evacuated with blood clots.*

Discussion

Bezoar fungal formation is a rare complication with only twenty cases reported since their first report in 1961 [4]. Immunocompromised patients such as diabetes mellitus, prolonged use of steroid therapy, broad spectrum antibiotics, a neurogenic bladder and an indwelling Foley catheter are common predisposing factors [5]. Like in our patients which have poor control of diabetes mellitus as a risk factor causing immunodeficiency and glycosuria, a good medium for fungal growth [6].

In terms of radiological imaging, intravenous urography can demonstrate presence of filling defects in the pelvicalyceal system or in the urinary bladder, but these findings lack specificity for the diagnosis to be made [2,7]. Sonographic appearance shows echogenic masses with or without posterior acoustic shadowing in contrast to the anechoic urine in the pelvicalyceal system [7]. Observing the CT image with the soft tissue window, we may see faecaloid material in the urinary bladder like in this case. The differential diagnosis includes colovesicular fistula, but differentiation can be established clinically. If we adjust wider window width, we can better depict a spherical shape of the numerous fungal bezoars packing in the urinary bladder. Window setting is a helpful method for diagnosing fungal bezoar.

Operative and non-operative management could be used for the treatment of this entity. Rohloff et al. [8] performed a study in which fifteen case reports were compared and concluded that both options had advantages. The operative management consists of cystoscopy bladder wash out and resection of the bezoars, while the non-operative management includes systemic antifungal medication, local antifungals, or spontaneous expulsion.

Conclusion

The case of urinary bladder fungal bezoar infection should be suspected in patients with compromised immune status. Radiological features of the fungal bezoar mimic the appearance of the faecal material in the large bowels. Adjusting windowing technique to a more wider windowing level may allow clinicians and radiologist to get an accurate diagnosis and can better depict the appearance of the fungal ball, thus helping the managing team to give the best treatment for the patient.

Conflicts of interest

The authors have no potential conflicts of interest to report regarding this presentation.

References

1. Fisher JF, Chew WH, Shadomy S, Duma RJ, Mayhall CG, House WC. Urinary tract infections due to Candida albicans. Rev Infect Dis 1982;4:1107–18. doi: 10.1093/clinids/4.6.1107.

2. Comiter CV, McDonald M, Minton J, Yalla SV. Fungal bezoar and bladder rupture secondary to candida tropicalis. Urology 1996;47:439-41. doi: 10.1016/S0090-4295(99)80470-1.

3. Henning GM, Chow AK. A bladder full of bezoars: A bizarre finding on CT imaging. Urology 2020;141:e28-9. doi: 10.1016/j.urology.2020.04.013.

4. McDonald DF, Fagan CJ. Fungus balls in the urinary bladder. Case report. Am J Roentgenol Radium Ther Nucl Med 1972;114:753–7. doi: 10.2214/ajr.114.4.753.5.

5. Kumari P, Kan VL. Bladder rupture attributed to candida albicans bezoar. Infect Dis Clin Pract 10:271-2. doi:10.1097/00019048-200106000-00006.

6. Takemura K, Takazawa R, Kohno Y, Yoshida S, Kato H, Tsujii T. Vesical fungus balls (fungal bezoars) by Candida albicans mimicking urothelial carcinoma in a patient with diabetic neurogenic bladder. Urol Case Rep 2018; 18:50–1. doi: 10.1016/j.eucr.2018.03.005.

7. Kale H, Narlawar RS, Rathod K. Renal fungal ball: an unusual sonographic finding. J Clin Ultrasound 2002;30:178–80. doi: 10.1002/jcu.10049.

8. Rohloff MA, Shakuri-Rad J, Dehaan AP. Candida bezoars in adults: determining optimal management. J Endourol Case Rep 2017;3:45–8. doi: 10.1089/cren.2017.0021.

Case Report

What is cheesier than a Whitmore's liver? An accidental diagnosis of melioidosis

Harika Vangara, M.D. (1)
Jayaprada Rangineni, M.D. (2)
Venkata Rami Reddy Vutukuru, M.D. (3)
Sarala Settupalli, M.D. (4)
Bhavya Kotapati, B.Sc. (5)
From (1) Department of Microbiology, Kasturba Medical College, Mangalore, Manipal Academy of Higher Education, Manipal, India,
(2) Department of Microbiology, Sri Venkateswara Institute of Medical Sciences, Tirupati, A.P, India,
(3) Department of Surgical Gastroenterology, Sri Venkateswara Institute of Medical Sciences, Tirupati, A.P, India,
(4) Department of Radiology, Sri Venkateswara Institute of Medical Sciences, Tirupati, A.P, India,
(5) Department of Microbiology, Sri Venkateswara Institute of Medical Sciences, Tirupati, A.P, India.
Address correspondence to H.V.(e-mail: mythili130791@gmail.com)

Received 21 September 2023; revised 4 November 2023; accepted 4 November 2023
doi:10.46475/asean-jr.v24i3.884

Abstract

Despite the endemicity of Melioidosis in India, there were no official reports of the same case in our area which can be attributed to a lack of awareness of its occurrence in this geographic region, varied manifestations and consequent misdiagnosis. We report a case of Melioidosis from Tirupati, Andhra Pradesh. A diabetic male presented with fever, jaundice, and breathlessness. Radiological investigations revealed abscesses in the liver and spleen with a swiss cheese or honey comb appearance on CECT abdomen. The patient rapidly succumbed to the illness even with appropriate antibiotics in view of delayed presentation. Pus aspirated from the patient isolated *Burkholderia* species which was later confirmed through molecular methods as *Burkhloderia pseudomallei.* Hence, it is advised to consider Melioidosis as a potential infection in this region, for a timely and appropriate management of the patient's conditions.

Keywords: *Burkhloderia pseudomallei,* Liver abscess, Melioidosis.

Introduction

"Melioidosis" (distemper of the horses) or "Pseudoglanders" (Glanders like) or "Whitmore's disease" (in honor of the pathologist who first documented) or the sinister name "Vietnam time bomb" (occurrence in USA soldiers returned from Vietnam war) is caused by *Burkholderia pseudomallei,* a Gram negative non-fermenting bacillus, also called the "Great Mimicker of diseases", because of its various manifestations ranging from fever of an unknown origin to sepsis, the most common being community acquiring pneumonia [1]. The disease is spread through inhalation, ingestion and inoculation with a surge in cases during the rainy season [2]. Melioidosis is endemic to the tropical belt of India, Pakistan, the Philippines, Malaysia, and other South Asian countries stretching to northern Australia and an approximate annual incidence of 52000 cases [3]. With the major risk factors for Melioidosis, namely, excessive alcohol consumption, cases of diabetes, chronic lung disease and chronic renal disease on the rise, it is safe to assume the burden of this disease would be escalating henceforth [4]. Not geographically reported from this particular area in Southern India, the microbiological suspicion lead to reconsideration of the patient's typical radiographic findings to be of hepatic Melioidosis by the radiologist.

Case Summary

A 42-year-old male patient who is a type – 2 diabetic, smoker and alcoholic was admitted in our hospital with complaints of fever with chills, cough, and breathlessness for 10 days. Prior to this, the patient was admitted in another hospital for one week due to yellowish discoloration of skin, passing yellow-colored stools, abdominal bloating, right sided abdominal pain, and nausea.

He was diagnosed with jaundice, multiple liver abscesses and splenic infarct with mild pleural effusion and was treated for those conditions. No further reports could be retrieved regarding the patient treatment regarding his previous hospitalization. He was transferred to our hospital for the further management in view of worsening patient condition.

The patient was febrile (101.4° F) and had icterus. Tenderness in right hypochondrium with hepatosplenomegaly was noted on palpation of the abdomen. On auscultation, diffuse crepitations were heard over the entire right lung. Other system examinations were normal.

Blood investigations

Blood culture and sensitivity was sterile after one week of aerobic incubation. Serum procalcitonin was >100 ng/mL.

Liver function test indicated impaired functioning with serum alkaline phosphatase – 158 IU/ml (90 to 120 IU/ml), serum alanine amino transferase (SGPT/ALT) – 42(10 to 40 IU/ml), serum aspartate amino transferase (SGOT/AST) – 85 (10 to 35 IU/ml). Serum bilirubin conjugated was 2.3 (0.1 to 0.3mg/dL) and serum bilirubin total was 4.4 (0.2 to 1.1 mg/dL).

Total leukocyte count was 11800 cells /mm^3 with neutrophilia – 86 % (50 – 70%) and lymphocytopenia – 7% (20-40%). The patient had anemia with hemoglobin - 6.4 mg/dL and red blood cells – 2.14 (4.5 – 6 million/ mm^3). Erythrocyte sedimentation rate was 110 mm/ first hour (0 to 9).

Radiological investigations

A contrast enhanced CT scan (CECT) of the abdomen and chest was conducted in which multiple liver and splenic abscesses with massive hepatosplenomegaly were noted on the coronal plane (Figure 1). In Figure 2, a large focal lesion with multiple cystic areas and enhancing walls is seen giving a characteristic honeycomb appearance. It can be seen that some of the abscesses are coalescing to give a cavity in segments V, VII, VIII and IV. Similar lesions are also noted in the spleen. Chest X ray showed an elevated right dome of diaphragm with moderate right sided pleural effusion that was loculated. Figures 3 and 4 show the culture plate with growth of pale pink colonies with metallic sheen resembling *Burkholderia pseudomallei*, along with Gram stain (safety pin appearance).

Under the ultrasound guidance, aspiration of the abscess was implemented which was sent to Microbiology for Gram stain, culture and antimicrobial susceptibility testing. A pigtail catheter was inserted into the liver to drain the abscess. The patient was started on Inj. Piperacillin tazobactam 4.5 gm TID and Inj. metronidazole 500 mg TID along with a supportive therapy.

As soon as the sample was received, Gram stain was done, which revealed plenty of neutrophils with occasional Gram-negative bacilli whose peculiar morphology could not be ascertained. Aerobic culture was done on blood, MacConkey agar and nutrient agars. After 24 hours of incubation, it revealed pale non-lactose fermenting colonies on MacConkey which were slow oxidase positive. On Blood agar, the colonies were translucent and non-hemolytic which were wrinkled with prolonged incubation. No pigmentation was observed on any culture media, while Gram stain from the culture plate revealed typical Gram-negative bacilli with a notable safety pin appearance (Figure 4).

The patient continued to be tachypneic and an X-ray chest revealed haziness of the entire right lung. In view of worsening oxygen saturation levels, the patient was intubated the following day and antibiotics changed to meropenam 1.5 gm TID and tigecycline 50 mg OD, by which time the preliminary report was conveyed to the treating surgeon. The fever was nonresponding despite the new regimen and the patient succumbed to the illness four days later due to sepsis and multiorgan dysfunctions.

The culture report of aspirated pus revealed *Burkholderia* species which was sensitive to cefoperazone-sulbactam, ceftazidime, chloramphenical, ciprofloxacin, cotrimoxazole, imipenem and meropenam. The isolate was resistant to amikacin, gentamicin, cefotaxime and netilmicin. The isolate was later sent to the Centre for Emerging and Tropical Diseases in Manipal, Karnataka for confirmation where, *Burkholderia pseudomallei* was confirmed by specific monoclonal antibody-based latex agglutination and type three secretion system (T3SS1) gene polymerase chain reaction (PCR).

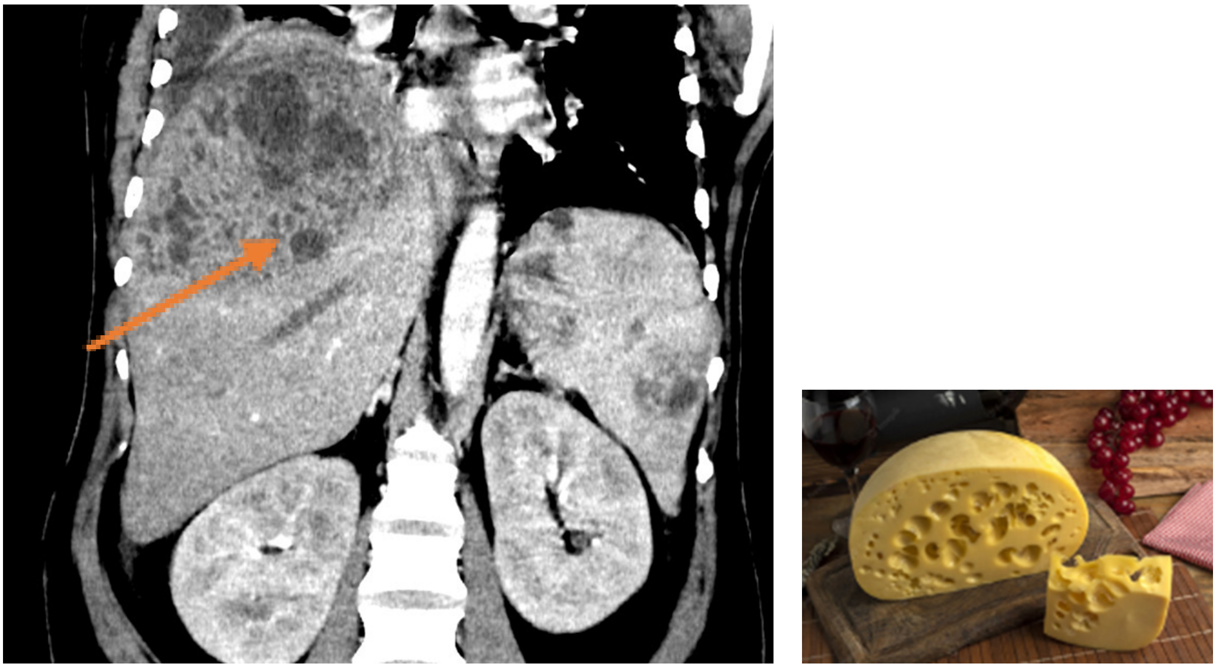

Figure 1. *Coronal abdominal CECT showing massive hepatomegaly and swiss cheese appearance of the liver abscess and similar findings in the spleen.*

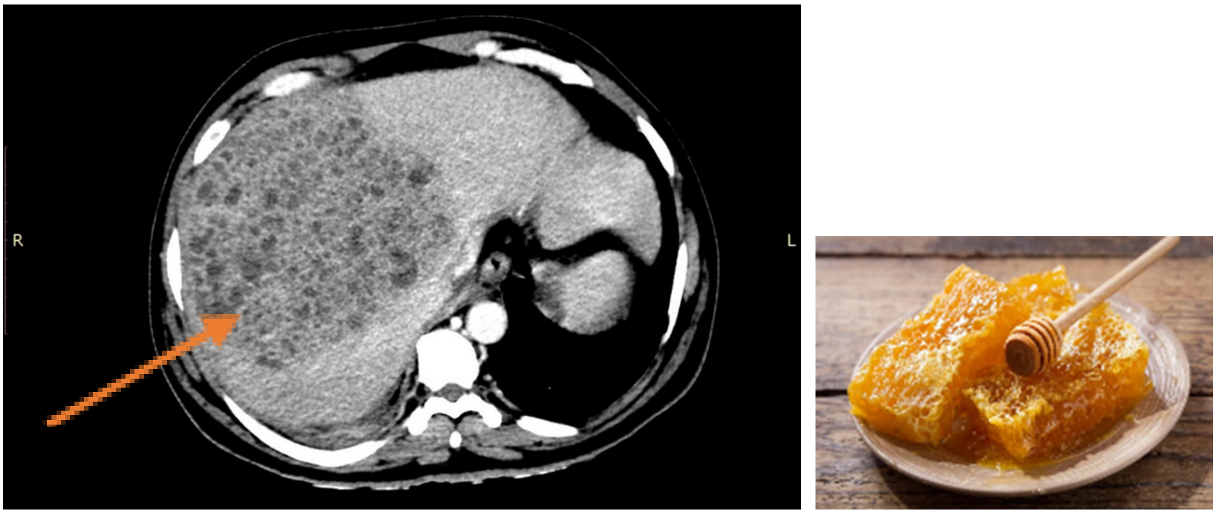

Figure 2. *Transverse abdominal CECT at the level of liver showing honeycomb appearance of the abscess.*

Figure 3. *MacConkey and Sheep blood agar plates showing growth of Burkholderia pseudomallei.*

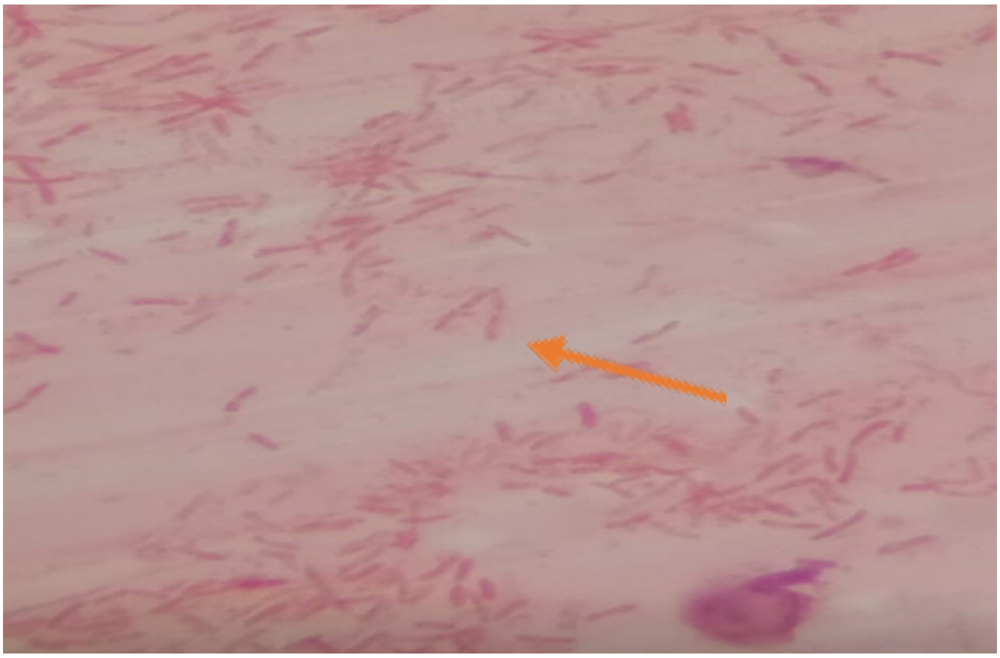

Figure 4. *Gram stain showing safety pin appearance of Burkholderia pseudomallei.*

Discussion

Burkholderia pseudomallei, an environmental saprophyte causing Melioidosis, has been classified as an agent of bioterrorism by the Centre for Disease Control (CDC) in nature of its easy transmissibility and high fatality (6). Paddy cultivating countries are known for their endemicity of Melioidosis, regardless of which, it is grossly under reported for diverse reasons. A lack of awareness of the Melioidosis burden in this geographic area due to under reporting resulted in an almost missed diagnosis despite typical radiographic features. While blood cultures may not be always positive, the culture of samples onto blood and MacConkey agars from specific site may be helpful. Colonies are 1-2 mm in diameter with a wrinkled surface and no haemolyis on Blood agar while on MacConkey colonies are pale, with a pinkish metallic sheen and oxidase positive. Unless looked with suspicion, these features can be easily misinterpreted as Pseudomonas or aerobic spore bearers. Automated tools like MALDI -TOF or VITEK 2 may not be definitive in identification of the organism as it happened with the current isolate. Amoxycillin clavulanate sensitivity and polymyxin resistance are more clues towards *Burkholderia pseudomallei.*

Most cases presented in the critical stages of illness with multiple internal organ abscesses, pneumonia and sepsis [7]. The chronic disease occurs because of the organism's ability to survive inside macrophages, and can mimic granulomatous diseases [8]. Early diagnosis and prompt administration of antibiotics can cut down the mortality rate drastically [7]. This is possible with a radiological diagnosis like CT or ultrasonography as microbiology can take more than 24 hours for the earliest definitive diagnosis. The revealing features of Melioidosis on CECT would be a thick-walled abscess with cavitation akin to Swiss cheese or honeycomb pattern, typically seen in the internal organs like lungs, liver and spleen [9,10]. Cluster sign can be used to describe the multiple small abscesses coalescing to form a single large abscess especially in liver [9]. The definitive diagnosis remains to be culture and confirmation with PCR.

The rate of recurrence can be 25% and is often fatal even in people who have been treated for Melioidosis [11]. Hence, the treatment is done in two phases:

1. Intensive phase (for sepsis) - Ceftazidime (2gm, TID) is the drug of choice for 10-14 days. Meropenem (1g, TID) in case of worsening condition, for >four weeks,

2. Eradication phase (prevent relapse) - Cotrimoxazole (800/160mg, BD) for three to six months. Amoxiclav in case of resistance or allergy to cotrimoxazole.

Despite invitro susceptibility, a clinical failure can occur for various reasons like overwhelming sepsis or biofilm production [5]. This calls for newer, quicker diagnostic methods and an increase in awareness of the burden, presentation and management of Melioidosis.

Conclusion

Melioidosis may escape diagnosis due to a lack of awareness of its occurrence. *Burkholderia* should be considered in case of Gram-negative bacteria which is non-fermentative, amoxicillin-clavulanate sensitive and polymyxin resistant. Prompt treatment with ceftazidime or meropenem can reduce mortality.

Conflicts of interest

None

Funding

None

Acknowlegments

Vandana K E (Professor and HOD, KMC Manipal), Dr. Gurlal Singh (M. Ch 1st year SGE, SVIMS), and Dr. M Harsha Choudhary (DM ID, KMC Manipal).

References

1. Mohapatra PR, Mishra B. Burden of melioidosis in India and South Asia: Challenges and ways forward. Lancet Reg Health Southeast Asia 2022;2:100004. doi: 10.1016/j.lansea.2022.03.004.

2. Koshy M. Melioidosis: an emerging infection in India. Curr Med Issues 2020;18:94-7.

3. Limmathurotsakul D, Golding N, Dance DA, Messina JP, Pigott DM, Moyes CL, et al. Predicted global distribution of Burkholderia pseudomallei and burden of melioidosis. Nat Microbiol 2016; 1:15008. doi: 10.1038/nmicrobiol.2015.8.

4. Savaj P, Shaw T, Munim FC, Mukhopadhyay C. Melioidosis in Gujarat: a neglected tropical disease. Trop Doct 2020;50:373-5. doi: 10.1177/0049475520928219.

5. Mukhopadhyay C, Shaw T, Varghese GM, Dance DAB. Melioidosis in South Asia (India, Nepal, Pakistan, Bhutan and Afghanistan). Trop Med Infect Dis 2018;3:51. doi: 10.3390/tropicalmed3020051.

6. Vinayan S, Bhat UP. Clinical, epidemiological and microbiological profile of a potentially pathogenic environmental saprophyte, Burkholderia pseudomallei; at a Tertiary Care Hospital in Coastal India. J Pure Appl Microbiol 2022;16:193-200.

7. Selvam K, Ganapathy T, Najib MA, Khalid MF, Abdullah NA, Harun A, et al. Burden and risk factors of melioidosis in Southeast Asia: a scoping review. Int J Environ Res Public Health 2022;19:15475. doi: 10.3390/ijerph192315475.

8. Wiersinga WJ, Virk HS, Torres AG, Currie BJ, Peacock SJ, Dance DAB, et al. Melioidosis. Nat Rev Dis Primers 2018;4:17107. doi: 10.1038/nrdp.2017.107.

9. Burivong W, Wu X, Saenkote W, Stern EJ. Thoracic radiologic manifestations of melioidosis. Curr Probl Diagn Radiol 2012;41:199-209. doi: 10.1067/j.cpradiol.2012.01.001.

10. Harsha M, Tirlangi PK, Varma M, Mukhopadhyay C. Dealing with the honey trap: a case of hepatic melioidosis. QJM 2023; Jul 18:hcad175. doi: 10.1093/qjmed/hcad175.

11. Dance D. Treatment and prophylaxis of melioidosis. Int J Antimicrob Agents 2014;43:310-8. doi: 10.1016/j.ijantimicag.2014.01.005.

Perspectives

Responsibility of the radiologists as a clinician: RCRT perspective and short message of the ESR International Forum 2023, Vienna, Austria

Tawika Kaewchur, M.D., FANMB.[(1) (2) (3)]
From [(1)]Division of Nuclear Medicine, Department of Radiology,
[(2)]PET/CT and Cyclotron Center, Center for Medicine Excellence,
Faculty of Medicine, Chiang Mai University, Thailand.
[(3)] Board of Directors, Royal College of Radiologists of Thailand, Bangkok, Thailand.
Address correspondence to T.K. (e-mail: tawika.k@cmu.ac.th)

Received 30 August 2023; accepted 5 September 2023
doi:10.46475/asean-jr.v24i3.875

Introduction

The European Society of Radiology (ESR) internal forum is held in the European Congress of Radiology (ECR) every year and this year, under the theme "Responsibility of the Radiologists as a Clinician", on March 3, 2023. The representatives of twenty-two international societies were invited to present their perspectives and discussions as ESR's global society stakeholders.

The "Responsibility of the Radiologists as a Clinician" was selected by ESR for sharing and engaging in deep discussions this year to enhance and emphasize diagnostic radiologists' value in engagement with referrers and directly answering patients' questions and offering explanations. From Thailand, both Assistant Professor Jaturon Tantivatana and I were the representatives of the Radiological Society of Thailand (RST) and the Royal College of Radiologists of Thailand (RCRT), respectively, to give the presentation and discussion on this topic.

A group photo of panellists in The European Society of Radiology (ESR) international forum 2023, Vienna International Conference Center (VIC), Vienna, Austria.

Roles of Diagnostic Radiologists as a Clinician: The Royal College of Radiologists of Thailand (RCRT) Perspective

A radiologist is a medical professional specializing in using imaging to diagnose and guiding the management and treatment. There are four significant specialists in radiology, including diagnostic radiologists, interventional radiologists (both body and neuroradiology), radiation oncologists and nuclear medicine physicians. Prominent roles as a clinician in direct contact with patients appear in interventional radiologists, radiation oncologists and nuclear medicine physicians. These three specialists use radiation for the objective of treatment in different ways.

With the dynamic advancement of radiological technologies, the role of traditional diagnostic radiologists in image interpretation to guide diagnosis may no longer be sufficient in the modern healthcare system. Therefore, we would enhance our positions in the patient care team by expanding our roles in the following:

1. Health delivery in disease screening,
2. Policy and management in radiation safety,
3. Research collaboration in developing innovations.

Health delivery in disease screening

Health promotion and disease screening for early abnormality detection are critical in modern medicine. Diagnostic imaging is the objective evidence for gross abnormality in the human body. Therefore, radiology investigations would be an effective disease screening tool.

Regarding the increased incidence of breast cancer in Thailand, diagnostic radiologists can be a considerable part of screening tool providers through mammography. This is because mammography shows highly cost-effective investigation with high sensitivity and specificity in detecting breast cancer. In addition, well-experienced technologists also play an essential role in generating good-quality images.

Liver ultrasonography is a powerful non-radiation tool in the early detection of parenchymal liver disease and primary liver cancers, e.g. hepatocellular carcinoma in cirrhotic liver and liver-fluke-associated cholangiocarcinoma in Northeastern Thailand. In addition, diagnostic radiologists can transfer these ultrasonography techniques and skills to general practitioners to promote health screening in remote areas.

Policy and management in radiation safety

Because of the increasing use of ionizing radiation, e.g. a plain radiograph and computed tomography (CT), as the screening, diagnosing and follow-up tool for many diseases, radiologists would be a leader in implementing radiation safety policies and establishing the radiation practice guideline at the national or societal level to minimize radiation exposure to be as low as possible without loss of adequate imaging quality. In addition, the centralized radiation exposure data collection and analysis would help promote radiation exposure monitoring and adjust image acquisition protocol to reduce unnecessary radiation exposure to patients and workers globally. Radiologists can contribute to the expansion of the responsibility in quality management, radiation-used appropriateness, and patient safety.

Research collaboration in developing innovations

Continuous lifelong education is essential in the dynamic world nowadays. Research collaboration in developing innovations is vital in today's world where technology disruption has become pervasive. Artificial Intelligence, or AI, is becoming more popular in helping with imaging diagnosis, and its development needs research collaboration support. Furthermore, extensive pool data analysis and validation are necessary to develop AI for image diagnosis. Radiologists also play a huge role in developing innovations related to diagnostic radiology and treatment techniques to lean our working process, particularly in limited-personal numbers or facilities and widespread emerging disease burdens.

Essential Skills for Clinical Radiologists

As clinical radiologists, we need to combine the knowledge of anatomy, medical understanding of the clinical context, pathology and the principle of imaging technique for diagnosis, and decrease error. There are many essential skills for radiologists in the era of modern medicine, including:

- Good communication and relationship,
- Problem-solving and decision-making,
- Cooperation in radiological teamwork,
- Cooperation in the multidisciplinary patient-care team,
- Organization.

Roles of Diagnostic Radiologists as a Clinician: International Forum Discussion from Other Societies

- Radiological Society of North America
- American College of Radiology
- Canadian Association of Radiologists
- Inter-American College of Radiology
- Mexican Federation of Radiology and Imaging
- Mexican Society of Radiology and Imaging
- Colombian Association of Radiology
- Brazillian College of Radiology and Diagnostic Imaging
- Radiological and Diagnostic Imaging Society of Sao Paolo
- Egyptian Society of Radiology and Nuclear Medicine
- Moroccan Society of Radiology
- Asian Oceanian Society of Radiology
- European Society of Radiology
- Indian Radiological and Imaging Association
- Radiological Society of Saudi Arabia
- Radiological Society of Thailand
- Chinese Society of Radiology
- Japan Radiological Society
- Korean Society of Radiology
- Royal Australian and New Zealand College of Radiologists
- International Society of Radiology

The consensus perspectives of the societies above include:

1. Direct contact with the patients while performing ultrasonography,
2. Keeping communication with referral physicians,
3. Establishing guidelines to improve quality and standardization.

Direct contact with the patients while performing ultrasonography

The sonographic probe appears to be a radiologist's stethoscope for disease screening, diagnosing, answering specific clinical questions and guiding non-invasive procedures. Other than that, direct communication during examination and verbal communication with the referring physicians help improve the quality of reports. Setting up outpatient units, e.g. thyroid radiology, breast imaging and interventional radiology, is another option to enhance a clinical radiologist's role and make it more visible.

Keeping communication with referral physicians

Other than direct verbal reports to the referral physicians, communication in the multidisciplinary care team or during the conference is another option to light up a radiologist's role and to express professionalism. Being a part of a patient care team and advising other medical professionals, particularly general practitioners, is essential in the new era of radiology with innovations.

Establishing guidelines to improve quality and standardization

To improve quality and standardization, developing and implementing the imaging investigation guidelines are essential for the health care system, together with the awareness of unnecessary radiation exposure. Radiologists should lead this working group, by incorporating radiologic technologists, medical physicists, and other related medical professionals.

Conclusion

In the ever-changing world, radiologists must come out of the reading room to expand their leadership roles in disease screening, radiation safety policy, research collaboration in developing radiology innovations, and continuing professional development.

Funding

Royal College of Radiologists of Thailand.

THE ASEAN JOURNAL OF RADIOLOGY
ISSN 2672-9393

Perspectives

Mission to study x-rays emitted from the most violent events in the universe

Arthur E Brown, M.D., M.P.H.
From Faculty of Medical Technology, Mahidol University, Bangkok, Thailand.
Address correspondence to A.E.B.(E-mail: aebrown800@gmail.com)

Received 7 December 2023; revised 7 December 2023 ; accepted 26 December 2023
doi:10.46475/asean-jr.v24i3.891

Keywords: Cosmic x-rays, X-ray telescope, XRISM.

In September of 2023, a bus-size x-ray telescope was launched into low-Earth orbit from the Japanese Space Center located on an island off the country's southern tip. This 2300 Kg satellite (Figure 1) called XRISM (X-Ray Imaging and Spectroscopy Mission; pronounced 'crism') now orbits around the Earth every 96 minutes at an altitude of 550 Km. XRISM is led by the Japan Aerospace Exploration Agency (JAXA) in collaboration with the U.S. National Aeronautics and Space Administration (NASA) and the European Space Agency.

Figure 1. *Artist's depiction of XRISM telescope. Credit: NASA website (https://heasarc.gsfc.nasa.gov/docs/xrism/gallery/index.html), accessed 5 Dec 2023.*

X-rays from space do not penetrate the Earth's atmosphere (Figure 2), protecting humans but also limiting their study. In the 1960s and 70s, rockets and then satellites overcame this limitation and allowed x-ray detectors to be utilized above the atmosphere. The most successful so far is NASA's Chandra X-ray Observatory which was launched in 1999. But it is aging and plans were made to replace it with Japan's Hitomi satellite which was launched in March of 2016. But after collecting data for only one month (Figure 3), control of Hitomi was unfortunately lost and the satellite broke up in late April of that year. Facing a multi-year gap in the ability to carry out x-ray astronomy, JAXA and NASA approved a rebuild (with improvements) of the Hitomi, the new version becoming XRISM.

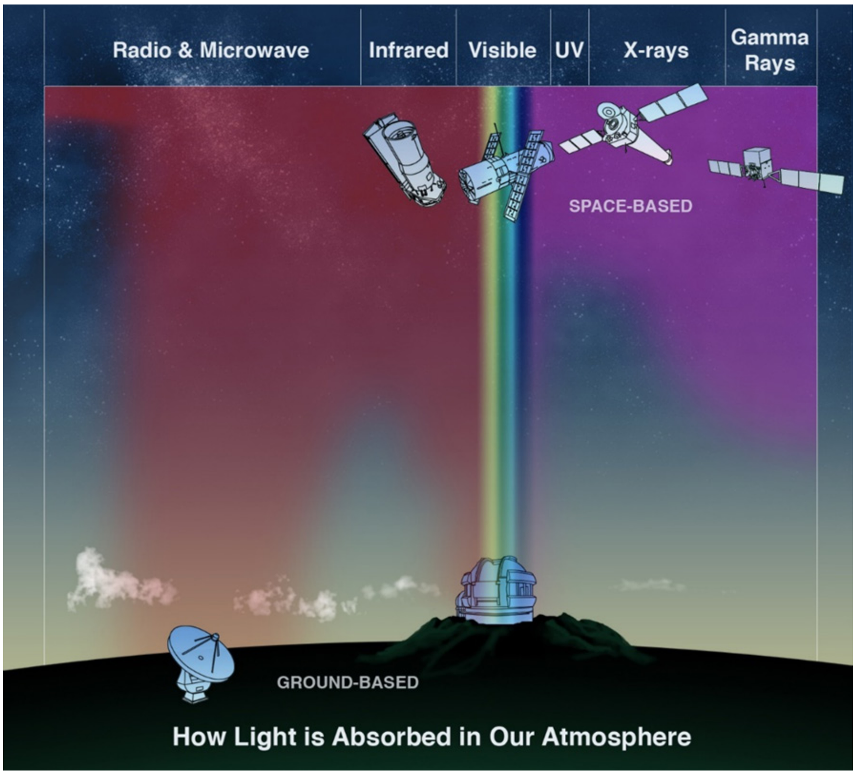

Figure 2. *The differential penetration of electromagnetic energy through the Earth's atmosphere. Penetrating radio waves and visible light can be studied with ground-based telescopes, while space-based telescopes are required to study x-rays originating in space. Credit: Chandra X-ray Observatory website (https://chandra.harvard.edu/graphics/resources/illustrations/absorption_new_300.jpg), accessed 6 Dec 2023.*

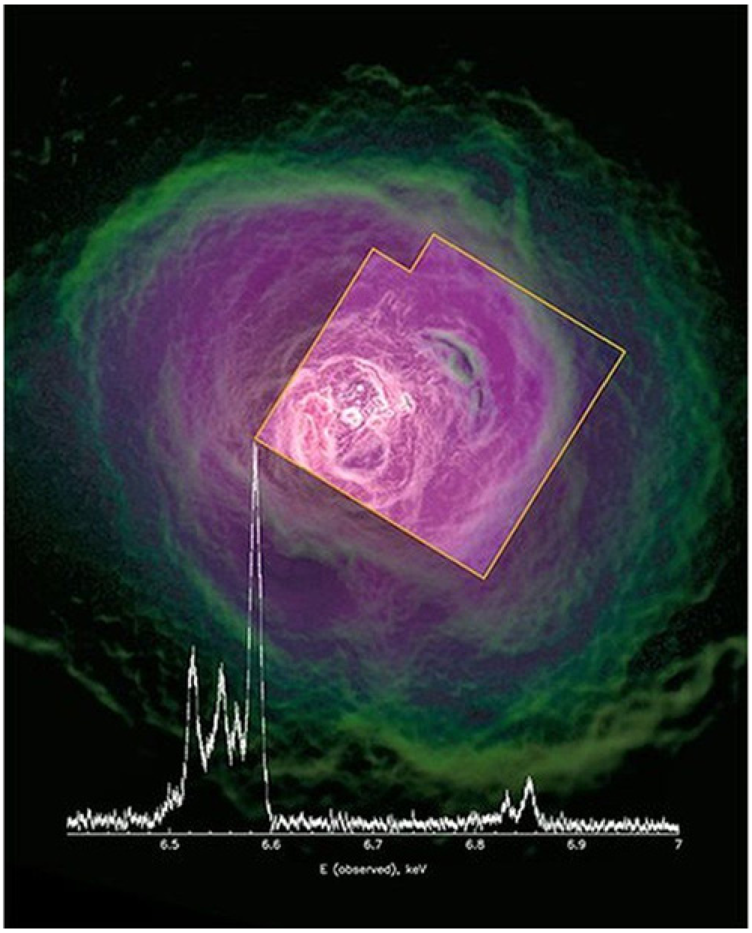

Figure 3. *Image of a galaxy cluster in the Perseus constellation taken by NASA's Chandra X-ray Observatory, overlaid with data collected by the Hitomi X-ray Satellite (just before it ceased functioning), outlined by an orange box, showing X-rays emitted by hot gases between the galaxies. Note the enhancement provided by Hitomi. Credit: BBC News (https://www.bbc.com/news/world-asia-36732336), accessed 5 Dec 2023.*

Some of the universe's most interesting objects and most explosive events emit x-rays. These include galaxy clusters, remnants of exploded stars and black holes. But this radiation cannot be studied even by such very sensitive telescopes as the James Webb Space Telescope which was launched in 2019, because it detects only the orange to mid-infrared part of the electromagnetic spectrum and not x-rays. Dr. Brian Williams, an astrophysicist at NASA who was on both the Hitomi and XRISM research teams, said "we realized that we really had to go and build this mission again, because this is the future of x-ray astronomy" [1].

XRISM carries two instruments, one called 'Resolve' and the other 'Xtend'. Resolve analyzes x-rays with a spectroscope which must be kept at a temperature close to absolute zero so that tiny temperature changes caused by the x-rays hitting the detector can be detected. Its resolution of spectroscopic data will be about 30-fold better than those of the Chandra X-ray Observatory. Working in parallel, Xtend will expand current imaging, observing areas of space about 60% larger than the apparent size of the full Moon.

The high frequency and short-wave lengths of x-rays determine the shape of x-ray telescopes. The mirrors essential in all telescopes to increase capture of light and focus it are large and require an extreme smoothness (at the microscopic level). But while mirror assemblies in telescopes for visible light are close to perpendicular to the path of the photons being studied, they would not work for x-rays. They would pass right through the mirrors. Instead, mirror assemblies for x-ray telescopes are set nearly parallel with the path of the photons, causing only tangential 'grazing' at very low angles. Thus, x-ray telescopes are long, with their mirrors lining the inner sides of a very elongated cone. For example, the main telescope of XRISM is 45 cm in diameter while having a focal length of 5.6 meters.

Scientific operations of XRISM are expected to begin in January 2024, but it may be a year or longer before data become public. JAXA and NASA worked hard on the $190M XRISM to minimize the likelihood of a repeat of the previous failure. This included improving safety measures and giving up some of Hitomi's instruments. Professor Makoto S. Tashiro, an astrophysicist and the XRISM Principal Investigator, states on the JAXA website "learning from the successes and failures of ASTRO-H [Hitomi], XRISM will open a new doorway for the x-ray astronomy world" [2]. Dr. Williams told the journal Science that XRISM "will be the predominant x-ray mission of the 2020s" [3].

Conflicts of Interest and Source of Funding

The author has no conflicts of interest to declare; no funding was involved in this article.

References

1. Miller K, Chang K. Japan joins the new moon race, and launches an X-ray telescope, too. The New York Times [Internet]. 2023 Sept 6 [cited 2023 Dec 7]. Available from: http://www.nytimes.com/2023/09/06/science/japan-launch-moon-xrism-slim.html

2. XRISM [Internet]. Japan Aerospace Exploration Agency; c 2018 [cited 2023 Dec 5]. Greetings from Project Team. Available from: http://xrism.isas.jaxa.jp/en/about/index.html#anc01

3. Clery D. Revolutionary x-ray sensor to probe workings of black holes and supernovae. Science 2023;381:720-1.

ASEAN Movement in Radiology

Report from the 2023 annual meeting of thoracic radiologists in Thailand: The development and reviews of the standards, guidelines, and advice concerning diagnostic radiology of thoracic disorders in Thailand

Chayaporn Kaewsathorn, M.D.[(1)]
Phakphoom Thiravit, M.D.[(2)]
Nitra Piyavisetpat, M.D.[(3),(4)]
Chayanin Nitiwarangkul, M.D.[(5)]
Kanyarat Totanarungroj, M.D.[(2)]
Wiwatana Tanomkiat, M.D.[(1)]
From [(1)] Department of Radiology, Faculty of Medicine, Prince of Songkla University, Songkhla, Thailand,
[(2)] Department of Radiology, Faculty of Medicine Siriraj Hospital, Mahidol University, Bangkok, Thailand,
[(3)] Department of Radiology, MedPark hospital, Bangkok, Thailand,
[(4)] Department of Radiology, King Chulalongkorn Memorial Hospital, Chulalongkorn University, Bangkok, Thailand,
[(5)] Department of Diagnostic and Therapeutic Radiology, Faculty of Medicine Ramathibodi Hospital, Mahidol University, Bangkok, Thailand.
Address correspondence to W.T.(e-mail: twiwadha@hotmail.com)

Received 27 November 2023; accepted 2 December 2023
doi:10.46475/asean-jr.v24i3.890


INTERSTITIAL LUNG DISEASE

The rising issues in practice related with thoracic diagnostic imaging in both private and public sectors were presented to a panel consisting of thoracic radiologist experts from all parts of Thailand in a meeting held on 20 October 2023 by the Royal College of Radiologists of Thailand (RCRT) in collaboration with the Foundation for Orphan and Rare Lung Disease (FORLD) at Asoke Conference Room on the fourth floor of Eastin Grand Hotel, Phaya Thai, Bangkok. The issues were grouped into 5 agendas: a post implementation review of the National HRCT Protocol, the safety and effectiveness of the diagnostic imaging, HRCT interpretation for suspected or at-risk or with known interstitial lung disease including the standard report of HRCT in patients with fibrotic lung disease, the recommended CT protocol for patients with thoracic malignancy in the public health universal coverage system, and a review of the guideline for determining fibrotic extent on HRCT.

Agenda 1: A post implementation review of the National HRCT Protocol and a question-and-answer session, presented and moderated by Chayaporn Kaewsathorn.

The conference revisited the proceedings of the annual meeting held in 2022, during which HRCT protocols from ten different institutes were compared with the National HRCT Protocol. A comprehensive summary of this meeting has been documented in The ASEAN Journal of Radiology under the title "Report from the 2022 Annual Meeting of Thoracic Radiologists in Thailand: National HRCT Protocol and its Applications in 10 Major Institutes” [1]. The conference facilitated discussions on the additional adjustments made to the protocol in each institute, detailed in Table 1. From an overarching standpoint, each hospital demonstrated an average radiation dose lower than 7 mSv, with the exception of Burapha University. Burapha University is currently in the process of acquiring a new machine, anticipated to be operational within the next 6 months.

Table 1. *The HRCT protocols practiced in ten institutes, in comparison with the National Protocol.*

	Position/ respiration	National protocol	Songklanagarind Hospital	Siriraj Hospital	Chulalongkorn Hospital	Ramathibodi Hospital
Scan coverage	Supine/Inspiration	Whole chest	Whole chest	Whole chest	Whole chest	Whole chest
	Supine/Expiration	Whole chest	Whole chest	Whole chest	Whole chest	Whole chest
	Prone/Inspiration	Optional Limit to ROI / whole chest	Optional Whole chest	Optional Whole chest	Optional Limit to ROI	Optional Limit to ROI
Technique	Supine/Inspiration	Volumetric	Volumetric	Volumetric	Volumetric and Sequential	Volumetric
	Supine/Expiration	Sequential / (optional) volumetric, ultralow dose	Sequential	Volumetric, dose not assessed	Sequential	Sequential / Volumetric, dose not assessed
	Prone/Inspiration	Sequential / (optional) volumetric at ROI, ultralow dose	Sequential / volumetric at whole chest, ultralow dose	Sequential (below carina)	Sequential	Sequential
Collimation	Supine/Inspiration	Thinnest (< 1.5 mm)	Thinnest (0.625 mm)	Thinnest (< 1.5 mm)	Thinnest (0.6 mm)	Thinnest (0.625 mm)
	Supine/Expiration					
	Prone/Inspiration					
Rotation time	Supine/Inspiration	Shortest (<0.5 s)	Shortest (0.33 s)	Shortest (<0.5 s)	Shortest (0.35 s)	Shortest (0.27 s)
	Supine/Expiration					
	Prone/Inspiration					
Pitch	Supine/Inspiration	Highest (>1)	Highest (>1)	0.992:1	1.2	1.234
	Supine/Expiration					
	Prone/Inspiration					
Radiation dose	Supine/Inspiration	120 kVp Auto mAs (1-3 mSv)	120 kVp Auto mAs (1-3 mSv)	120 kVp Auto mAs (dose not assessed)	120 kVp Volumetric Auto mAs Sequential 40-60 mAs (2-4 mSv)	120 kVp Auto mAs (dose not assessed)
	Supine/Expiration	120 kVp 20-60 mAs (<1mSv) *100 Kvp, 40-60 mAs (<1mSv)	120 kVp Auto mAs (<1mSv)	100 kVp Auto mAs (dose not assessed)	100 kVp 40-60 mAs (<1 mSv)	100 kVp 20-60 mAs (dose not assessed)
	Prone/Inspiration	120 kVp 40-80 mAs (<1mSv)	120-100 kVp Auto mAs (<1mSv)"	100 kVp 50 mAs (dose not assessed)"	100 kVp 60 mAs (<1 mSv)	100 kVp 40-50 mAs (dose not assessed)
Reconstruction	Supine/Inspiration	1. Axial, lung-window (high-spatial algorithm) ≤1.5 mm thickness overlap (30-50%) 2. Axial, mediastinal-window (low-spatial algorithm) ≤1.5 mm thickness overlap (30-50%) 3. Coronal, mediastinal window (low-spatial algorithm) ≤1.5 mm thickness contiguous	1. Axial, lung-window (high-spatial algorithm) 1.0-1.5 mm thickness overlap (30-50%) 2. Coronal and sagittal, lung-window (high-spatial algorithm) 1.0-1.5 mm thickness overlap (30-50%) 3. Axial, mediastinal-window (low-spatial algorithm) 2.5-3 mm thickness 4. No coronal, mediastinal window	1. Axial, lung-window (high-spatial algorithm) Inspiration 0.625 mm Expiration 1.25 mm thickness overlap (30-50%) 2. Axial, mediastinal-window (low-spatial algorithm) 1.25 mm thickness 3. Coronal, mediastinal window (low-spatial algorithm) 5 mm thickness contiguous **estimate BW and HT before scan	1. Axial, lung-window (high-spatial algorithm) 1.0-1.25 mm thickness overlap (30-50%) 2. Axial, mediastinal-window (low-spatial algorithm) 1.0-1.25 mm thickness overlap (30-50%) 3. Coronal and sagittal, mediastinal window, 5 mm thickness, 3 mm increments	1. Axial, lung-window (high-spatial algorithm) 1.0 mm thickness overlap (30-50%) 2. Axial, mediastinal-window (low-spatial algorithm) 1.0 mm thickness 3. Coronal and sagittal, mediastinal window 4. Axial MIP, mediastinal window, 7 mm thickness, 3 mm increments **estimate BW and HT before scan

	Position/ respiration	Rajavithi Hospital	Maharaj Nakorn Chiang Mai Hospital	Srinagarind Hospital	Thammasat University Hospital	Burapha University Hospital	MedPark Hospital
Scan coverage	Supine/Inspiration	Whole chest	Whole chest	Whole chest	Whole chest	Whole chest	Whole chest
	Supine/Expiration	Whole chest	Whole chest	Whole chest	Whole chest	Whole chest	Whole chest
	Prone/Inspiration	Optional Whole chest	Optional Limit to ROI	Optional Whole chest	Optional Whole chest	Optional Whole chest	Optional Limit to ROI
Technique	Supine/Inspiration	Volumetric	Volumetric	Volumetric	Volumetric	Volumetric	Volumetric and Sequential
	Supine/Expiration	Volumetric, not ultralow dose	Volumetric, not ultralow dose	Volumetric, dose not assessed	Volumetric, not ultralow dose	Volumetric, not ultralow dose	Volumetric, ultralow dose
	Prone/Inspiration	Volumetric at whole chest, not ultralow dose	Volumetric at ROI, not ultralow dose	Volumetric at whole chest, dose not assessed	Volumetric at whole chest, not ultralow dose	Volumetric at whole chest, not ultralow dose	Volumetric at ROI, ultralow dose
Collimation	Supine/Inspiration	Thinnest (< 1.5 mm)	Thinnest (0.6 mm)	Thinnest (< 1.5 mm)	Thinnest (0.625 mm)	Thinnest (0.5 mm)	Thinnest (< 1.5 mm)
	Supine/Expiration						
	Prone/Inspiration						
Rotation time	Supine/Inspiration	Shortest (<0.5 s)	Shortest (<0.5 s)	Shortest (<0.5 s)	Shortest (<0.5 s)	Shortest (<0.5 s)	Shortest (<0.5 s)
	Supine/Expiration						
	Prone/Inspiration						
Pitch	Supine/Inspiration	1.2	1	1.2	1	1.4	1.2
	Supine/Expiration						
	Prone/Inspiration						
Radiation dose	Supine/Inspiration	120 kVp Auto mAs (3-4 mSv)	120 kVp 110 mAs (1-3 mSv)	120 kVp Auto mAs (dose not assessed)	120 kVp Auto mAs (1-3 mSv)	120 kVp Auto mAs (10 mSv)	120 kVp Volumetric Auto mAs Sequential 220 mAs (4.1 mSv)
	Supine/Expiration	120 kVp Auto mAs (2 mSv)	120 kVp 65 mAs (1-2 mSv)	120 kVp Auto mAs (dose not assessed)	120 kVp Auto mAs (1-2 mSv)	120 kVp 150 mAs (5 mSv)	120 kVp Auto mAs (<1mSv)
	Prone/Inspiration	120 kVp Auto mAs (2 mSv)	120-100 kVp 110 mAs, (1-3 mSv)	120 kVp Auto mAs (dose not assessed)	120-100 kVp Auto mAs (1-2 mSv)	120 kVp 150 mAs (5 mSv)	120 kVp Auto mAs (<1mSv)
Reconstruction	Supine/Inspiration	1. Axial, lung-window (high-spatial algorithm) 2.0 mm thickness overlap (30-50%) 2. Axial, lung-window, (high-spatial algorithm) 1.0 mm, interval 10 mm. 3. Coronal and sagittal , lung-window, (high-spatial algorithm) 2.0 mm thickness 4. Axial, mediastinal-window (low-spatial algorithm) 2.0 mm thickness 5. No coronal, mediastinal window	1. Axial, lung-window (high-spatial algorithm) 0.7-1.0 mm thickness overlap (30-50%) 2. Coronal and sagittal, lung-window (high-spatial algorithm) 1-5 mm thickness 3. Axial, mediastinal-window (low-spatial algorithm) 1 mm thickness 4. No coronal, mediastinal window	1. Axial, lung-window (high-spatial algorithm) 0.6-1.0 mm thickness overlap (30-50%) 2. Coronal and sagittal, lung-window (high-spatial algorithm) 1 mm thickness 3. Axial, mediastinal-window (low-spatial algorithm) 2.0 mm thickness 4. No coronal, mediastinal window	1. Axial, lung-window (high-spatial algorithm) 1.0 mm thickness overlap (30-50%) 2. Coronal and sagittal, lung-window (high-spatial algorithm) 2.5 mm thickness 3. Axial, mediastinal-window (low-spatial algorithm) 2.5 mm thickness 4. No coronal, mediastinal window	1. Axial, lung-window (high-spatial algorithm) 1.0 mm thickness overlap (30-50%) 2. Coronal and sagittal, lung-window (high-spatial algorithm) 3 mm thickness 3. Axial, mediastinal-window (low-spatial algorithm) 2.0 mm thickness 4. No coronal, mediastinal window	1. Axial, lung-window (high-spatial algorithm) 1.0 mm thickness overlap (30-50%) 2. Coronal and sagittal, lung-window (high-spatial algorithm) 2 mm thickness 3. Axial, mediastinal-window (low-spatial algorithm) 1 mm thickness 4. Coronal and sagittal mediastinal window (thickness not provided)

Agenda 2: A review of safety and effectiveness of the diagnosis of thoracic disorders using imaging.

2.1 Mass miniature chest radiography, presented by Chayaporn Kaewsathorn and moderated by Wiwatana Tanomkiat.

Image intensifier photofluorography or mass chest radiography is still in limited use in Thailand and image interpreters are general doctors, without the reliance on an illuminator and a magnifying machine to enlarge the image to facilitate an interpretation even in the contemporary healthcare practices. Therefore, the sensitivity, specificity, and accuracy cannot be compared with reports from other countries. Because the mass miniature chest image is the screen film radiograph, it needs to be digitized to store in the Picture Archive and Communication System (PACS) or its use in mass screening in public health can be limited. For the same reason, artificial intelligence (AI) for screening or triaging cannot be applied on the digitized mass chest. Moreover, in 1974, the World Health Organization (WHO) released the ninth report claiming that mobile mass radiography should be abandoned in the screening for tuberculosis [2].

Participants' conclusion: The conference participants unanimously agreed that mass miniature chest radiography is not a recommended method in a medical check-up or a health screening. There should be a clear communication about the limitations of using mass miniature chest radiography in terms of sensitivity, specificity, and accuracy, which might not be effective enough and diseases could stay unnoticed.

2.2 The use of low-dose CT (LDCT) and Lung-RADS, presented by Nitra Piyavisetpat.

LDCT

As CT scans have become more widely used in lung cancer screening nowadays, a meeting was convened to establish a common understanding regarding the definition of LDCT, responsibilities of the individuals in charge of LDCT, and the limitations and risks associated with LDCT.

Definition of LDCT: Until the present days, there has not been an exact definition of how much radiation falls into the low-dose category. In practice, many institutes in Thailand follow the following:

- The low-dose quantity is defined as 10-30% of the standard-dose CT [3],
- The general aim of LDCT is to decrease the effective dose, calculated by multiplying the Dose Length Product (DLP) by a specific conversion factor of 0.0146. The DLP itself is derived from computed tomography dose index (CTDI) multiplying by scan length (in cm). To reduce the effective dose, changes can be made not only by lowering the tube current and tube voltage but also by limiting the scan length specific to the lungs.

The use of LDCT: It is widely accepted that the use of LDCT could reduce the mortality rate, as indicated by numerous studies. According to the US Preventive Services Task Force guidelines, patients aged 50 years or older, with a smoking history of 20 or more pack years, and who are either current smokers or quit smoking less than 15 years ago, are considered at risk [4].

Whether or not there should be a CT protocol guideline: In low-dose screening trials, the effective dose ranges from 0.2-2.36 mSv. In the National Lung Screening Trial (NLST), an average effective dose estimate is 2 mSv per CT, and in the Nelson trial the estimated effective dose is less than 2 mSv. Based on the National Diagnostic Reference Levels in Thailand 2023 [5], the DLP of standard non-contrast chest CT chest is 417 mGy.cm, which corresponds to an effective dose of approximately 6.09 mSv. Therefore, in Thailand, LDCT should be at least 50% lower than the standard non-contrast chest CT.

Possible dangers: The primary concern regarding LDCT is the potential harmful effects of radiation. Even though the radiation dose in LDCT is significantly lower than in standard chest CT, patients often require multiple CT scans, not only for initial screening but also for diagnostic evaluations of lesions detected during LDCT screening. This leads to cumulative radiation exposure. Furthermore, the lungs become more sensitive to radiation as individuals age, with a peak sensitivity typically occurring around 50-55 years. Smoking also amplifies the damage caused by radiation [6]. Therefore, the risk of radiation exposure is not negligible.

LDCT is generally considered inferior to standard dose CT in detecting lesions such as ground glass nodule and other mediastinal lesions, especially in the obese patients. It can also lead to false negative results, particularly for small cell lung cancer which is not generally detected at an early stage. Therefore, a negative LDCT result does not rule out the possibility of lung cancer.

In Thailand, there is widespread confusion regarding the use of LDCT for diagnostic purposes. Some decision-makers mistakenly believe that LDCT should be inexpensive due to its lower radiation dose, leading physicians to request LDCT to cut healthcare costs. However, achieving diagnostic quality with reduced radiation demands sophisticated, high-level CT scanners. These advanced machines are meticulously engineered to minimize radiation doses while ensuring diagnostic accuracy. Consequently, these high-quality CT scanners come at a significant cost. This misunderstanding poses challenges for radiologists using LDCT, potentially compromising the quality of diagnoses. Therefore, it is imperative for responsible individuals to educate decision-makers about the intricacies of LDCT technology and its associated costs.

Participants' conclusion: The participants achieved the following:

1) In terms of the definition of LDCT, an effective dose is at least 10-30% of the standard-dose non-contrast chest CT,

2) The CT machine used to conduct LDCT should be the 16 slices model or newer, as this specific model offers sufficient image resolution to detect nodules even with reduced radiation,

3) Although the radiation dose in LDCT is low, multiple CT scans are performed in the screening group. Moreover, the peak sensitivity of lungs to radiation occurs between the ages of 50-55, and there is a synergistic effect with smoking. Hence, radiation harm cannot be disregarded. Patients entering screening programs should meet the specified screening criteria. Additionally, it is crucial not only to undergo low-dose CT screening but also to focus on smoking cessation,

4) LDCT has limitations in its interpretation across various aspects. The interpretation of other diseases using LDCT relies on the judgment of radiologists for deriving additional benefits,

5) LDCT screening for lung cancer is valuable for detecting slow-growing cancers, but it may miss rapidly progressing tumors between screenings. A negative low-dose CT result does not guarantee the absence of lung cancer and can yield high false-positive rates, particularly in areas with a high prevalence of tuberculosis and granulomatous infections.

Lung-RADS

To ensure consistent interpretation based on Lung-RADS version 2022 [7], discussions were conducted regarding its application. Lung-RADS 2022 is intended for interpreting scans of patients meeting specific screening criteria, namely, those aged 50 years or older, with a smoking history of 20 or more pack years, and either current smokers or individuals who quit smoking less than 15 years ago. Conversely, the 2017 Fleischner Society guidelines should be applied to the general population with incidentally detected nodules [8].

Participants' conclusion: All were in agreement with the established approach.

Agenda 3: HRCT interpretation for suspected or at-risk or with known interstitial lung disease (ILD) by Wiwatana Tanomkiat, Chayanin Nitiwarangkul, Chayaporn Kaewsathorn, and Kanyarat Totanarungroj.

The increasing prevalence of lung fibrosis has prompted concerns among referring physicians regarding the adequacy of information provided in certain HRCT reports for subsequent clinical decision-making. Consequently, the delineation of key components within HRCT reports has been suggested for enhanced diagnostic interpretation.

Recommended topics and information for inclusion in an HRCT report:

- Date of scan and date of image comparison.
- Patient history/demographic data.
- Scanning technique (including image quality).
- HRCT findings, including details such as:
    - Changes in the lung volume,
    - Descriptive findings of lung fibrosis findings and distributions,
    - Disease extent (both global disease and fibrotic extents),
    - Other associated features.

- Impression details, including:
    - Identification of disease patterns (e.g., "UIP pattern," "probable UIP pattern," "indeterminate for UIP pattern," and "alternative diagnosis – specify the most likely disease/diagnosis if possible") as per the 2022 ATS/ERS/ARS/ALAT guideline [9],
    - Fibrotic extent and global disease extent,
    - Presence of radiological progression of the disease [9],
    - Other significant findings/associated findings.

Additional clarifications:

- Disease extent: fibrotic extent and global disease extent as determined in the administrative meetings of 2021, published in The ASEAN Journal of Radiology in December 2021 [10] and April 2022 [11,12], respectively.
- Presence of radiological progression indicating progressive pulmonary fibrosis (PPF): PPF refers to cases with certain underlying diseases (non-IPF ILD) causing pulmonary fibrosis, which meet the 2 in 3 criteria in the past year with no alternative explanation. Criteria include radiological characteristics indicating an increased extent or increased severity of lung fibrosis.

HRCT of the lungs

Technique: (including limitations (if any), e.g., poor image quality, motion artifact)
History:
Comparison:

Findings:

Lung volume: Increase/Decrease

Pattern:
- Honeycombing: Y/N
- Traction bronchiectasis/bronchiolectasis: Y/N
- Reticulations/GGO: Y/N

Distribution:
- Axial: central/peripheral/diffuse
- Craniocaudal: upper/mid/lower/diffuse

+/- Extent:
- Global disease extent % (nearest to 5)
- Fibrotic extent % (nearest to 5)

Associated features:
- Cysts (consider LAM, PLCH, LIP, and DIP)
- Mosaic attenuation/air-trapping/ or three-density sign (consider HP)
- Predominant GGO (consider HP, smoking-related disease, drug toxicity, and acute exacerbation of fibrosis)
- Nodules (Y/N) >> random/ centrilobular/perilymphatic/ profuse centrilobular micronodules (consider HP or smoking-related disease)
- Consolidation (consider organizing pneumonia, etc.)
- Pleural plaques (consider asbestosis)
- Dilated esophagus (consider CTD)
- Pulmonary ossifications
- Emphysema (centrilobular/paraseptal/panacinar)
- Lymphadenopathy
- Pulmonary artery dilatation/enlargement
- Airway abnormalities; bronchiectasis
- Bony structures; joint erosion

Impression:
- Findings suggestive of "UIP pattern", "probable UIP pattern", "indeterminate for UIP pattern", and "alternative diagnosis – specify the most likely disease/diagnosis if possible").
- Fibrotic extent and global disease extent
- Presence of radiological progression of the disease.
- Other significant findings/associated findings

Figure 1. *Example of detail in HRCT report in patients with suspected or at-risk or with known ILD.*

Participants' conclusion: A shared understanding of the report guideline's purposes was affirmed among participants:

1. It is intended to be used with patients suspected of developing pulmonary fibrosis with an unknown cause, such as IPF or connective tissue disorder (CTD),
2. It aims for comprehensive information to enhance more effective patient treatment,
3. It is acknowledged that this guideline specifically pertains to reporting HRCT in patients with ILD and may not be universally applicable to all patient reports.

Agenda 4: The CT protocol for cancer patients in the system under the Universal Health Coverage (UHC) by Wiwatana Tanomkiat and the panellists.

Because the National Health Security Office (NHSO) aims to elevate medical services, enhance the efficiency and medical service quality, reduce the waiting period to receive a computed tomography (CT) for cancer patients who are in the system under UHC by allowing cancer patients to receive CT in private health services. The NHSO asked for advice from the RCRT on a CT protocol that serves as a guideline to be employed in private health services that offer CT to eligible cancer patients in order to deliver quality CT that reaches the standard in terms of safety and optimal benefits for a treatment. Therefore, the CT protocol has been proposed to perform as a guideline for the private medical institutions to appropriately adopt and adapt.

Participants' conclusion: During the discussion, diverse opinions regarding the CT protocol employed in each participant's institution were exchanged. Taking into account the well-being of patients, the efficiency of procedures, and the practical aspects involved, Table 2 was formulated.

Table 2. *shows the CT chest protocol for primary lung cancer and metastatic surveillance.*

Phase	- Lung cancer (first diagnosis)	- Pre-contrast at the tumor (optional) - Venous
	- Lung cancer (follow-up) - Surveillance for metastasis - Surveillance for metastasis in extrathoracic soft tissue sarcoma (first diagnosis)	- Venous
	- Surveillance for metastasis in extrathoracic soft tissue sarcoma (follow-up)	- Low dose non-contrast
Coverage	Supraclavicular area to adrenal gland	
Slice thickness	$\leq$ 3 mm	
Increment (optional)	Less than slice thickness	
Field of view	Cover chest wall	
Rotation time	Shortest as possible	
Scanning time	Should be within single breath hold	
Radiation exposure	Automatic exposure control	
Reconstruction	Lung algorithm and soft tissue algorithm	
Reconstruction	High spatial lung window	Axial view (2-3 mm)
	Low-spatial algorithm/kernel for soft tissue window	Axial view (2-3 mm), Coronal and sagittal views (3 mm) Optional: MIP 5-7 mm
Total radiation dose	Recommendations regarding doses applied in chest CT without contrast media examination were formulated based on the National Diagnostic Reference Levels of Thailand in 2022. This included the reference levels of DLP <417 mGy.cm and CTDI <18 mGy, For CT chest with contrast media examination, recommendations were formulated, including the reference levels of DLP <665 mGy.cm and CTDIVOL <18 mGy.	

Agenda 5: A review of the guideline for determining fibrotic extent on HRCT by Phakphoom Thiravit.

The fibrotic extent of ILD in CTD patients could affect treatments such as using immunosuppressive drugs in patients with systemic sclerosis with fibrosis covering over 20% of the lung. For this reason, the use of HRCT to determine the fibrotic extent is crucial.

There are four popular methods in the determination of the fibrotic extent and the global disease extent, based on the different levels of lung parenchyma selected on HRCT:

Method 1: Using the 3 levels by Sanchez et al. [13],
Method 2: Using the 5 levels by Well et al. [14],
Method 3: Using the 5 levels by Goh et al. [15],
Method 4: Using the 6 levels by chest radiologists in Thailand [12]. This group modified the Method 3 by adding the 6th level, located below the diaphragm.

Chest radiologists from Siriraj Hospital conducted a comparative research study by applying methods 1, 2, and 4 to evaluate the fibrotic extent in IPF. The results revealed:

Method 1 gave the highest mean fibrotic score or global disease extent score among the three methods,
Method 2 gave the lowest mean fibrotic score or global disease extent score among the three methods,
Method 4 gave the mean fibrotic score or global disease extent score in between the Method 1 and Method 4.

Moreover, AI was created to calculate the fibrotic score whose results linger between Method 2 and 4. However, the AI usage is still in its developmental stage.

Participants' conclusion: Method 4 can be adjusted by removing the 4th level and relocating the last level to 5 centimeters above the posterior costophrenic angle (CPA). The additional coronal or sagittal view might be helpful to determine the fibrotic extent more accurately.

Participant list:

Panellists

1. Wiwatana Tanomkiat	Songklanagarind Hospital, Prince of Songkla University.
2. Sitang Nirattisaikul	Songklanagarind Hospital, Prince of Songkla University.
3. Chayaporn Kaewsathorn	Songklanagarind Hospital, Prince of Songkla University.
4. Sutarat Tungsagunwattana	Central Chest Institute of Thailand, Department of Medical Services, Ministry of Public Health.
5. Kittika Jiamjit	Central Chest Institute of Thailand, Department of Medical Services, Ministry of Public Health.
6. Rungaroon Tangsrikertikul	Central Chest Institute of Thailand, Department of Medical Services, Ministry of Public Health.
7. Thitiporn Suwatanapongched	Ramathibodi Hospital, Mahidol University.
8. Warawut Sukkasem	Ramathibodi Hospital, Mahidol University.
9. Chayanin Nitiwarangkul	Ramathibodi Hospital, Mahidol University.
10. Nisa Muangman	Siriraj Hospital, Mahidol University.
11. Kanyarat Totanarungroj	Siriraj Hospital, Mahidol University.
12. Phakphoom Thiravit	Siriraj Hospital, Mahidol University.
13. Krittachat Butnian	Siriraj Hospital, Mahidol University.
14. Wariya Chintanapakdee	King Chulalongkorn Memorial Hospital, Chulalongkorn University.
15. Itthi Itthisawatpan	King Chulalongkorn Memorial Hospital, Chulalongkorn University.
16. Nitra Piyavisetpat	King Chulalongkorn Memorial Hospital, Chulalongkorn University. Department of Radiology, MedPark hospital.
17. Juntima Euathrongchit	Maharaj Nakorn Chiang Mai Hospital, Chiang Mai University.
18. Yuttaphan Wannasopha	Maharaj Nakorn Chiang Mai Hospital, Chiang Mai University.
19. Panaya Tumsatan	Srinagarind Hospital, Khon Kean University.
20. Wannaporn Soontrapa	Srinagarind Hospital, Khon Kean University.

21. Krisna Dissaneevate	Rajavithi Hospital, Department of Medical Services, Ministry of Public Health.
22. Watanya Jaidee	Faculty of Medicine, Burapha University.
23. Amolchaya Kwankua	Faculty of Medicine, Thammasat University.

Observers

1. Pakorn Prakaikietikul	Maharaj Nakorn Chiang Mai Hospital, Chiang Mai University.
2. Natnicha Seehirunwong	Songklanagarind Hospital, Prince of Songkla University.
3. Apisada Siripraiwan	Songklanagarind Hospital, Prince of Songkla University.
4. Tanaporn Eiambanapong	Songklanagarind Hospital, Prince of Songkla University.
5.Thamonpon Pholpraserth	Songklanagarind Hospital, Prince of Songkla University.
6. Phum Inseeyong	Songklanagarind Hospital, Prince of Songkla University.

Meeting recorder Chayaporn Kaewsathorn, MD.
Reviewer Wiwatana Tanomkiat, MD.

References

1. Kaewsathorn C, Thiravit P, Tongbai T, Chintanapakdee W, Itthisawatpan I, Sukkasem W, et al. Report from the 2022 annual meeting of thoracic radiologists in Thailand: National HRCT Protocol and its applications in 10 major institutes. ASEAN J Radiol [Internet]. 2023 Apr 30 [cited 2023 Oct 29];24(1):44-58. Available from: https://www.asean-journal-radiology.org/index.php/ajr/article/view/214.

2. WHO-expertem-Komitee für Tuberkulose, 9. Bericht. Technische Berichtsreihe Nr. 552; WHO, Genf, 1974 Deutsche Ubersetzung [WHO-Expert Committe on Tuberculosis, Ninth Report. Technical Report Series No. 552; WHO, Geneva, 1974 (author's transl)]. Z Erkr Atmungsorgane 1975 ;143:162-93. German.

3. Larke FJ, Kruger RL, Cagnon CH, Flynn MJ, McNitt-Gray MM, Wu X, et al. Estimated radiation dose associated with low-dose chest CT of average-size participants in the National Lung Screening Trial. AJR Am J Roentgenol 2011;197:1165-9. doi: 10.2214/AJR.11.6533.

4. US Preventive Services Task Force; Krist AH, Davidson KW, Mangione CM, Barry MJ, Cabana M, et al. Screening for Lung Cancer: US Preventive Services Task Force Recommendation Statement. JAMA 2021;325:962-970. doi: 10.1001/jama.2021.1117.

5. อนงค์ สิงกาวงไชย์, ศุภวัฒน์ ทัพสุริย์, ปานฤทัย ตรีนวรัตน์, บรรณาธิการ. National Diagnosis Reference Level in Thailand 2023 (ค่าปริมาณรังสีอ้างอิงในการถ่ายภาพรังสีวินิจฉัยทางการแพทย์ของประเทศไทย 2566) [อินเทอร์เน็ต]. นนทบุรี: กรมวิทยาศาสตร์การแพทย์ กระทรวงสาธารณสุข; 2566 [เข้าถึงเมื่อ 3 ธันวาคม 2566]. เข้าถึงได้จาก:https://www.rcrt.or.th/wp-content/uploads/2023/10/National-DRLs-in-Thailand-2023.pdf

6. Pozzessere C, von Garnier C, Beigelman-Aubry C. Radiation Exposure to Low-Dose Computed Tomography for Lung Cancer Screening: Should We Be Concerned? Tomography 2023;9:166-177. doi: 10.3390/tomography9010015.

7. American College of Radiology Committee on Lung-RADS [Internet]. Lung-RADS 2022 [cited 2023 Dec 3]. Available from: https://www.acr.org/-/media/ACR/Files/RADS/Lung-RADS/Lung-RADS-2022. Accessed October 29, 2023.

8. MacMahon H, Naidich DP, Goo JM, Lee KS, Leung ANC, Mayo JR, et al. Guidelines for Management of Incidental Pulmonary Nodules Detected on CT Images: From the Fleischner Society 2017. Radiology 2017;284:228-43. doi: 10.1148/radiol.2017161659.

9. Raghu G, Remy-Jardin M, Richeldi L, Thomson CC, Inoue Y, Johkoh T, et al. Idiopathic Pulmonary Fibrosis (an Update) and Progressive Pulmonary Fibrosis in Adults: An Official ATS/ERS/JRS/ALAT Clinical Practice Guideline. Am J Respir Crit Care Med 2022;205:e18-e47. doi: 10.1164/rccm.202202-0399ST.

10. Tanomkiat W, Nitiwarangkul (Thongprasert) C, Euathrongchit J, Thiravit P, Tongbai T, Suwatanapongched T. Multidisciplinary working group for interstitial lung disease in Thailand: Part 1-rationale in developing a guide to estimate the global disease and fibrotic extents on high-Resolution computed tomography. ASEAN J Radiol [Internet]. 2021 Dec 31 [cited 2023 Oct 29];22(3):47-60. Available from: https://www.asean-journal-radiology.org/index.php/ajr/article/view/158.

11. Euathrongchit J, Thiravit P, Tanomkiat W, Nitiwarangkul C, Tongbai T, Wannosopha Y, et al. Multidisciplinary working group for interstitial lung disease in Thailand: Part 2 – a concise review of published visual scoring methods for interstitial lung disease. ASEAN J Radiol [Internet]. 2022 Apr 30 [cited 2023 Oct 29];23(1):42-55. Available from: https://www.asean-journal-radiology.org/index.php/ajr/article/view/170.

12. Suwatanapongched T, Nitiwarangkul C, Euathrongchit J, Thiravit P, Tongbai T, Tanomkiat W. Multidisciplinary working group for interstitial lung disease in Thailand: Part 3 – the proposed visual scoring method for quantifying the global disease and fibrotic extents on high-resolution CT. ASEAN J Radiol [Internet]. 2022 Apr 30 [cited 2023 Oct 29];23(1):56-65. Available from: https://www.asean-journal-radiology.org/index.php/ajr/article/view/171.

13. Sánchez RP, Fernández-Fabrellas E, Samper GJ, Montañana MLD, Vilar LN. Visual HRCT score to determine severity and prognosis of idiopathic pulmonary fibrosis. Int J Respir Pulm Med 2018; 5:084. doi.org/10.23937/2378-3516/1410084.

14. Wells AU, Hansell DM, Corrin B, Harrison NK, Goldstraw P, Black CM, et al. High resolution computed tomography as a predictor of lung histology in systemic sclerosis. Thorax 1992;47:738-42. doi: 10.1136/thx.47.9.738.

15. Goh NS, Desai SR, Veeraraghavan S, Hansell DM, Copley SJ, Maher TM, et al. Interstitial lung disease in systemic sclerosis: a simple staging system. Am J Respir Crit Care Med 2008;177:1248-54. doi: 10.1164/rccm.200706-877OC.

ISSN 2672-9393
ASEAN J Radiol 2023; 24(3) : 340-344

ASEAN Movement in Radiology

Report on the 2023 ASNR Osborn Professorship to Thailand

Mai-Lan Ho, M.D.
From Department of Radiology, University of Missouri, Columbia, United States of America.
Address correspondence to M-L.H.(e-mail: mailanho@gmail.com)

Received 17 December 2023; accepted 17 December 2023
doi:10.46475/asean-jr.v24i3.892

Abstract

Professor Mai-Lan Ho reported on her two weeks of activities during 16 November –2 December as the 2023 Anne G. Osborn ASNR International Outreach Professor to Thailand, jointly supported by the American Society of Neuroradiology and Royal College of Radiologists of Thailand. Medical and radiological trainings in Thailand were summarized. Academic and social activities were described at three institutes in Bangkok and Chiang Mai.

Keywords: Advanced, ASNR, International, Neuroimaging, Neuroradiology, Outreach.

It was my great honor to serve as the 2023 Anne G. Osborn ASNR International Outreach Professor to Thailand, jointly supported by the American Society of Neuroradiology and Royal College of Radiologists of Thailand [1]. My visit lasted a total of two weeks, during which I gave 23 talks at three leading institutions, all videoconferenced to other hospitals across the country. My interests in advanced imaging, pediatric neuroimaging, and head & neck imaging aligned well with my host institutions, who each selected different topics for me to speak on during my visits.

Medical trainings and practices in Asia are very different from those practiced in North America. Medical schools begin directly after high school, including six years of integrated basic science and clinical training. Medical graduates are assigned to internships in rural areas of Thailand for 1–3 years. After completing their internships, medical doctors can continue working as general practitioners or choose to apply for subspecialty residencies. Radiology residency programs last for three years, with the number of available spots determined by the faculty: trainee ratio of 2:1. Radiology fellowships are two years long and lead to a subspecialty certification, which is required to interpret advanced imaging studies. Academics in the radiology faculty are supported to complete 1–2 years of overseas education, which greatly enhances their research skills and helps them to forge international connections during their careers. Patient records and radiology reports are typed in medical English, although verbal communication is mostly conducted in Thai.

My first stop was at Siriraj Hospital in Bangkok, which is the oldest and largest hospital in Thailand and a hub for medical tourism in Asia. I delivered nine lectures at Siriraj on different focus areas including advanced imaging, adult neuroimaging, pediatric neuroimaging, and head & neck imaging. In the afternoons, I attended multidisciplinary working conferences and interesting case presentations, during which referring clinicians and local radiologists presented challenging cases and unknowns from the past year. My input was requested for several unusual neurogenetic, metabolic, congenital, and parasitic disorders. We also discussed advanced topics including clinical protocoling, research technology, and artificial intelligence (Figure 1).

Figure 1. *Visiting with radiologists and clinicians at Siriraj Hospital.*

Next, I flew north to Chiang Mai, the second largest city in Thailand and formerly a separate country known as the Lanna Kingdom. The city's profound natural beauty makes it an international destination for remote workers or "digital nomads." At Chiang Mai University, I gave four talks and provided diagnostic and management advice on complicated cases of pediatric congenital malformations, tumors and tumor mimics, and inflammatory and metabolic disorders (Figure 2).

Figure 2. *Lecturing at Chiang Mai Hospital.*

Finally, I returned to Bangkok to visit Phramongkutklao Hospital, the largest military hospital in Thailand. Phramongkutklao is a rapidly growing academic center with strong government support and a burgeoning neuroradiology service. My ten lectures covered the breadth of neuroradiology practices and were well received by the faculty, trainees, and military physician leaders. I also liaised with referring neurology and ophthalmology clinicians on complex systemic, autoimmune, and parasitic conditions (Figure 3).

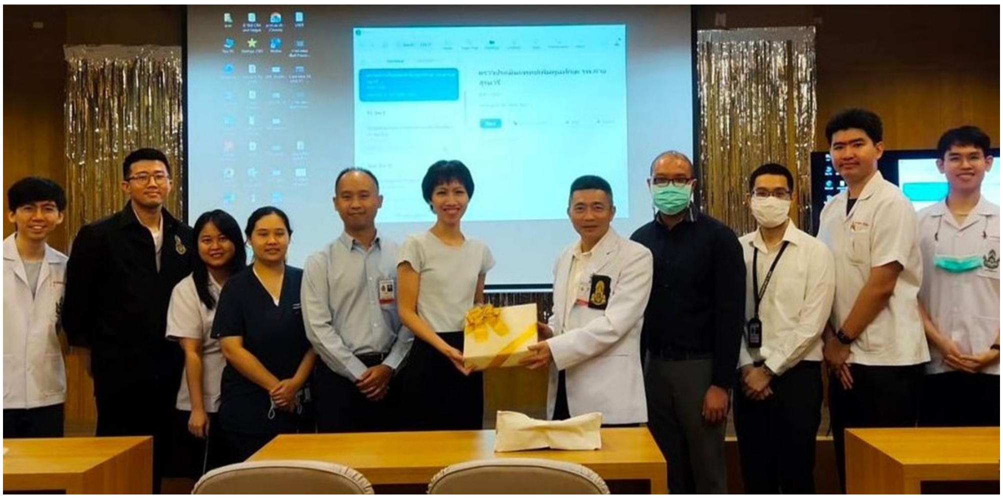

Figure 3. *Teaching at Phramongkutklao Hospital.*

Interspersed with the busy teaching schedule, my hosts found the time to take me to various tourist attractions including the Royal Palace, Loy Krathong festival, temples, museums, street markets, and shopping malls. There is an impressive melting pot of cultures, religions, and cuisines included within this part of Southeast Asia. Everyone I met was incredibly welcoming, curious, and enthusiastic to learn and collaborate in cutting-edge areas. My hosts and I plan to continue corresponding via multidisciplinary conferences, lectures, research, and exchange programs. I am incredibly grateful to ASNR and The Royal College for this once-in-a-lifetime opportunity, and highly recommend the program to future applicants (Figure 4).

Figure 4. *Touring the Grand Palace in Bangkok.*

References

1. ASNR.Org [Internet]. Oak Brook (IL): ASNR; c2005-2023 [cited 2023 Dec 18]. Anne G. Osborn ASNR International Outreach Professor Program. Available from: https://www.asnr.org/international-collaboration/anne-g-osborn-asnr-international-outreach-professor-program/

THE ASEAN JOURNAL OF RADIOLOGY
ISSN 2672-9393

Memorial (Part 2)

Professor Emeritus Chaleow Piyachon (1938-2023) was a scholar, an active citizen and an active member

Received 23 November 2023; accepted 7 December 2023
doi:10.46475/asean-jr.v24i3.889

Professor Chaleow and the author in Hobart, Tasmania (Australia), in 2006.

Some time has passed since the lamentable death of our revered Professor Emeritus Chaleow Piyachon, one of the pioneers in the field of diagnostic radiology in Thailand and a member of the Faculty of Medicine, Chiang Mai University. In the previously published memorial article [1], his particular interest in literature was introduced. Here, his prodigious authorship of numerous works is explored.

During his working years in diagnostic radiology, Professor Chaleow wrote numerous academic works. One of his most renowned textbooks is a pictorial essay of "non-traumatic emergency cases", published in 1984. This montage offers head-to-toe basic knowledge for the interpretation of radiographs, in the era when CT scans and radiologists in Thailand were both scarce. In the days prior to smart phones and online medical material, this portable textbook provided significant knowledge for doctors.

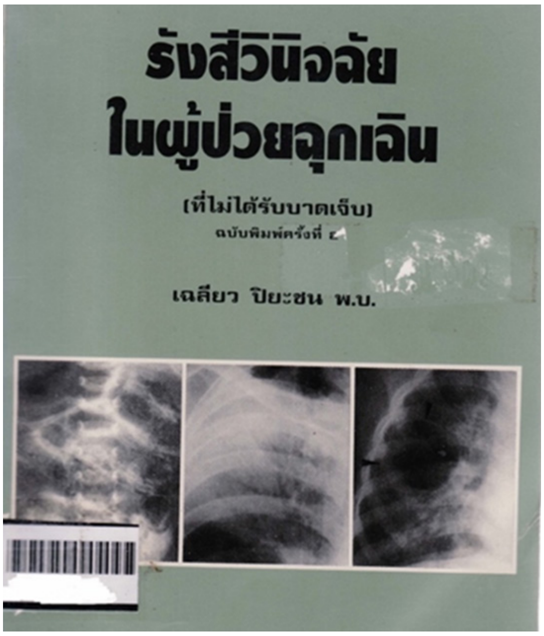

Diagnostic Radiography in Non-traumatic Emergencies (1984): His most widely known academic text providing a vast array of knowledge and pictorials, not only for radiologists but for practitioners as well.

In his retirement years, Professor Chaleow's curiosity shifted to Thai alternative medicine and arts, leading to his writing several non-academic books accordingly. They combine his expertise in Western and traditional Thai medicine, and cover voluminous health topics, including cancer, cardiovascular disease and holistic care.

A non-academic book sharing medical knowledge on atherosclerosis (the 5th edition in 2008).

Apart from his academic writings, Professor Chaleow was acclaimed to be a leading enthusiast in Thai art and culture. His noteworthy books, written in Thai, include:

- "Roeun Kalae" (lit. Northern Thai Houses),
- Heritage in Thai Pottery and Ceramics,
- Sculptures of Mythological and Celestial Beings in Northern Thailand.

These books were drafted and crafted with his unwavering passion, with most of the illustrations and photographs devised and obtained by the professor himself. His work regarding Northern Thai Houses was highly praised by one of the honorary National Artists of Thailand as the finest of its kind.

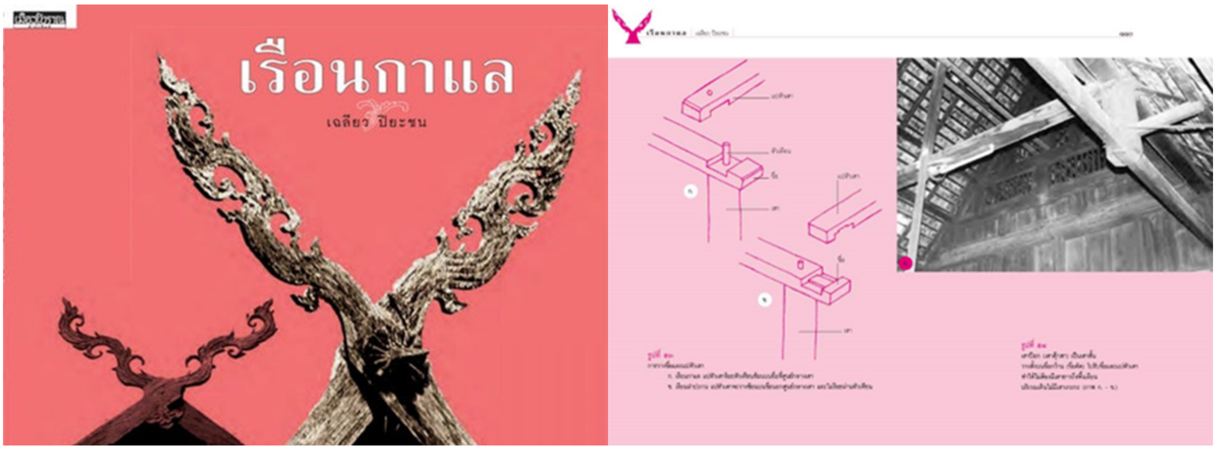

Roeun Kalae (1989): An illustrative guide for Northern Thai Traditional Houses. One of his most cherished and an opus magnum.

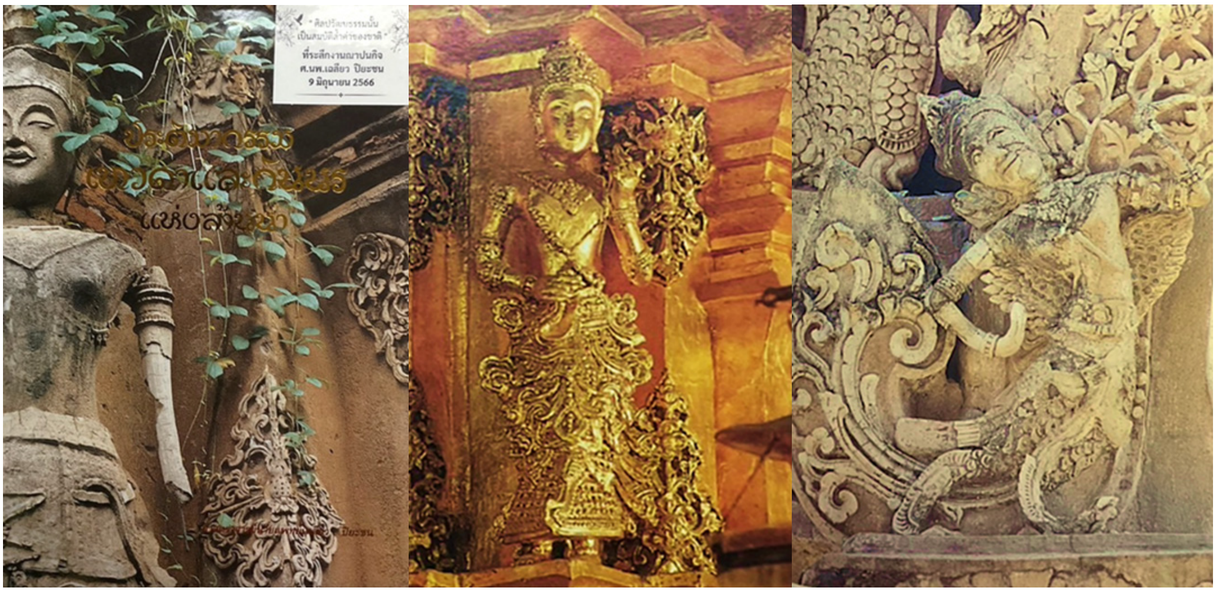

Sculptures of Mythological and Celestial Beings in Northern Thailand (1997) is a testament to both his photographic skill and diligent authorship.

In these days when emphasis on academic achievement usually outweighs personal interests, and the so-called “work-life balance” has become increasingly elusive in our field, one finds the passion for living slowly to be fading away. This article reflects on Professor Chaleow as the epitome of the dedicated radiologist who was always keen on his interests, and did not hesitant to share them with society. This is perhaps a manifesto that work and life can coexist in certain ways, and encourage us to pursue the widely-acclaimed “work-life balance” way of life.

Pavarit Piyachon, M.D.

References

1. Piyachon P. MEMORIAL: PROFESSOR EMERITUS CHALEOW PIYACHON. ASEAN J Radiol [Internet]. 2023Aug.31 [cited 2023Nov.25];24(2):199-200. Available from: https://www.asean-journal-radiology.org/index.php/ajr/article/view/872.

ASEAN

This journal provide 4 areas of editorial services: language editing, statistical editing, content editing, and complete reference-citation check in 8 steps:

Step	Services to authors	Services providers
I	Manuscript submitted	Editor
II	Language editing/ A reference-citation check	Language consultant/Bibliographer
III	First revision to ensure that all information remains correct after language editing	Editor
IV	Statistical editing	Statistical consultant
V	Content editing*	Three reviewers
VI	Second revision	Editor
VII	Manuscript accepted/ rejected	Editor/Editorial board
VIII	Manuscript published	Editorial office

*Content editing follows a double-blind reviewing procedure

JOURNAL OF RADIOLOGY